Understanding the role of alpha-synuclein in Japanese encephalitis virus replication and evaluation of pyrazole derivatives as therapeutics against its infection

A Thesis for

Doctor of Philosophy

by

Ms. ANJALI GUPTA

Department of Biosciences and Bioengineering
Indian Institute of Technology Guwahati
Guwahati-781039, Assam, India
February, 2024

INDIAN INSTITUTE OF TECHNOLOGY GUWAHATI
Department of Biosciences and Bioengineering
Guwahati- 781039, Assam, India

Declaration

I hereby declare that the research work embodied in this thesis entitled "**Understanding the role of alpha-synuclein in Japanese encephalitis virus replication and evaluation of pyrazole derivatives as therapeutics against its infection**" is the result of the scientific investigation carried out by me in the Department of Biosciences and Bioengineering, Indian Institute of Technology Guwahati, India, under the supervision of Prof. Sachin Kumar and Prof. Nitin Chaudhary. And, in keeping with the general practice of reporting scientific observations, due acknowledgments have been made wherever the findings of other investigators have been cited in the thesis.

Date: 19th February, 2024

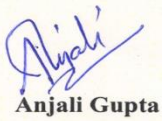

Anjali Gupta

(Roll No. 176106107)
Department of Biosciences and Bioengineering,
Indian Institute of Technology Guwahati,
Assam, India

INDIAN INSTITUTE OF TECHNOLOGY GUWAHATI
Department of Biosciences and Bioengineering
Guwahati- 781039, Assam, India

Certificate

It is certified that the work described in this thesis entitled "**Understanding the role of alpha-synuclein in Japanese encephalitis virus replication and evaluation of pyrazole derivatives as therapeutics against its infection**" by Anjali Gupta (Roll No. 176106107) for the award of the degree of Doctor of Philosophy is an authentic record of the results obtained from the research work carried out under our supervision at the Department of Biosciences and Bioengineering, Indian Institute of Technology Guwahati, India. This work has not been submitted elsewhere for any other degree or diploma award.

February 2024

Prof. Sachin Kumar
Thesis Supervisor
Department of Biosciences and Bioengineering
Indian Institute of Technology Guwahati, Assam, India

Prof. Nitin Chaudhary
Thesis Supervisor
Department of Biosciences and Bioengineering
Indian Institute of Technology Guwahati, Assam, India

Acknowledgments

The accomplishment of the present research work has been made possible with the blessings of god and the generous support of many individuals. Hence, I would like to express my sincere gratitude to all of them for their esteemed contributions.

I am profoundly thankful to my mentors, **Dr. Sachin Kumar** and **Dr. Nitin Chaudhary**, whose unwavering support and guidance have been instrumental in this journey. Their enduring patience and motivation have been persistently helpful. It is with deep appreciation that I recognize their constructive feedback and insightful suggestions, without which this work could not have evolved into its present form.

I wish to express my sincere appreciation to the esteemed members of my doctoral committee: **Dr. Vishal Trivedi** (Chairperson), **Dr. S. Senthilkumar**, and **Dr. Shirisha Nagotu**. Their timely and constructive comments, along with insightful suggestions, have significantly enhanced the execution of this work.

I sincerely acknowledge **Dr. Baldev Raj Gulati** (National Examiner), Director, ICAR-NIVEDI and **Dr. Mark S. Parcells** (Foreign Examiner), Professor, Molecular Virology, Department of Animal and Food Sciences, University of Delaware, for comprehensive evaluation of my doctoral thesis. I want to thank my Ph

I am also thankful to **Dr. Hari Mohan**, Centre for Medical Biotechnology, Maharshi Dayanand University, for his generous help with animal house facility and with related experiments. I also want to thank **Dr. Vidya G Desai**, Department of Chemistry, Dnyanprassarak Mandal's College and Research Centre, for assistance in compound synthesis work.

I would like to extend my acknowledgment to **Prof. Kannan Pakshirajan**, **Prof. Latha Rangan**, and **Prof. Rakhi Chaturvedi**, Department of Biosciences and Bioengineering (BSBE), IIT Guwahati, for lending their support as respectable Heads of the Department during my Ph.D. tenure.

I also thank the Department of BSBE, IIT Guwahati, for providing the infrastructural facility for the research work. My thanks are also due to the technical and non-technical staff of the Department of BSBE, IITG for their kind cooperation during my entire Ph.D. duration.

I sincerely acknowledge the Ministry of Human Resource and Development (MHRD), Government of India, for providing me with the research fellowship and the Department of Biotechnology (DBT) and Indian Council of Medical Research (ICMR) for providing research grants to our laboratory.

I owe my heartfelt gratitude to all my senior lab members, **Dr. Manisha Pandey**, **Dr. Sudhir Morla**, **Dr. Rakesh Kumar**, **Dr. Anshuman Mohapatra, and Dr. Ajay Kumar,** for their needful help and cooperation, especially during my initial phase of Ph.D.

My heartfelt thanks to other past and present lab members: **Ferrin**, **Karam**, **Imdhiyas**, **Vishnu, Purvita di, Shambhavi, Vijay, Kamal, Sushil, Shivani, Priyanka, Shinjini, Nilave, Kiran, Deepa, Aditya** for being great lab mates.

I also want to thank **Uttariya**, **Sweta**, **Sosmitha**, and **Saddam**, with whom I had the best times at IIT Guwahati. I am grateful for all the wonderful moments and their presence, even during unfavorable times in my Ph.D.

I want to thank my former supervisor and mentor, **Dr. Mrinal Kumar Maiti**, Professor, Department of Biotechnology, IITKGP, for being the building block of my professional career. Exposure to his lab and research work has greatly influenced me to be who I am today. I want to mention **Dr. Sudip Kumar Ghosh**, Professor, Department of Biotechnology, IITKGP, for his mentorship and guidance. He has been a constant source of positive feedback and inspiration.

I want to acknowledge **Prabir sir** and **Brijesh,** who have greatly helped me with their thoughtful suggestions and constant faith in me.

I want to express my gratitude towards my **parents**, **Anuj** and **Pinku**, for being the driving force behind my accomplishments and for their love, care, and everything else.

Table of Contents

List of Abbreviations x

List of figures i

Abstract 1

Chapter 1. Introduction 2

1.1 Introduction 2

1.1 Virus Genome 3

1.2 Structural Proteins 4

1.3 Non-Structural proteins 5

1.4 Genotypes 6

1.5 Virus Replication 6

1.7 Diagnostics 8

1.6 Vaccines and Therapeutics 8

1.7 Neuropathogenesis 9

1.8 Alpha-synuclein: neuronal specific protein 11

1.9 Oxidative stress in JEV pathogenesis 13

Chapter 2. Review and literature 15

2.1 Alpha-synuclein in viral pathogenesis 15

2.2 Alpha-synuclein mediated modulation of oxidative stress 16

2.3 Role of pyrazole based derivatives in modulating oxidative stress 17

2.4 Aim and scope of current research 18

2.5 Objectives 20

Chapter 3. Understanding the role of α-syn in JEV replication 21

3.1 Abstract 21

3.2 Introduction 22

3.3 Material and Methods 23

3.3.1 Cells and viruses 23

3.3.2 Expression and Purification of Exoα-syn protein 24

3.3.3 Characterization of Exoα-syn protein 24

3.3.4 Time course analyses of α-syn expression 25

3.3.5 *In vitro* anti-JEV activity 25
3.3.6 Small Unilaminar Vesicles (SUV) preparation 26
3.3.7 Circular Dichroism (CD) analyses 26
3.3.8 Calcein entrapped vesicle preparation 27
3.3.9 Overexpression and knockdown of α-syn 27
3.3.10 Overexpression and endogenous silencing of SOD1 28
3.3.11 Gene expression and viral particle estimation 28
3.3.12 ROS estimation 29
3.3.13 Statistical analysis 29
3.4 Results 30
3.4.1 Modulation of α-syn post JEV infection in neuronal cells 30
3.4.2 α-syn inhibits JEV replication 31
3.4.3 Effect of overexpression and silencing of α-syn on JEV replication 36
3.4.4 α-syn modulates oxidative stress via decreasing ROS in neuro2a cells 37
3.4.5 α-syn positively regulates SOD1 expression 38
3.4.6 Increase in JEV infectivity post treatment with LCS-1 39
3.5 Discussion 42
Chapter 4. Understanding the effects of JEV replication on phosphorylation and oligomerization of α-syn 47
4.1 Abstract 47
4.2 Introduction 48
4.3 Material and Method 49
4.3.1 RNA and protein quantification of phosphokinases 49
4.3.2 Phosphorylated α-syn estimation 50
4.3.3 Aggregation of α-syn 50
4.3.4 ThioflavinT Assay 50
4.4 Results 51
4.4.1 Modulation of phosphokinases post JEV infection 51
4.4.2 Oligomerization of α-syn 52
4.5 Discussion 53
Chapter 5. 3. Designing and assessment of pyrazole derivatives against JEV infection. 56
5.1 Abstract 56

5.2 Introduction 57
5.3 Materials and methods 57
5.3.1 General methods 57
5.3.2 General procedure for the synthesis of pyrazole derivatives 58
5.3.3 Cytotoxicity assay of pyrazole-based compounds. 58
5.3.4 *In vitro* antiviral assay of pyrazole compounds 59
5.3.5 *In vitro* time-dependent kinetics of JEV 59
5.3.6 *In vitro* dose-dependent response of JEV 60
5.3.7 Dose and time-course study of compounds in mice 60
5.3.8 Evaluation of anti-JEV effect of the compounds in mice 61
5.3.9 ROS estimation 61
5.4 Results 62
5.4.1 Synthesis of pyrazole derivatives 62
5.4.2 Evaluation of the anti-JEV effect of compounds in cells 66
5.4.3 Time and dose-dependent kinetics of JEV in cells 68
5.4.4 Anti-JEV potential of 1b and 1f in mice 70
5.4.5 Anti-JEV mechanism 72
5.5 Discussion 73
Chapter 6. Conclusions 78
Chapter 7. Future prospects 80
Bibliography 82
Research Achievements 95

List of Abbreviations

AES	Acute Encephalitis Syndrome
ARE	Anti-Oxidant Response Element
α-syn	Alpha-synuclein
BBB	Blood Brain Barrier
BHK-21	Baby hamster kidney cells
C	Capsid
CD	Circular Dichroism
CK2	Casein Kinase 2
CNS	Central Nervous System
CSF	Cerebrospinal Fluid
DAT	Dopamine Active Transporter
DCFH-DA	2′,7′-dichlorodihydrofluorescin diacetate
DENV	Dengue virus
DLS	Dynamic Light Scattering
DMEM	Dulbecco's modified eagle medium
D2R	Dopamine D2 Receptor
E	Envelope
ER	Endoplasmic Reticulum
Exoα-syn	Exogenous alpha-synuclein
FBS	Fetal Bovine Serum
FITC	Fluorescein isothiocyanate
G	Genotype
GRKs	G-protein-coupled receptor kinases

GSH	Glutathione
GPx	Glutathione Peroxidase
H	Hour
HBV	Hepatitis B virus
HCV	Hepatitis C viruses
HIV	Human Immunodeficiency virus
HO-1	Heme Oxygenase 1
HSV	Herpes Simplex virus
H_2O_2	Hydrogen Peroxide
IAV	Influenza-A virus
IC_{50}	Inhibitory Concentration 50
JEV	Japanese encephalitis virus
Keap1	Kelch-like ECH associated protein 1
LBs	Lewy Bodies
M	Membrane
MOI	Multiplicity of infection
MTT	3-(4,5- dimethylthiazol-2-yl)-2,5-diphenyltetrazolium bromide
NRF2	Nuclear Factor Erythroid 2-Related Factor 2
NS	Non-Structural
NQO1	NAD(P)H: Quinone oxidoreductase 1
ORF	Open Reading Frame
PBS	Phosphate Buffer Saline
PCR	Polymerase Chain Reaction
PD	Parkinson's Disease
PFU	Plaque forming unit

PLC	Phospholipase C
PLKs	Polo-like Kinases
POPC	1-palmitoyl-2-oleoyl-sn-glycero-3-phosphocholine
POPS	1-palmitoyl-2-oleoyl-sn-glycero-3-phospho-L-serine sodium
POPE	1-palmitoyl-2-oleoyl-sn-glycero-3-phosphoethanolamine
RC	Replication Complex
RNA	Ribonucleotide acid
ROS	Reactive Oxygen Species
RSA	Radical Scavenging Activity
SDS-PAGE	Sodium Dodecyl Sulfate Polyacrylamide Gel Electrophoresis
SM	Sphingomyelin
SOD	Superoxide dismutase
ss	single stranded
SUVs	Small Unilaminar Vesicles
SQSTM1	Sequestosome 1
TBEV	Tickborne encephalitis virus
$TCID_{50}$	Tissue culture infectious dose
TH	Tyrosine Hydroxylase
ThT	ThioflavinT
TLRs	Toll like Receptors
VZV	Varicella-Zoster virus
WNV	West Nile virus
YFV	Yellow Fever virus
ZIKV	Zika virus

List of figures

Chapter 1: Introduction

Figure 1.1 Schematic representation of JEV virion

Figure 1.2 Genomic arrangement of JEV + sense ssRNA of ~11Kb. Whole genome codes for three structural proteins: C, preM, E and seven Non-Structural proteins: NS1, NS2a, NS2b, NS3, NS4a, NS4b, NS5. At both ends untranslated region are present acting as cis-regulatory elements during replication and translation process. Single ORF is present at 5' end of which single precursor polypeptide is produced. Further viral and host proteases act to produce single mature functional viral protein.

Figure 1.3 JEV replication cycle inside host cell. **1)** Virion surface proteins bind with cell receptors. **2)** Virion enters through clathrin- coated vesicles inside cell. **3)** Fusion between membrane vesicle and early endosome takes place. Virion enters endosome. **4)** Due to low pH the conformation of E protein changes and virion structural proteins get dissemble. Nucleocapsid structure is released out of late endosome. **5)** Genomic RNA is released in cytoplasm. Multiple copies of positive sense RNA are produced through RNA dependent RNA polymerase activity of NS5 and other accessory proteins. Simultaneously, positive sense RNA act as template and viral proteins are also produced. **6)** Viral proteins and RNA strands are carried to Endoplasmic Reticulum (ER) where premature virion assembly takes place. **7)** Newly synthesized virion particle is carried to inside network where protein modification takes place. **8)** Mature virion is carried towards cell membrane in Golgi vesicle. Virus particles are released through exocytosis

Figure 1.4 Diagrammatic representation of different structural domains of α-syn protein. N-terminal region including NAC domain of the protein forms a broken, amphipathic alpha-helix structure whereas, C-terminal tail remains in flexible and disordered conformation.

Chapter 3: Role of alpha-synuclein in JEV pathogenesis

Figure 3.1 Quantification of endogenous α-syn in neuro2a cells. Real-time PCR analysis of viral RNA at 12 h interval till 96 h post-infected with 0.1 MOI JEV (A). Fold change expression of α-syn in JEV-infected neuro2a cells compared to mock-infected cells till 96 h where GAPDH is used as a control (B). Fold change is calculated keeping mock-infected cells as control. Western blot along with densitometric analysis of α-syn protein in JEV-infected neuro2a cells compared to mock-infected cells till 96 h (C).

Figure 3.2 Characterization of purified Exoα-syn. The SEC profile of the anion exchange-purified α-syn (A). A 12% SDS-PAGE of Exoα-syn SEC fractions. The BioRad Precision Plus Protein™ ladder marked as M. The SEC fractions were loaded in L1-L8 (B). MALDI-TOF mass spectrometric analyses of Exoα-syn protein. Expected monoisotopic mass: 14,451.22 Da, observed

m/z: 14,476.18. Doubly-charged species is seen at m/z 7,233.25 (C). DLS profile of the freshly prepared Exoα-syn protein (D).

Figure 3.3 Modulation of JEV in neuro2a cells after co-treatment, pre-treatment, and post-treatment of Exoα-syn at 0.25, 0.5, and 1 µM concentrations. JEV vRNA quantification after 72 h of infection in differentially-treated cells. Fold change is calculated with respect to uninfected cells as control (A). Western blot analysis to quantify the viral protein after 72 h of JEV infection in cells differentially treated with Exoα-syn (B). Virus titration of supernatant collected after 72 h of JEV-infected cells differentially-treated with Exoα-syn protein (C).

Figure 3.4 Characterization of liposomes (SUVs) and interaction with Exoα-syn protein. Graphs representing DLS size distribution profile of the plain and calcein-loaded SUVs (A). Circular dichroism spectra of Exoα-syn (2 µM) in phosphate buffer and in the presence of SUVs at protein:lipid ratio of 1:200 (B). Graphs representing fluorescence intensities of calcein-loaded SUVs in buffer, in the presence of Triton X-100 (1% v/v), and with Exoα-syn at 1:50 protein:lipid ratio (C).

Figure 3.5 Modulation of JEV upon up and down regulations of α-syn gene. Western blot analysis of JEV protein after 48 h of its infection in cells transfected with plasmid expressing α-syn (A). The graph representing the percentage reduction in the plaque number. Downregulation of α-syn mRNA by siRNA treatment in neuro2a cells (B). Western blot analysis of JEV protein and plaque assay of neuronal cells transfected with siRNA and infected with JEV at 0.1 MOI (C).

Figure 3.6 Reactive oxygen species (ROS) estimation using flow cytometry. Flow cytometry analysis to quantify ROS in JEV infection at 24 h interval till 96 h. DCFH-DA dye was used to stain the cells 30 min prior estimation in live cells in FITC channel. Graph representing median FITC (%) in mock-infected and JEV-infected cells (A). Median FITC (%) of ROS estimation in cells 6 h post-treatment with H_2O_2, 12 h post-ascorbic acid and α-syn protein treatment and untreated control (B). Modulation of JEV infection post-treatment with H_2O_2, ascorbic acid, α-syn protein, and untreated control. Western blot analysis along with viral titration through plaque assay from the whole cell lysate and supernatant of the treated cells, respectively (C). Graph representing the percent plaque numbers in differentially treated cells.

Figure 3.7 Modulation of genes involved in oxidative stress post-treatment with Exoα-syn protein at 0.25, 0.5, and 1 µM concentrations. Western blot analyses of SOD1, SQSTM1, DJ-1, and NQO1 proteins after 24 h of treatment. Untreated neuro2a cells are used as control cells and GAPDH as loading control (A). Modulation of SOD1 post-α-syn gene silencing. Real-time PCR and western blot analyses to estimate SOD1 specific mRNA and protein post α-syn siRNA treatment (B). Fold change is calculated by keeping SOD1 expression in untransfected (CON) cells as baseline.

Figure 3.8 Modulation of ROS post-treatment with SOD1 inhibitor LCS-1. Graph representing median FITC (%) post 6 h and 12 h of 5 µM LCS-1 treatment in neuro2a cells (C). Untreated (CON) neuro2a cells are kept as control cells. Modulation of JEV post-treatment with 5 µM LCS-

1. Viral titer analyses through plaque assay and graph representing plaques (%) in differentially-treated cells (D).

Figure 3.9 Modulation of JEV post-overexpression and silencing of SOD1. Modulation of JEV post-overexpression of SOD1. Western blot analyses were performed after 48 hours to estimate the JEV NS1-specific protein. Cells without infection (CON) and cells with JEV infection (JEV) were used as control groups. Graph representing the percentage of plaque obtained from the supernatant of treated cells after 48 h (A). Modulation of JEV post-SOD1 siRNA treatment. Western blot analyses and plaque assays were carried out for virus titration in treated groups. Cells treated with universal scrambled siRNA were used as the control group. Graph representing the percentage of plaque obtained from the supernatant of the differentially treated groups post 48 h (B). Statistical analyses were determined using ordinary one-way ANOVA ($p<0.05$, $p<0.001$, and $p<0.001$ are described as *, **, and ***).

Figure 3.10 Modulation of JEV post overexpressing and silencing of α-syn along with SOD1 silencing and overexpression. Differential treated cells along with controls; non-transfected, -ve siRNA, SOD1 siRNA, α-syn siRNA, α-syn overexpression were infected with 0.1MO1 of JEV. Western blot analyses using GAPDH, NS1, SOD1, α-syn specific antibodies and plaque estimation were performed after 48 hours of JEV infection. Graph representing the percentage of plaque obtained from the supernatant of differentially treated cells. Statistical analyses were determined using ordinary two-way ANOVA ($p<0.05$, $p<0.001$, and $p<0.001$ are described as *, **, and ***).

Chapter 4: To study aggregation of alpha-synuclein in JEV infected neuronal cells

Figure 4.1 Real time analyses of CK2 and PLK2 in JEV infected and CON neuro2a cells (A). Fold change has been calculated keeping CON as base line expression and GAPDH as control gene expression. The western blot analyses using PLK2, CK2 and GAPDH specific antibodies in JEV infected and CON cells at 24, 48, 72 h intervals (B). Western blot analyses to evaluate the pα-syn in JEV infected and non-infected neuro2a cells which are transfected α-syn expression plasmids (C). Total α-syn is kept as control to analyze the change in pα-syn

Figure 4.2. Analyses of aggregation α-syn by western blotting and ThT fluorescence. Western blot analyses of whole cell lysate post 0.05% glutaraldehyde mediated protein cross-linking. α-syn specific antibody was used to detect the oligomers of different sizes in CON and JEV infected sample (A). Spectrophotometric analyses of aggregated intracellular proteins via ThT dye. Graphs representing fluorescence intensities from 450 to 650 nm (B). CON cells without ThT is used to measure base line fluorescence from cells (ThT). The samples CON, JEV, α-syn and α-syn+JEV were mixed with 300 µl of 20 µM ThT dye and all the samples were excited at 445 nm wavelength.

Chapter 5: Analysis of fluoro based pyrazole analogues as a potential therapeutics' candidate against JEV modulating host proteins

Figure 5.1 Substrate scope of the synthesized 2,4-dinitrophenyl pyrazole derivatives (**A**). Structural representation newly synthesized six pyrazole derivatives (**B**).

Figure 5.2 ^{1}H NMR and ^{13}C NMR spectral analysis of compounds 1a-1f.

Figure 5.3 Cytotoxicity analyses of six compounds in Neuro2a cells. MTT assay was done after 48hr. Concentrations from 100µM to 100nM were selected for the experiment (**A**). Data are shown as the mean ± SD.

Figure 5.4 Evaluation of antiviral effect of 1b and 1f derivatives in Neuro2a cells. Different treatment groups are marked as: cell control (CON), virus infected (V), virus along with 1b treated cells (V+1b) and virus along with 1f treated (V+1f). Schematic presentation of post-treatment and co-treatment performed for 72 h at 15µM concentration (**A**). Virus titration using plaque assay of supernatant collected from post and co-treated cells after 72 h of incubation (**B**). Real-time analyses of viral RNA using JEV E gene specific amplification (**C**). For all the treated groups CON, V,V+1b, V+1f analyses is done at 72 h time points. GAPDH is used as an internal control and values are represented as mean fold change in multiple of 100 with respect to cell control. *** representing p-value < 0.001. Western blot analyses using JEV NS1 specific monoclonal antibody (GTX633820, GeneTex) and GAPDH (BB-AB0060, BioBharti) as an internal control (**D**). Analyses was done using whole cell lysates after 72 h of treatments. JEV NS1 band is detected at ~45 kDa normalised with protein band of GAPDH at around 37 kDa.

Figure 5.5 Time and Dose-dependent kinetics of JEV in Neuro2a cells. Multi-step growth kinetics of the JEV in Neuro2a cells upon treatment with 15 µM of 1b and 1f (**A**). Cells from CON are shown as base line. Supernatant were collected after every 24 h till 120th h post treatment and replaced with equal volume of fresh medium. Virus yield were determined by $\log_{10}$ $TCID_{50}$. Standard deviations indicated as error bars. Dose response analyses of JEV from (15 to 5) µM concentration of 1b and 1f (**B**). Western blot analyses with JEV NS1 and GAPDH specific antibody post. Whole cell lysates collected post 72 h of treatment were used for analyses.

Figure 5.6 Evaluation of IC_{50} value of 1b and 1f through plaque assay at 72th h. (**A**). Graph representing percentage of plaque reduction at 15 µM, 10 µM, 5 µM and 1 µM (**B**).

Figure 5.7 Graph representing time escalation study of 1b and 1f in mice (**A-B**). Mice were injected intraperitoneal with 10, 50 and 100mg/kg of 1b or 1f first day in different groups (n=3). Mice of control group received DMSO of equal volume. Body weight of each mice were observed till five days and plotted as mean body weight in grams. Graph representing dose escalation study of compounds in mice (**C-D**). Intraperitoneal injection of 100mg/kg of 1b or 1f were given two, three and four times at 24 h interval in different groups. Body weight of each mice was observed till 5th day of experiment and plotted in graph as mean body weight in grams

Figure 5.8 Schematic presentation of anti-JEV experiment in mice (**A**). Real time analyses of JEV E viral RNA in spleen (**B**) and brain (**C**) tissues harvested at 24, 48, 72, 96, 120th h time points.

Graph representing JEV E RNA fold change in multiple of 100 with respect to group CON+DMSO. GAPDH is used as internal control**.** *** representing p-value < 0.001. Standard deviations indicated as error bars

Figure 5.9 Western blot analyses using DJ-1 (SQSTM1 (8025, CST) specific antibody and beta-actin as a loading control (MA1-91399, Invitrogen) at 48th h. **(A).** Flow cytometry analyses to estimate ROS generation in differential treated group with respect to CON group at 48th h in Neuro2a cells **(B).** FITC channel is used to detect fluorescence of DCFH-DA dye. Y-axis representing median FITC intensity**.** Base line drawn at intensity of CON group. *** representing p-value < 0.001

Abstract

In the prognosis of Japanese encephalitis virus (JEV) infection, many host factors have been identified as being involved in the various steps of the viral life cycle. Since it is a neurotropic virus, understanding the role of neuronal-specific proteins and local cellular homeostasis in developing therapeutics against JEV is an active area of research. Alpha-synuclein (α-syn) is one of the neuronal-specific proteins regulating synaptic plasticity and has been reported to have antiviral potential in related neurotropic viruses. JEV-infected patients displaying Parkinson's disease (PD)-like symptoms have been reported to have α-syn overexpression in the brain regions. As per reports, phosphorylation at S129 position plays a major role in aggregation and α-synucleinopathy. Therefore, exploring the function of α-syn in JEV induced death of dopaminergic neurons and α-synucleinopathy is essential. To this day, the present study reports the functional role of α-syn in JEV pathogenesis as well as explores the anti-JEV therapeutic candidates. There is a significant increase in endogenous α-syn expression during JEV replication, demonstrating a substantial reduction in JEV replication, suggesting an anti-JEV effect. α-syn was found to modulate the anti-oxidative pathway by increasing the expression of superoxide dismutase 1 (SOD1). The pathological implications of α-syn phosphorylation were carried out by studying casein kinase 2 (CK2) and Polo-like kinase (PLK2) involved in α-syn phosphorylation. Detailed analyses of CK2 and PLK2 reveal a notable reduction in these kinases, particularly during the late phase of JEV replication, thereby reducing the phosphorylated α-syn (pα-synS129) protein level. The intracellular α-syn oligomerization was increased in JEV-infected cells. Pyrazole derivatives with anti-oxidative properties were found to have anti-JEV activity. Comprehensive *in vitro* and *in vivo* studies showed compounds suppressed JEV-induced reactive oxygen species (ROS) generation through NRF2-SQSTM1 signaling mechanisms. This study contributes valuable insights into the interplay between α-syn and JEV, shedding light on avenues to study further the potential role of α-syn aggregation in JEV pathogenesis and exploit it to develop broad-spectrum antiviral therapeutics.

Chapter 1. Introduction

1.1 Introduction

Encephalitis is an uncommon but serious condition in which severe brain inflammation develops. Out of various factors like autoimmune disease and exaggerated immune response against pathogens, viral encephalitis is a more common cause of Acute Encephalitis Syndrome (AES) cases (1, 2). Flaviviruses are the most prevalent arthropod-borne viral diseases of humans. Among flaviviruses, dengue viruses (DENV), Japanese encephalitis virus (JEV), tickborne encephalitis virus (TBEV), yellow fever virus (YFV), West Nile virus (WNV), and zika viruses (ZIKV) are most common cause of encephalitis with high mortality rate (3).

JEV is a serious vector-borne cause of encephalitis and a significant public health problem leading to high morbidity and mortality. After its first outbreak in Japan in 1871, its endemic area extends to eastern and southeastern Asia, including India, Nepal, Japan, China, Korea, Thailand, Indonesia, Malaysia, Vietnam, Taiwan, and the Philippines (4). The transmission vector of JEV is the *Culex*. mosquito especially *Cx. tritaeniorhynchus* and the primary amplifying vertebrate host are pigs (5). It is estimated that approximately 60,000 JE cases occurs within endemic areas every year, with 25-30% rate mortality and severe residual neurological or psychiatric complications in up to 50% of survivors (6). In humans, the incubation period is believed to last for 5 to 15 days followed by sudden onset of flu-like symptoms, such as a high temperature, headache, photophobia, vomiting (7). More severe symptoms develop over days or weeks, including confusion or disorientation, seizures (fits), changes in personality and behavior, difficulty in speaking, weakness or partial loss of movement, loss of consciousness, hallucinations, and coma (7). With the low number of JE cases in the higher age group due to the development of immunity,

either by sub-clinical infections or due to earlier vaccination, mortality rates are higher among children from 0–10 age group.

1.1 Virus Genome

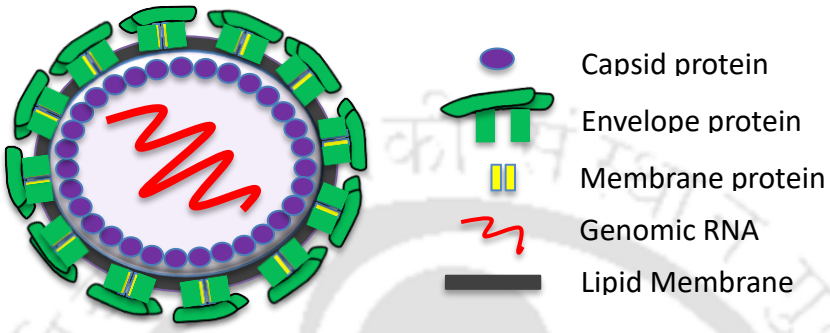

Figure 1.1 Schematic representation of JEV virion

JEV has a single-stranded, positive-sense RNA genome of approximately 11 kb in length (Figure 1.1) (8). The virion of JEV contains three structural proteins - capsid (C), membrane (M), and envelope (E), as well as seven non-structural (NS) proteins - NS1, NS2A, NS2B, NS3, NS4A, NS4B, and NS5 (Figure 1.2) (8, 9). The JEV genome contains a single open reading frame (ORF) encoding single polyprotein, which goes post-translational cleavage and modification by viral proteases and host signalases (10). After infection, transcription and translation are modulated by cis-acting non-coding regions present at both 5` and 3` sides of JEV genome (11).

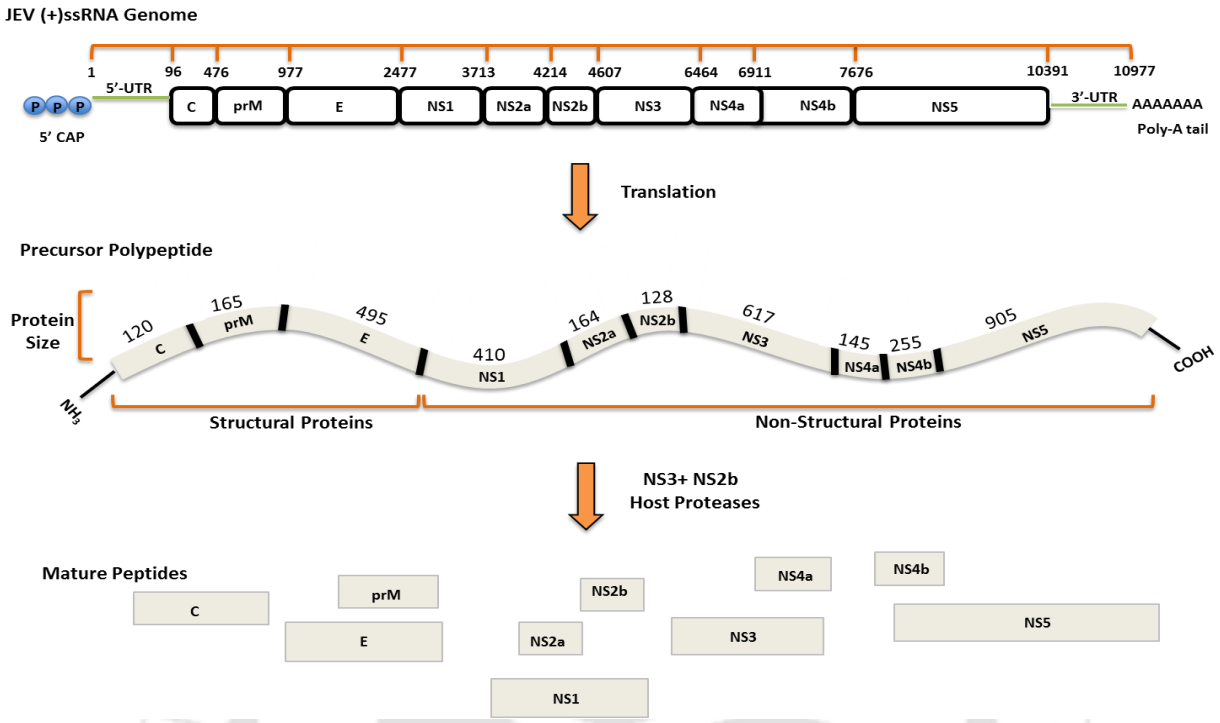

Figure 1.2 Genomic arrangement of JEV + sense ssRNA of ~11Kb. Whole genome codes for three structural proteins: C, preM, E and seven Non-Structural proteins: NS1, NS2a, NS2b, NS3, NS4a, NS4b, NS5. At both ends untranslated region are present acting as cis-regulatory elements during replication and translation process. Single ORF is present at 5' end of which single precursor polypeptide is produced. Further viral and host proteases act to produce single mature functional viral protein.

1.2 Structural Proteins

C protein of JEV contains ~120 amino acids and are found in homodimer (12). Multiple copies of the C protein are organized into a capsid that covers the viral genome to form a nucleocapsid structure (13). The amino acid identity between different flavivirus C proteins ranges from 15 to 90% (14). M and E are the viral glycoproteins. prM (~165 amino acids) and E (~495 amino acids) contain two transmembrane helices. The prM protein functions as a chaperone for the folding and assembly of the E protein before it is cleaved during particle maturation to yield the pr peptide and the M protein (~75 amino acids) (15). E protein among the flavivirus share ~40% amino acid identity. It contains a cellular receptor-binding site(s) and a fusion peptide (16). With the three characteristic domains, namely the domain I lateral ridge, fusion loop, domain III

lateral ridge, and domain I-II hinge, JEV facilitates cellular attachment and membrane fusion and is the primary target of neutralizing antibodies (17). The number and position of potentially glycosylated residues is not conserved among different strains of the JEV, which modulate receptor binding specificity prevailing targeted pathogenicity (16, 18).

1.3 Non-Structural proteins

NSPs of the flaviviruses play an essential role in its post-entry biology inside the host cell. Most are multifunctional proteins and mediate the replication and translation processes of the virus genome to form new particles (19). NS1, a secreted protein, plays a role early in replication, immune modulation, and immune evasion through the wide range of interactive host proteins (20). NS2A is a small, hydrophobic, transmembrane protein part of the replication complex and inhibits interferon response (21, 22). Recently, the role of the flavivirus NS2A protein is found to be essential in virus assembly (23, 24). NS3 is also a multidomain protein. The N-terminal domain (NS3Pro), combined with NS2B, has the viral serine protease activity. In contrast, the C-terminal part contains the RNA triphosphatase (NS3RTPase) and RNA helicase (NS3Hel) activities involved in capping and viral RNA synthesis, respectively (25, 26). NS4b facilitates the formation of the viral replication complexes and counteracting innate immune responses. It has an overall impact on (i) type I IFN signaling, (ii) RNA interference, (iii) formation of stress granules, and (iv) the unfolded protein response (27, 28). NS5 is the largest and the most conserved viral protein. The N-terminal region of NS5 is a methyltransferase that methylates the N-7 and 2′-O positions of the viral RNA cap structure. In contrast, the C-terminal region has an RNA-dependent RNA polymerase (RdRp) activity (29, 30).

1.4 Genotypes

JE was described in Japan from the 1870s onwards, and the prototype Nakayama strain was isolated from a fatal case in 1935 (31). Since then, the disease spread across Asia to affect most of China and the Asian subcontinent, all of southeast Asia, and the Pacific Rim, reaching northern Australia in 1998 (32). JEV isolates are divided into 5 genotypes based on envelope structural protein genes for phylogenetic reconstruction (33, 34). Historically, JEV genotype (G) GIII virus was the dominant genotype epidemic in Asia. However, JEV GI gradually replaced the GIII viruses and has become dominant in Eastern and Southeastern Asian countries like Japan, Korea, and Vietnam since the 1990s (4). JEV GI originated in Indonesia and circulated in Thailand and Cambodia in the 1970s (4).

1.5 Virus Replication

Many different proteins have been reported to interact with JEV at the cell surface. It enters the host cell by receptor-mediated endocytosis in clathrin-coated vesicles (35). Further acidic pH of the endosome causes structural changes in the E protein resulting in the release of genome into the cytoplasm.

JEV undergoes asymmetric and semi-conservative replication, forming the plus strands about 10–100 folds more than the minus strands through the formation of viral replication complex (RC) (Figure 1.3) (36). During these processes, the (+) ssRNA viral genome acts as a template for (1) the synthesis of the intermediate (−) ssRNA strand, which in turn acts as a template solely for the synthesis of (+) ssRNA genomic RNAs (by the NS5), and (2) the synthesis of the viral polyprotein (37, 38).

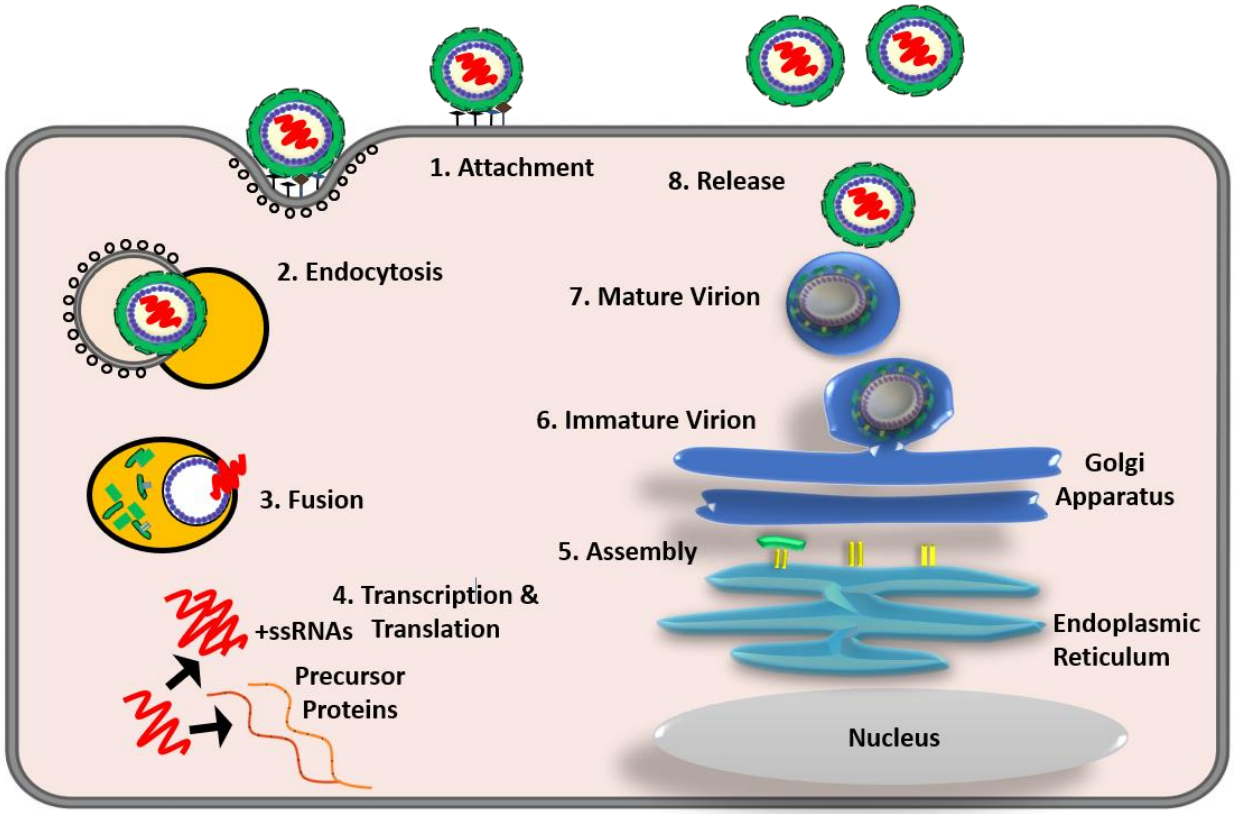

Figure 1.3 JEV replication cycle inside host cell. **1)** Virion surface proteins bind with cell receptors. **2)** Virion enters through clathrin- coated vesicles inside cell. **3)** Fusion between membrane vesicle and early endosome takes place. Virion enters endosome. **4)** Due to low pH the conformation of E protein changes and virion structural proteins get dissemble. Nucleocapsid structure is released out of late endosome. **5)** Genomic RNA is released in cytoplasm. Multiple copies of positive sense RNA are produced through RNA dependent RNA polymerase activity of NS5 and other accessory proteins. Simultaneously, positive sense RNA act as template and viral proteins are also produced. **6)** Viral proteins and RNA strands are carried to Endoplasmic Reticulum (ER) where premature virion assembly takes place. **7)** Newly synthesized virion particle is carried to inside network where protein modification takes place. **8)** Mature virion is carried towards cell membrane in Golgi vesicle. Virus particles are released through exocytosis.

Non-structural proteins (NS3 and NS5), along with host factors, causes the cyclization of viral genome. Double stranded replicative form (dsRF) is formed to ensures the full length viral RNAs synthesis and complementary to the parent strand (11). The additional role of cis-acting RNA elements in viral genome replication have been identified at 3'NCR of JEV with six domains: V, X, I, II-1, II-2, and III in the 5′-to-3′ direction (39). The domains II-2 and III have been reported to be sufficient for replication, but other domains are also required for maximum replication

efficiency. Generally, the cytoplasm is the major site for the presence of JEV RC. RC has been reported to be surrounded by a membrane which protects RC from extensive protease treatment (34).

1.7 Diagnostics

The detection of JE infection from clinical samples can be accomplished by testing serum or cerebrospinal fluid (CSF) to detect virus-specific IgM antibodies. Diagnostic assays available are enzyme-based immunoassays and lateral flow assay-based kits, which target IgM/IgG antibodies. Usually, antibodies against JEV are detectable three to eight days after onset of infection. Confirmatory tests are done by plaque reduction neutralization testing and nucleic acid amplification. Laboratory diagnostic methodologies include virus neutralization, haemagglutination inhibition, complement fixation, ELISA.

1.6 Vaccines and Therapeutics

Multiple vaccines against JEV can be broadly categorized into three types:

1. Inactivated JE vaccines

   The attenuated strain SA-14-14-2 is grown in Vero cells and further formalin inactivated. It is sold as IXIARO in Europe and Americas and as JESPECT in Australia and New Zealand. The Beijing-1 strain of JEV grown in Vero cells is inactivated and sold as JEBIK and ENCEVAC.

2. Live-attenuated JE virus vaccines

   The live-attenuated Chinese vaccine SA-14-14-2 is derived from a virulent strain SA14, isolated from a pool of mosquito larvae. To attenuate SA14, it was passaged more than a hundred times in primary hamster kidney (PHK) cells.

3. Live yellow fever virus (YFV)-JEV chimeric recombinant vaccine.

   Known as Chimerivax-JE, this vaccine was generated by inserting the prM and E genes of attenuated SA-14-14-2 vaccine strain on the cDNA backbone of the yellow fever 17D vaccine strain using reverse genetics.

Apart from vaccine, there are currently no available licensed therapeutic options for the treatment, and supportive care remains the primary treatment option. Although some drugs showed anti-viral properties against JEV *in-vitro* conditions, however, proved ineffective in the clinical setting once symptomatic patients arrived in the hospital. Hence, there is need to understand JEV in context to its neurobiology. Alternatively, identifying a biomarker could be a way forward to develop its therapeutics and/or diagnostics.

1.7 Neuropathogenesis

JEV is of zoonotic importance, which can be both enzootic and epizootic. Pigs are the major reservoir/amplifying host, water birds are carriers and mosquitoes are vectors (40). Humans are the dead end hosts because of the low levels of viremia that are insufficient to infect feeding mosquitoes (32). *Culex tritaeniorhynchus* belonging to the *Culex vishnui* subgroup of mosquitoes are the primary vector for JEV. *Culex gelidus*, *Culex fuscocephala* and *Culex annulirostris* are considered as secondary or regional vectors (40).

The molecular pathogenesis of JEV infection is not well understood. JEV causes neuronal cell death in two ways—direct neuronal killing due to viral multiplication within infected neuronal cells and the other is indirect mode of killing, wherein massive inflammatory response causes an up-regulation of reactive oxygen species and cytokines such TNFα (41). Severe symptoms perhaps start after overreacted-host immune response when JEV enters brain and attack microglial cells

(42). The indirect neuronal cell death during JE is the uncontrolled over activation of microglia cells, which release proinflammatory cytokines such as IL-6, TNFα monocyte chemotactic protein 1 (MCP1), and RANTES (regulated upon activation, normal cell expressed and secreted) (43).

The breaching of blood-brain barrier (BBB) is one of the most distinctive pathophysiologies of JEV. JEV replication has found to be localized mainly at thalami, substantia nigra, basal ganglia, cerebral cortex, cerebellum, and brain stem of clinically infected patients (44, 45). It can infect brain dopaminergic neurons, microvascular endothelial cells, astrocytes, microglia, and pericytes. Neurological complications associated with the critical phase of the illness include encephalopathy movement disorders such as parkinsonism (46, 47). Parkinsonism includes symptoms like tremors, a masked face, microphonia, impaired consciousness, saccadic eye tracking and neck stiffness (48, 49). Apart from JEV, these symptoms are associated with various other enveloped RNA virus infections like WNV and DENV (50, 51).

Neuron-specific proteins in JEV infection is likely to play major role in JEV prognosis in CNS. Recent work has shown that innate immune responses to viral infections in the CNS contribute to neuron-specific injury patterns and susceptibility to viral infection. JEV causes neuronal cell death by direct neuronal killing due to viral multiplication within infected neuronal cells. The other is indirect mode of neuronal damage, wherein massive inflammatory response and cytokine release such as TNFα causes cell damage (52). Severe symptoms may start after overreacted-host immune response when JEV enters the brain and attacks microglial cells (42). The indirect neuronal cell death during JE is the uncontrolled over-activation of microglia cells, which release proinflammatory cytokines.

Researchers have identified a few surface receptors mainly responsible for the entry of JEV into the nerve cells, namely C-type lectin domain family 5 member A, glucose regulated protein 78, caveolin-1, dopamine 2 receptor, toll-like receptors (TLRs), and src protein (53). JEV has been found to utilize dopamine mediated signaling pathways via targeting dopaminergic neurons (54). Dopamine is a primary catecholamine neurotransmitter that regulates a wide range of biological functions such as cognition, endocrine regulation, and voluntary movement. Furthermore, tyrosine hydroxylase (TH) phosphorylation regulates dopamine biosynthesis and converts tyrosine to L-DOPA [82]. Alpha-synuclein (α-syn), is associated with dopaminergic neurons, modulating dopamine homeostasis by reducing TH's phosphorylation state (55). It also binds and influences the activity of dopamine active transporter (DAT) (56-58). The absence of α-syn exerts a considerable impact on dopaminergic system because of reduced striatal dopamine levels and DAT function.

1.8 Alpha-synuclein: neuronal specific protein

Alpha-synuclein (α-syn) is one of the neuronal-specific protein regulating functions associated with the synapse, such as synaptic plasticity, neurotransmitter release, dopamine metabolism, and vesicle trafficking (59). It is extensively expressed in the thalamus, substanti nigra, basal ganglia. It is a protein of 140 amino acid residues with an amphipathic alpha-helix structure similar to apolipoproteins at its N-terminal due to seven 11-mer repeats with a KTKGEV consensus (Figure 1.4) (60). This N-terminal domain (residues 1-60) mediates high-affinity, reversible lipid interactions and functions as a lipid-binding protein (61, 62).

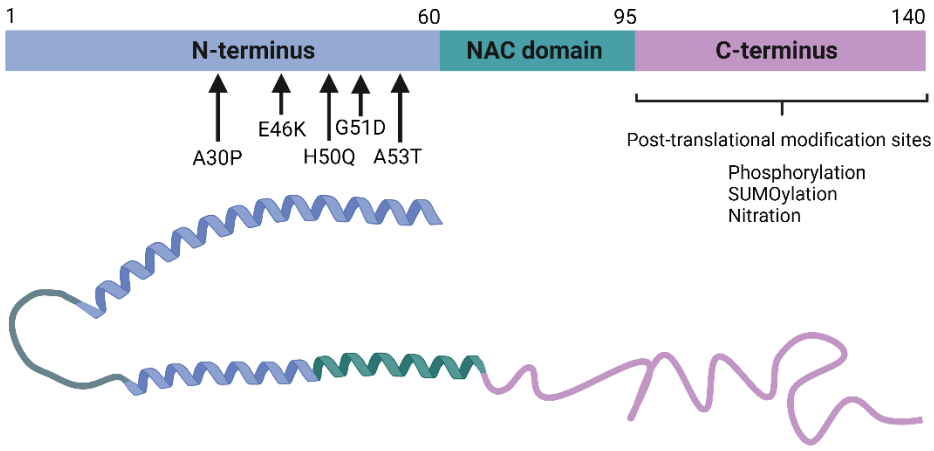

Figure 1.4 Diagrammatic representation of different structural domains of α-syn protein. N-terminal region including NAC domain of the protein forms a broken, amphipathic alpha-helix structure whereas, C-terminal tail remains in flexible and disordered conformation.

It has aggregation-prone central domain (NAC) (residues 61–95) that can form cross β-structures and, therefore is involved in amyloid fibril formation (Figure 1) (63). Different mutations like A30P, E46K, H50Q, G51D and A53T in the N-terminal region have been found to modulate the functions of α-syn, largely by influencing local structural propensity (64-67). The C-terminus of α-syn (residues 96–140) is highly acidic and largely unstructured. α-syn has been responsible for membrane remodeling by inducing membrane curvature and convert large vesicles into highly curved membrane tubules, micelles and vesicles (68, 69). It also inhibits phospholipases D1 and D2 *in vitro* and *in vivo*, and is involved in cleavage of membrane lipids and membrane biogenesis. The c-terminal part is known to be the target of various post-translational modifications like phosphorylation, ubiquitination, and sumoylation and are believed to be responsible for altered binding affinities or interactions with proteins and lipids (70). The aggregation of the α-syn forming intracellular cytoplasmic inclusions (Lewy bodies) in dopaminergic neurons is the histopathologic hallmark of Parkinson's disease (PD).

1.9 Oxidative stress in JEV pathogenesis

Some virulent strains of flaviviruses have established mechanisms to hijack host cell machinery for its replication. Oxidative stress-induced ROS plays a significant role in shaping the cellular milieu to favor JEV propagation. JEV replication induces toxicity by increasing reactive oxygen species (ROS) inside the cytoplasmic neuron body, eventually causing harm to mitochondria and other organelles. In a biological system, ROS, for example, hydrogen peroxide (H_2O_2), superoxide anion ($O_2^{\bullet-}$), hydroxyl radical ($^{\bullet}OH$), and singlet oxygen ($^1O_2$) are oxidants and mediators of cell injury, disease, homeostasis, and signaling activation (71, 72). Cell injury, disease, homeostasis, or signaling alteration increasingly produces reactive oxygen species (ROS), as a byproduct in mitochondria, endoplasmic reticulum (ER), and peroxisome compartments (73, 74). Many continuous cell lines can support the production of JEV, and early studies show that JEV infection produces the toxic oxygen species in neutrophils, ROS intermediates in murine neuroblastoma cells, and superoxide anion and nitric oxide in rat cortical glial cells (75-77). UV-inactivated JEV causes oxidative stress in mouse neuronal N18 cells (78). JEV induces massive inflammatory responses, which upregulates ROS (79). The production of ROS is involved in the oxidative stress-induced apoptosis (43). In the rat model, JEV is able to cause an imbalance of oxidants and antioxidant systems in different brain regions (80). Other than JEV, many other flaviviruses like DENV, WNV, Zika, TBEV virus cause oxidative stress resulting from an imbalance between levels of ROS/oxidants and anti-oxidants (78, 81-86).

In the prognosis of JEV infection, many host factors have been identified as being involved in the various steps of the viral life cycle (74). Previous studies showed that elevated ROS can react to form peroxynitrite, which triggers the loss of ATP and mitochondrial membrane potential. This cascade further leads to the activation of caspase 3, causing neuronal apoptosis (87, 88). In

human astrocytoma and astroglioma cell lines, JEV infection produces ROS and regulates RANTES (89). ROS is also produced due to activation of M1 macrophages (CD11b+CD68+CD64+) which have a predominantly proinflammatory activity (90).

JEV infection of human promonocyte cells downregulates thioredoxin, induces ROS and ASK1-ERK/p38 MAPK signaling, and leads to apoptosis (86). The endogenous (or adaptive) anti-oxidants are enzymatic and non-enzymatic molecules. Many of these enzymatic anti-oxidants (e.g., NAD(P)H: Quinone oxidoreductase 1 [NQO1] peroxiredoxins, heme oxygenase [HO-1], Superoxide dismutase [SOD], catalase, and glutathione peroxidase [GPx]) are modulated by the NRF2 (nuclear factor erythroid 2-related factor 2-) -Keap1 (kelch-like ECH associated protein 1) pathways (91). NRF2 is a transcription factor that regulates the expression of numerous ROS detoxifying and anti-oxidant genes through its binding to the anti-oxidant response element (ARE) (92). Upon cellular oxidative stress, p62 protein also known as sequestosome 1 (SQSTM1) prevents Keap1 from binding to NRF2, thereby up-regulates ARE-associated genes (93). NRF2 has been shown to get stabilized by DJ-1 protein, which is a redox-sensitive and triggers the activation of anti-oxidant genes through NRF2/ARE pathway (94, 95). Knockdown of DJ-1 has suggested decrease in NRF2 as well its dependent proteins NQO1 and HO-1 (94, 96).

Chapter 2. Review and literature

2.1 Alpha-synuclein in viral pathogenesis

Apart from PD more recently, α-syn has been linked to the neurotropic RNA viruses. It exhibits individual and regionally heterogeneous roles that influence the extent of neuroinvasion viruses that specifically target the CNS. To date, various neurotropic viruses are characterized including the members of the families *Picornaviridae*, *Flaviviridae*, *Rhabdoviridae*, *Togaviridae*, *Paramyxoviridae*, *Bunyaviridiae*, and *Coronaviridae* (97). Viruses like Influenza-A (IAV), JEV, WNV, and DENV, are known to induce acute or chronic PD-like symptoms (50, 51). Retrospective cohort studies reported an increased risk of developing PD after infection with hepatitis C and B viruses (HCV and HBV) (98-100). With other viruses such as JEV, WNV, human immunodeficiency virus (HIV) and SARS-CoV-2, the upregulation of α-syn in the brains of infected patients has been observed (101-105). Moreover, experimentally, mice infected with neurotropic IAV virus exhibit α-syn inclusions in dopaminergic neurons, inflammatory processes, and microglial activation (106). Mostly, neuronal expression of α-syn is hypothesized to restrict the replication of RNA viruses (101, 103, 107, 108). In WNV, α-syn has been reported to control the levels of PERK, phosphorylated eIF2α, Ero1L-1α, PDI, and ATF6 expression, all of which are known to support viral replication and contribute to virus-induced apoptosis (101).

Additionally, the α-syn-mediated chemotaxis of protective immune cells in response to WNV infection has been described (108, 109). α-syn is also involved in the activation of microglial cells and monocytes (110). A study revealed that the fibril form of α-syn participates in the inflammasome activation to release mature form of IL-1β. Through similar pathways, the indirect role of α-syn has been shown to play in SARS-CoV-2 infection (107). However, the potential

relationship between the neuro-protective properties of α-syn and its aggregation, specifically concerning the elevated expression and inflammatory response, is a topic of debate that requires more fundamental research.

2.2 Alpha-synuclein mediated modulation of oxidative stress

The aggregated α-syn has been reported to induce toxicity by increasing ROS inside cytoplasmic body of the neuron, eventually causing harm to mitochondria and other cellular organelles (111, 112). The behavior or function of α-syn seems to differ based on cell type, its mutational status (wild type or mutated), and the conformation of the protein (aggregated or non-aggregated). Several studies have demonstrated a relationship between mutated and aggregated α-syn and oxidative stress, leading to neurotoxicity and its involvement in neurodegenerative diseases. However, besides the well-documented neurodegenerative activity of α-syn, the role of monomeric and wild-type α-syn is neuroprotective in many studies (113).

The loss of normal function of α-syn has been reported to cause accumulation of dopamine leading to oxidative damage. Increased free cytosolic dopamine readily auto-oxidizes to ROS as well as the highly reactive dopamine quinone, ultimately changing the cellular redox environment that inhibits the electron transport chain (114). This process further leads to oxidative stress by opening the mitochondrial permeability pore. In a separate study, wild-type α-syn was reported to block rotenone- and maneb-induced ROS production and cell toxicity. In contrast, the mutated versions of α-syn, such as A30P, A53T, and E46K, aggravated ROS production induced by rotenone and maneb (115). Moreover, administration of aggregated wild-type α-syn in microglial cells showed a dose-dependent increase in ROS production, whereas non-aggregated α-syn had no significant modulation of ROS (116). Thus, the ability of α-syn to induce ROS appears to depend on the protein's conformational form. Viruses like JEV, WNV, and DENV utilize oxidative stress-

induced ROS in shaping the cellular milieu to favor viral propagation (73). Various anti-oxidative proteins like glutathione S-transferase, NADPH-oxidase, NF-κB, superoxide dismutase 1 (SOD1), DJ-1, SQSTM1, and thioredoxin are reported to get manipulated differentially by most of the members of family *flaviviridae* (83, 85, 86, 117-119).

α-syn has been reported to directly interact with supercoiled DNA and RNA-interacting proteins to regulate specific gene expression (120). Probably due to this gene transcriptional activity, α-syn has been reported to increase the expression of anti-oxidative proteins like SOD1 in SH-SY5Y cells through unknown mechanisms and significantly attenuate rotenone-induced cell apoptosis (121). SOD1 is known to convert the superoxide radical into hydrogen peroxide and molecular oxygen through redox reactions. Other than JEV, the role of α-syn in directly influencing the anti-oxidative pathway in response to viral infections is not identified in any viral infection. Hence, more research is needed to explore the anti-oxidative potential of α-syn regulating viral infections.

2.3 Role of pyrazole based derivatives in modulating oxidative stress

Pyrazole is an important five-membered heterocyclic compound containing two nitrogen atoms. This heterocyclic ring is integral to the wide range of biopharmaceutical properties like antianxiety, anti-inflammatory, antipsychotic, anticancer, anti-obesity, analgesic, antipyretic etc. (122-124). By virtue of its prominent biological properties and therapeutic applications, its scaffold has attracted many researchers to synthesize derivatives for the advancement of potent drug molecules (125-127). Its antiviral activities have been reported for HIV, herpes simplex virus (HSV-1 and HSV-2), and varicella-zoster virus (VZV) (128, 129). Some pyrazole-based compounds with anti-West Nile virus activity have been reported but with inappropriate EC_{50} values (130).

In previous studies, the anti-oxidative properties of pyrazole has been explored where it has been shown to increase both nuclear NRF2 proteins and NRF2-ARE binding activity, suggesting their role in ROS scavenging (131, 132). Pyrazole has been shown to attenuate cisplatin-induced nephrotoxicity by increasing GPx, glutathione (GSH) and diminishing lipid peroxidation (LPO). Another derivative, 6-sulfonamido-pyrano[2,3-c]-pyrazole–based RalA inhibitors, increased SQSTM1 against hepatocellular carcinoma (133). Recently, a hybrid scaffold in which 3-naphthyl pyrazole was substituted with pyrazoline/isoxazoline ring at position 3 derivatives of 3-(2-naphthyl)-1-phenyl-1H-pyrazole showed significant radical scavenging activity (RSA) *in vitro* (134).

Since, JEV tends to modulate oxidative stress to enhance its replication, the role of pyrazole against its infection could be explored. The pyrazole derivatives with direct radical scavenging properties or modulating anti-oxidative enzymes like SOD1, catalase, GPx, GST could be targeted for antiviral therapeutics.

2.4 Aim and scope of current research

Prior studies have highlighted the antiviral potential of α-syn in other related neurotropic viruses although the exact mechanism is poorly understood. In relation to JEV, clinical patients showing PD-like symptoms are hypothesized to be due to non-functional or damaged dopamine transporter (DAT) protein. Also, overexpression of α-syn is reported in the brains of JEV-infected patients. Recently, evidence has been provided that the JEV exploits dopamine signaling and modulates its level to facilitate viral infection. Moreover, the dopamine D2 receptor (D2R) is utilized to enhance viral entry by activating phospholipase C (PLC) signaling cascades (135). Both, dopamine level and D2R activity depend upon α-syn and is therefore of critical importance to maintain synaptic homeostasis (136).

Thus, our initial study was to understand if α-syn promotes or inhibits JEV replication in neuronal cells. In our research, we focused on exploring the anti-oxidative potential of α-syn, which may modulate JEV replication. Through literature review, we have understood that α-syn alters ROS level which is requisite for JEV replication. JEV is able to cause an imbalance of oxidants and antioxidant systems in different brain regions and utilizes oxidative stressed homeostasis to enhance its replication.

Secondly, we wanted to resolve if there is any pathological effect of increased expression of α-syn by host cell, in response of JEV infection. In a healthy brain, most α-syn is unphosphorylated; however, more than 90% of abnormally aggregated α-syn in Lewy bodies of patients with PD is phosphorylated at Ser129, which is presumed to be of pathological significance. It is known that phosphorylation of α-syn at Ser129 is mediated by several kinases such as G-protein-coupled receptor kinases (GRKs), casein kinase II, polo-like kinases (137). However, none of the research highlighted the modulation or the impact of phosphorylated α-syn or its aggregation in JEV pathogenesis. Hence, we wanted to evaluate the modulation of different kinases in the presence of JEV replication at different time points and to understand if there is α-syn oligomerization.

The lack of anti-JEV therapeutics to treat critically ill patients have been the reason of mortalities among symptomatic cases. Several potential anti-oxidative compounds like minocycline, arctigenin, fenofibrate, and curcumin have been explored for anti-JEV activities, but only minocycline and ribavirin have been tested by randomized clinical trials (138-141). However, the treatment with both the drugs showed no statistically significant differences in the mortality rate as compared to placebo-treated controls (138-141). Pyazole derivatives have been explored with a wide range of applications in agriculture, pharmaceuticals, synthetics, etc. Its antiviral

activities have been reported for HIV, HSV-1 and HSV-2 and varicella-zoster virus (VZV) (128). Some pyrazole-based compounds with anti-WNV activity have been reported but with inappropriate EC_{50} values (142). The anti-JEV property of pyrazole or its derivatives has not been explored. Therefore, we have tried to explore the anti-oxidative potential of pyrazole derivatives against JEV *in vitro* and *in vivo*.

Overall, the present thesis research intends to understand the role of α-syn in JEV replication: including the mechanism, phosphorylation and its oligomerization. We also focused on utilizing the same mechanism to design anti-JEV therapeutic candidates and characterize it *in vitro* and *in vivo* systems. The current study will be a step ahead to uncover the role of neuronal-specific proteins and local cellular homeostasis to develop therapeutics against JEV.

2.5 Objectives

Based on our research focus, the following objectives were framed;

1. Understanding the role of α-syn in JEV replication
2. Understanding the effects of JEV replication on phosphorylation and oligomerization of α-syn
3. Designing and assessment of pyrazole derivatives against JEV infection.

Chapter 3. Understanding the role of α-syn in JEV replication

3.1 Abstract

JEV stands as a prominent vector-borne zoonotic pathogen, displaying neurotropism and eliciting PD-like symptoms among most symptomatic survivors. The characteristic feature of PD is aggregation of mutated α-syn which contributes to the loss of dopaminergic neurons. Having a potential link between JEV-induced PD-like symptoms and α-syn pathogenesis, we explored the supportive or inhibitory role of α-syn in JEV infectivity within neuronal cells. Our investigation revealed a significant increase in endogenous α-syn expression during JEV replication. Additionally, treatment with exogenous α-syn (Exoα-syn) protein substantially reduced JEV replication, suggesting its anti-JEV effect. Furthermore, the findings indicated a non-significant role of α-syn in inhibiting JEV entry inside cells or directly disrupting JEV virions. We delved into α-syn's role in modulation of host intracellular proteins implicated in oxidative stress mechanisms. Treatment with Exoα-syn post JEV infection led to the upregulation of superoxide dismutase 1 (SOD1). Flow cytometry analyses unveiled a reduction in reactive oxygen species (ROS) upon Exoα-syn treatment in JEV-infected cells. The results were validated via endogenous α-syn-knockdown, which decreased SOD1 and raised ROS, similar to SOD1 inhibition via LCS-1, which also intensified ROS and JEV infection. Overall, our results suggest that α-syn exerts an anti-JEV effect by regulating proteins involved in oxidative stress inside neuronal cells. This study contributes valuable insights into the interplay between α-syn and JEV, shedding light on avenues to study further the potential role of α-syn aggregation in JEV pathogenesis.

3.2 Introduction

Japanese encephalitis (JE) is the most serious infectious disease of the central nervous system (1, 2, 6, 7). Approximately 15% of JE patients die during the acute phase of the illness, and most survivors present with neurological aftereffects, including striatal dysfunction (143, 144). JEV replication has found to be localized mainly at thalami, substantia nigra, basal ganglia, cerebral cortex, cerebellum and brain stem in clinically infected JE patients (44, 45). Neurological complications associated with the critical phase of the illness include encephalopathy, movement disorders such as parkinsonism (46, 47). Parkinsonism include symptoms like tremors, a masked face, microphonia, impaired consciousness, saccadic eye tracking, neck stiffness (48, 49). Apart from JEV, these symptoms are associated with various other enveloped RNA virus infections like WNV and DENV (50, 51). Neuron-specific proteins in JEV infection is likely to play major role in JEV prognosis in CNS. Recent work has shown that innate immune responses to viral infections in the CNS contribute to neuron-specific injury patterns and susceptibility to viral infection. However, expression of a neuron-specific restriction factor for viral infections has not been described much.

The role of α-syn is explored much in terms of PD. In most of the Parkinson clinical patients, missense mutations in the α-syn gene (A30P, E46K, A53T) are likely to cause aggregation of these mutated α-syn proteins and formation of LBs into the cytoplasm (145). These aggregated α-syn induce toxicity by increasing ROS inside cytoplasmic neuron body, eventually causing harm to mitochondria and other organelles (111, 112). ROS are oxidants and mediators of cell injury, disease, homeostasis, killing of phagocytosed pathogens, and signaling activation in a biological system. The function of normal or monomeric α-syn is not inspected in much detail as of mutated ones.

Contrary to PD, α-syn plays a role in neuroprotective functions. α-syn is somewhere found to be important in pathogen-activated immune responses and lymphocyte maturation (146). In microglia cells, monomeric α-syn increases Th1 and Th2 cytokine expressions (147). Moreover, α-syn has been reported to directly interact with supercoiled DNA and RNA-interacting proteins to regulate specific gene expression (120). In some studies, nuclear translocation of α-syn is found important in modulating DNA repair (148). These data suggest that α-syn may play a pivotal role in pathophysiological responses involved in inflammatory disease to invading pathogens.

Besides these reports, the role of α-syn in viral pathogenesis has not been fully characterized. Recently, evidence has been provided stating the JEV exploits dopamine signaling and modulates its level to facilitate viral infection. As well as D2R is also utilized to enhance viral entry by activating PLC signaling cascade (135). Both dopamine level and D2R activity are dependent upon α-syn and are therefore of critical importance to maintain synaptic homeostasis (136).

This study aims to explore α-syn's multifaceted potential roles in JEV pathogenesis. We have carried out *in vitro* studies in mouse neuronal cells. Apart from analyzing the effect of JEV progression on endogenous α-syn, we have used exogenous Exoα-syn to explore its probable mechanism in JEV pathogenesis.

3.3 Material and Methods

3.3.1 Cells and viruses

The JEV stock preparation, along with all the plaque assays were carried out in Baby hamster kidney cells (BHK-21). We used JEV strain SA14-14-2 and mouse neuronal cells (Neuro2a) for all *in vitro* experiments. Both, BHK-21 and Neuro2a cells were maintained in Dulbecco's modified eagle medium (DMEM) medium containing 1X penicillin streptomycin

antibiotic and 10% fetal bovine serum (FBS) in 5% CO_2 at 37 °C. The JEV strain SA14-14-2 (GenBank accession number JN604986) was obtained from the Department of health and family welfare, Government of Assam, India. For stock preparation, BHK-21 cells at 80% confluency in T75 flasks were infected with JEV at MOI 0.1 in DMEM without FBS. After 2 h of virus adsorption, infection media was removed and replaced with DMEM media containing 2% FBS post washing cells once with phosphate buffer saline (PBS). The T75 flask was incubated for 72 h. Thereafter, cells were lysed by multiple freeze thaw cycles and clear lysate was collected after centrifugation. The lysates were in -80 °C after aliquoting it in 1.5ml microcentrifuge tubes.

3.3.2 Expression and Purification of Exoα-syn protein

Exogenous alpha-synuclein (Exoα-syn) protein was expressed in *E. coli* BL21(DE3) expression system. The pET21a-alpha-synuclein was obtained from Michael J Fox Foundation MJFF (Addgene plasmid # 51486) as a kind gift. Briefly, the plasmid was transformed into *E. coli* BL21(DE3) cells. The recombinant cells were grown up to an OD_{600} = 0.6 in Luria-Bertani broth enriched with 100 µg/ml ampicillin at 37 °C and 150 rpm shaking. The culture was induced using 1 mM IPTG and further grown for 15 h at 25 °C. The cell suspension was pelleted at 7000 rpm for 5 min and resuspended in 100 ml Buffer A (20 mM Tris-Cl, 5 mM EDTA, pH 8.0) containing 1 mM PMSF. The cells were sonicated for 45 min with 8 s 'ON' and 22 s 'OFF' cycle at 33% amplitude. The sonicated sample was boiled for 10 min at 95 °C, afterwards, the insoluble white precipitate was pelleted at 20,000 g for 1 h. The clear supernatant was passed through a 0.45 µm filter before further purifying using chromatographic methods as described elsewhere (149).

3.3.3 Characterization of Exoα-syn protein

The purified protein was characterized using an SDS PAGE. The molecular weight of the purified protein was determined using MALDI-TOF mass spectrometry on a Bruker Autoflex

Speed MALDI-TOF-TOF mass spectrometer using α-cyano-4-hydroxycinnamic acid matrix. The Dynamic Light Scattering (DLS) measurements of the freshly purified Exoα-syn were performed using a Malvern Zetasizer NANO-ZS DLS instrument. The DLS measurements were performed at room temperature using a 173° backscattering angle and analyzed using the Zetasizer software version 7.11.

3.3.4 Time course analyses of α-syn expression

Neuro2a cells were seeded in 6-well plate at a density of 2×10^6 cells/well in DMEM supplemented with 10% FBS. Post 12 h incubation, cells were washed by PBS followed by addition of 500 µl diluted JEV stock at 0.1 MOI per well. Mock-infected cells received plain DMEM 500 µl per well. The cells were collected post 12, 24, 36, 48, 60, 72, 96 h of incubation and processed for RNA isolation and protein lysate preparation.

3.3.5 *In vitro* anti-JEV activity

The Neuro2a cells were seeded in 6-well plate at a density of 2×10^6 cells per well. For co-treatment, JEV infection media at 0.01 MOI was incubated with Exoα-syn at three different concentration of 0.25, 0.5 and 1 µM for half an hour in three separate 1.5 ml tubes. One more tube was added with JEV without Exoα-syn. Total volume of each tube was kept around 500 µl only. Following incubation, infection medium was added on top of cells and kept for 2 h for adsorption. The infection media was removed, and fresh 2ml of DMEM with 2% FBS was added in each well. For post-treatment, Exoα-syn was added after 2 h of JEV adsorption. Whereas for pre-treatment, Exoα-syn was added 6 h before JEV infection. Cells and supernatant from differentially treated (CON, JEV, JEV along with 0.25, 0.5, 1 µM of Exoα-syn) samples were collected at 72 h time point. Virus titration was done via viral RNA and JEV NS1 protein detection through real-time

and western blot analyses, respectively. Also, plaque assay was performed using supernatant of each samples for viral particle quantification.

3.3.6 Small Unilaminar Vesicles (SUV) preparation

1-palmitoyl-2-oleoyl-sn-glycero-3-phosphocholine (POPC), 1-palmitoyl-2-oleoyl-sn-glycero-3-phospho-L-serine sodium salt (POPS), 1-palmitoyl-2-oleoyl-sn-glycero-3-phosphoethanolamine (POPE), and sphingomyelin (SM) were from Avanti Polar Lipids, Inc. The lipids POPC:POPS:POPE:SM in the molar ratio 57:25:3:15 were aliquoted into a clean glass tube. As described elsewhere, a lipid thin film was prepared by slowly swirling the lipids in the glass tube under a stream of nitrogen gas (150). Further, the lipid thin film was left to dry overnight in a desiccator. The next day, the lipid thin film was hydrated using 1 mL of PBS for six hours. The hydration was followed by vigorous vortexing and five freeze-thaw cycles in an ice bucket and warm water bath. Later, the suspension was kept at room temperature to equilibrate and sonicated in a water bath sonicator until the solution cleared out to form SUVs. The SUVs prepared were analyzed using DLS.

3.3.7 Circular Dichroism (CD) analyses

Circular dichroism spectroscopic characterization of Exoα-syn in PB (25 mM phosphate buffer, pH 7.5.) was made using the J-1500 Jasco CD spectropolarimeter. A far UV CD spectrum was recorded with eight accumulations from 300 nm up to 190 nm with 0.1 nm data pitch, 1 nm bandwidth, 2 sec D.I.T., and a 100 nm/min scan speed. The CD spectra were smoothened 25 points using the second polynomial function of the Savitzky-Golay algorithm. The protein lipid-interaction studies were carried out with 2 μM Exoα-syn at Exoα-syn:SUV (1:200) molar ratio and analyzed under CD.

3.3.8 Calcein entrapped vesicle preparation

The lipid film was prepared in the same composition as above in a clean glass tube and hydrated using 80 mM calcein solution in PB, pH 7.4. The calcein entrapped SUVs were prepared as described above and cleared through a HiTrap PD10 desalting column in PB. The early fractions containing calcein entrapped SUVs were collected and characterized with DLS and used for calcein release assay. The fluorescence was recorded for 600 s in a Jasco FP-8500 spectrofluorometer. The protein lipid-interaction studies were carried out with 0.5 μM Exoα-syn at Exoα-syn:calcein SUVs (1:10), Exoα-syn:calcein SUVs (1:25) and Exoα-syn:calcein SUVs (1:50) molar ratio. Triton X- 100 (1%v/v) was used a positive control.

3.3.9 Overexpression and knockdown of α-syn

Plasmid pHM6-alphasynuclein-WT which was a kind gift from David Rubinsztein (Addgene plasmid # 40824) was used for the overexpression of α-syn in neuro2a cells (151). The neuro2a cells were seeded in four 35 mm cell culture petri dishes at a density of 2×10^6 cells per dish. Cells from two dishes were transfected with 2μg of plasmid using Lipofectamine 3000 (Invitrogen, USA) following the manufacturer's protocol. After 12 h, cells transfected with plasmid and untransfected cells were infected with 0.1MOI JEV. Post 72 h of incubation, supernatant and whole cell lysate were collected for plaque and protein estimation. The knockdown of endogenous α-syn was carried out via combined transfection of two siRNAs at total 75 picomole concentration. The following sequence of siRNAs sense strands -CUAAGUGACUACCACUUAU[dT][dT] and CACAGGAAGGAAUCCUGGA[dT][dT] (Merck, Germany), targeted two different exons of α-syn. The transfection reagent Lipofectamine RNAiMAX (Invitrogen, USA) was used following manufacturer’s protocol, along with siRNA universal negative control #1 (SIC001, Sigma-

Aldrich, Germany) as negative control (-ve siRNA). The knockdown of α-syn was estimated post 24 h of transfection by real-time analyses and western blotting.

3.3.10 Overexpression and endogenous silencing of SOD1

For overexpression studies, the gene encoding mouse SOD1 protein was amplified from neuro2a cells and cloned into a c-flag pcDNA3 vector (#20011, Addgene), flanking XbaI and BamHI restriction sites. The expression was confirmed using SOD1-specific antibody post-transfection in neuro2a cells. The silencing of endogenous SOD1 was carried out via transfection of siRNA of the following sequences: AUCCUCACUCUAAGAAACA [dT][dT] and GGUGGAAAUGAAGAAAGUAC [dT] [dT] (Eurogentec, Belgium). The knockdown of SOD1 was estimated by western blotting after 24 h of transfection using RNAiMAX reagent (Invitrogen, USA).

3.3.11 Gene expression and viral particle estimation

Total RNA was isolated using RNAiso reagent (Takara, Japan) and converted into cDNA using iScript™ cDNA Synthesis Kit (Biorad, USA). Real-time PCR analysis was carried out in system QuantStudio5 (Applied Biosystems, USA) using Power-up SYBR master mix (Invitrogen, USA). GAPDH was used as an internal control and values are represented as mean fold change with respect to cell control (CON). Protein estimation were carried out using SDS-PAGE and western blotting. Western blotting was performed using antibodies specific to JEV nonstructural protein 1 (NS1) (GTX633820, GeneTex, USA), α-syn (32-8100, Invitrogen, USA), SOD1 (A0274, Abclonal, USA), and DJ-1(5933), SQSTM1 (39749), and NQO1 (62262) from CST, USA. The β-actin (MA1-91399, Invitrogen, USA) or GAPDH (MA1-16757, Invitrogen, USA) were used as a loading control for all the experiments. The relative quantification was done using ImageJ

software. For JEV particle quantification, plaque assay was performed in BHK-21 cells using standard protocol (152).

3.3.12 ROS estimation

For all flow cytometry studies, neuro2a cells were seeded at 2×10^6 cells/well density in 6-well plate and incubated for 12 h at 37 °C, 5% CO_2 incubator. ROS was estimated in JEV-infected and mock-infected cells at 24, 48, 72, and 96 h time points. Briefly, 0.1 MOI JEV was added in 4 wells and equal number of wells were kept as controls. The cells were detached every 24 h post-infection, resuspended in 500 µl PBS containing 10 µM of 2′,7′-dichlorodihydrofluorescin diacetate (DCFH-DA) dye, and incubated for 30 min at 37 °C. The stained cells were analyzed using flow cytometry (BC, CytoFlex S Analyser). FITC filter channel was used to record the emission of DCFH-DA dye. Flow cytometry analysis was done post-treatment with compounds; H_2O_2, ascorbic acid, Exoα-syn, and LCS-1 at different time intervals and concentrations. Ascorbic acid and Exoα-syn treatment were given 12 h before flow cytometry at 0.2 and 1 µM concentrations, respectively. Cells were treated with 500 µM of H_2O_2 for 6 h, whereas for LCS-1, ROS was estimated after 6 and 12 h of treatment with 5 µM of LCS-1.

3.3.13 Statistical analysis

The data presented in the results are the average of three independent experiments. Significance values were calculated through two-tailed analyses using Student's t-test in Microsoft Excel. Asterisk marks; ** represent a p-value < 0.01, while * represents a p-value < 0.05.

3.4 Results

3.4.1 Modulation of α-syn post JEV infection in neuronal cells

Time course analysis of α-syn expression upon JEV infection was carried out in neuro2a cells for 96 h. The mRNA estimation using real-time PCR indicated gradual increase in α-syn from 24 h till 60th h. The maximum ~3.7-fold change, with respect to the mock-infected neuro2a cells, was obtained at 60th h. Thereafter, with the rapid increase of JEV E RNA, α-syn mRNA decreased to ~2.4-fold level (Figure 3.1 [A, B]).

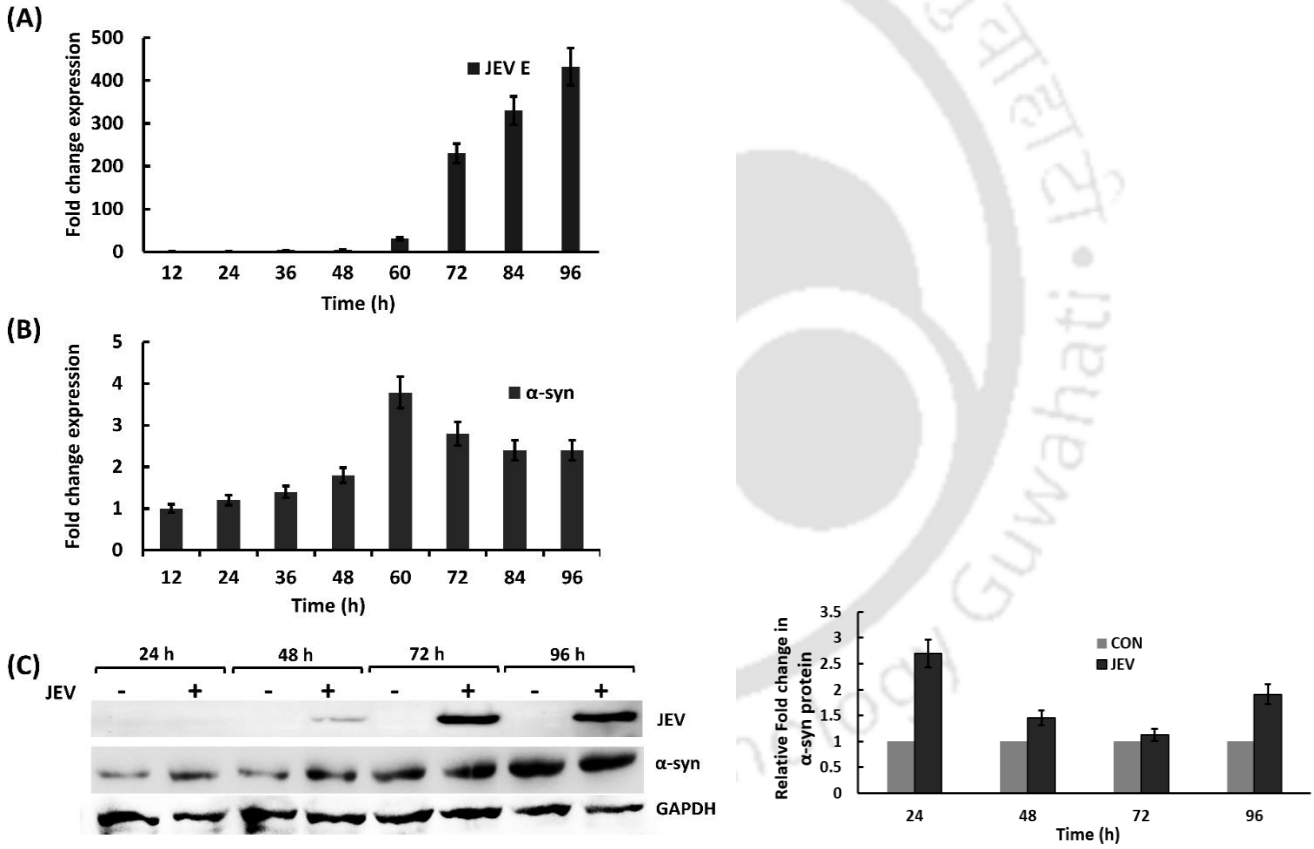

Figure 3.1 Quantification of endogenous α-syn in neuro2a cells. Real-time PCR analysis of JEV E RNA at 12 h interval till 96 h post-infected with 0.1 MOI JEV (A). Fold change expression of α-syn in JEV-infected neuro2a cells compared to mock-infected cells till 96 h where GAPDH is used as a control (B). Fold change is calculated keeping mock-infected cells as control. Western blot along with densitometric analysis of α-syn protein in JEV-infected neuro2a cells compared to mock-infected cells till 96 h (C).

At the protein level, a gradual increase in α-syn was observed with time in both mock-infected and JEV-infected cells. However, with respect to mock-infected neuro2a, there was significant upregulation of α-syn in JEV-infected cells at all the time points (Figure 3.1 C).

3.4.2 α-syn inhibits JEV replication

The purified Exoα-syn was characterized before proceeding towards experiments. The anion exchange-purified chromatogram of Exoα-syn showed elution around 55 min on a gel filtration column (Figure 3.2 A). The different 55 min fractions were run on 12% SDS PAGE that showed ~15 kDa protein band (Figure 3.2 B). The MALDI-TOF mass spectrum showed peaks at 7233.25 and 14,476.18 m/z values (Figure 3.2 C).

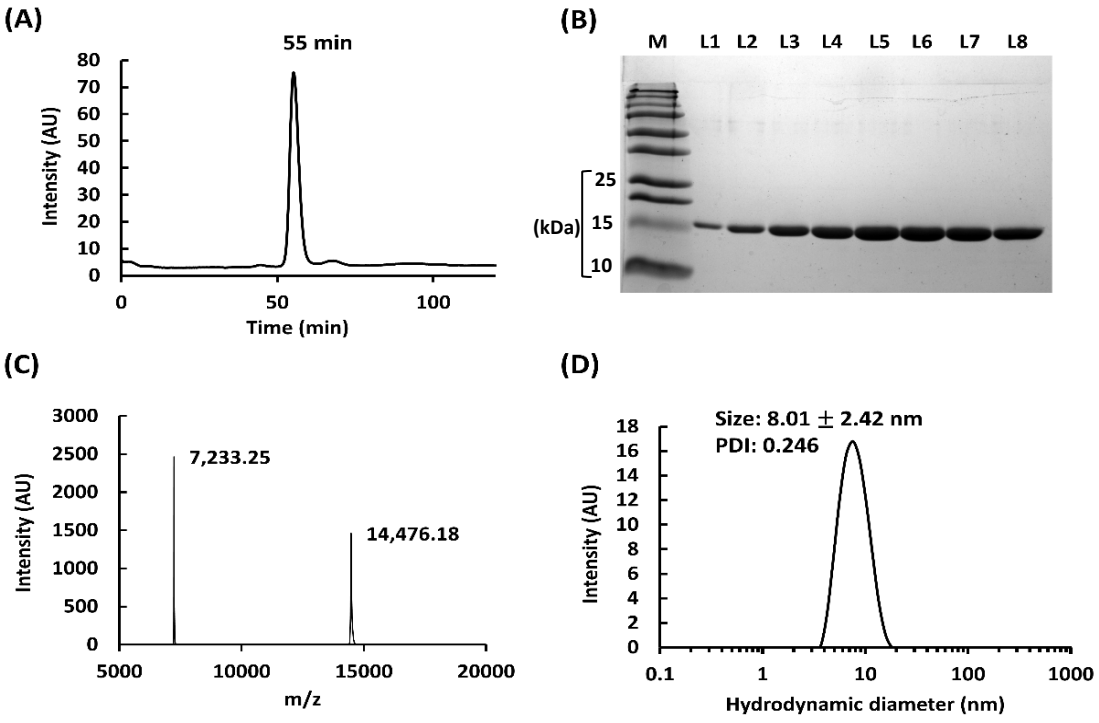

Figure 3.2 Characterization of purified Exoα-syn. The SEC profile of the anion exchange-purified αS (A). A 12% SDS-PAGE of Exoα-syn SEC fractions. The BioRad Precision Plus Protein™ ladder marked as M. The SEC fractions were loaded in L1-L8 (B). MALDI-TOF mass spectrometric analyses of Exoα-syn protein. Expected monoisotopic mass: 14,451.22 Da, observed

m/z: 14,476.18. Doubly-charged species is seen at m/z 7,233.25 (C). DLS profile of the freshly prepared Exoα-syn protein (D).

The peak at 14,476.18 corresponds to the $[M + Na]^+$ adduct of Exoα-syn whereas the smaller m/z value corresponds to the doubly-charged Exoα-syn. DLS analysis revealed a single peak with mean hydrodynamic diameter of 8.01 nm with PDI of 0.246, indicating a monodispersed protein preparation (Figure 3.2 D). This hydrodynamic diameter is comparable to those reported in the literature for monomeric α-syn (153, 154). To analyze the role of Exoα-syn in JEV replication, differential treatment of neuro2a cells was carried out with Exoα-syn along with JEV infection. Significant downregulation of NS1-specific RNA was observed in pre- and post-α-syn treatment. In pre-treatment, the vRNA gradually decreased with an increase in α-syn concentration (Figure 3.3 A).

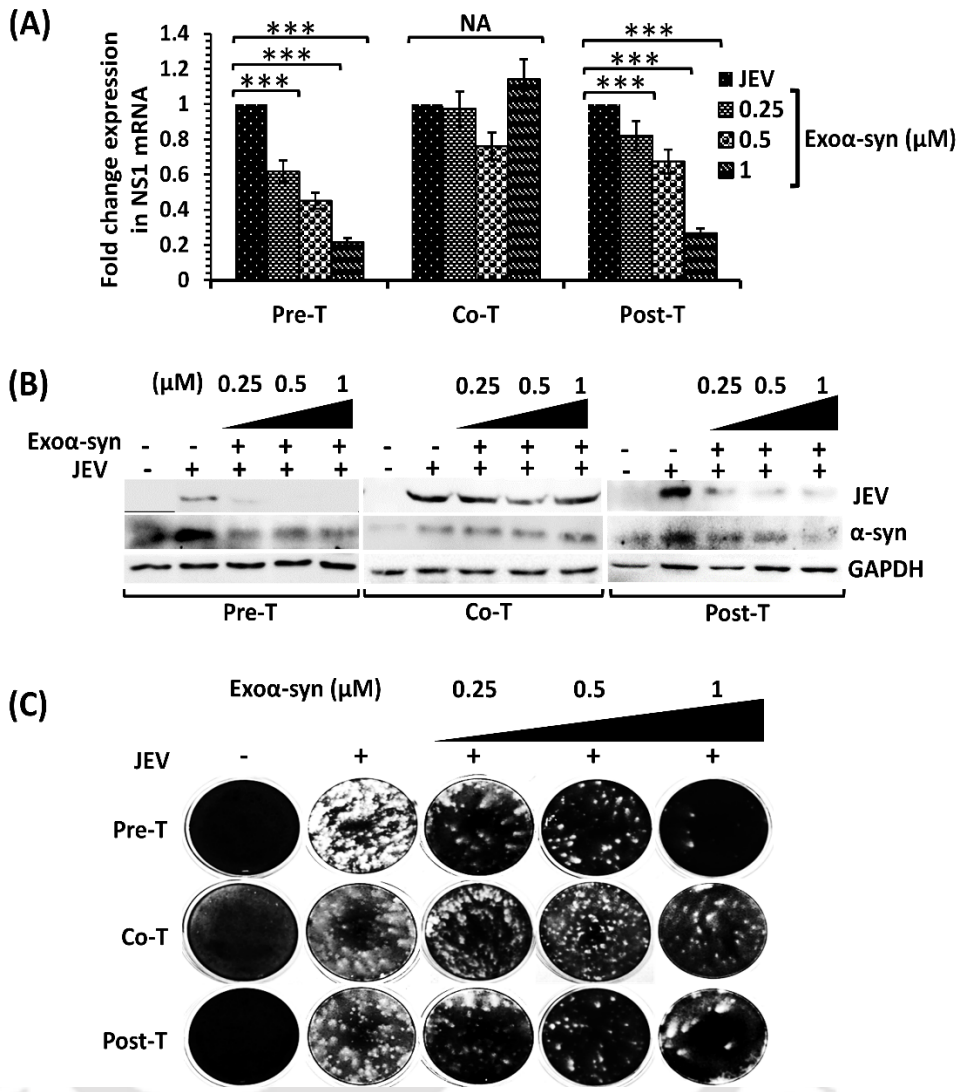

Figure 3.3 Modulation of JEV in neuro2a cells after co-treatment, pre-treatment, and post-treatment of Exoα-syn at 0.25, 0.5, and 1 μM concentrations. JEV vRNA quantification after 72 h of infection in differentially-treated cells. Fold change is calculated with respect to uninfected cells as control (A). Western blot analysis to quantify the viral protein after 72 h of JEV infection in cells differentially treated with Exoα-syn (B). Virus titration of supernatant collected after 72 h of JEV-infected cells differentially-treated with Exoα-syn protein (C).

Treatment with 1 μM α-syn caused around 80% reduction in the NS1 vRNA level. Similar results were obtained for the post-treatment samples as well. Around 75% reduction in the vRNA level was observed at 1 μM α-syn concentration. Inhibition in pre-treatment was slightly better than post-treatment. In co-treatment, no significant difference in viral vRNA levels was observed

at any Exoα-syn concentration. The cellular protein estimation indicated the similar trend as observed in gene expression studies. Upon α-syn pre-treatment (0.25 µM α-syn), JEV protein amount reduced to about 84% compared to untreated JEV infected control.

In post-treatment samples, JEV protein amount got reduced to 69-91% compared to infected control. Endogenous α-syn expression also seems to get regulated with JEV replication. The JEV-infected control exhibited the highest α-syn expression, whereas cells with lower JEV replication displayed reduced α-syn levels both in pre- and post-treatment samples (Figure 3.3 B). In co-treatment, uniform JEV replication across differentially treated cells resulted in consistent endogenous α-syn expression. In plaque assay, more than 60 % decrease in JEV titer were observed in 0.25 µM of Exoα-syn pre- and post-treated cells. In 1 µM of Exoα-syn treatment, more than 85 % decrease in JEV titer was observed. In co-treatment, about 42% decrease in JEV titer was observed only at 1 µM of Exoα-syn treatment (Figure 3.3 C).

As α-syn is known to bind lipid vesicles, its interaction with SUVs made up of lipids that constitute viral lipid bilayer was investigated. The diameters of plain and calcein-loaded SUVs, as determined by DLS, were around 32 nm and 55 nm, respectively (Figure 3.4 A). Circular dichroism spectrum of Exoα-syn in the absence of SUVs suggest a random coil conformation, as is expected for a monomeric α-syn. In the presence of SUVs, on the other hand, the protein folds to take up an α-helical conformation (Figure 3.4 B).

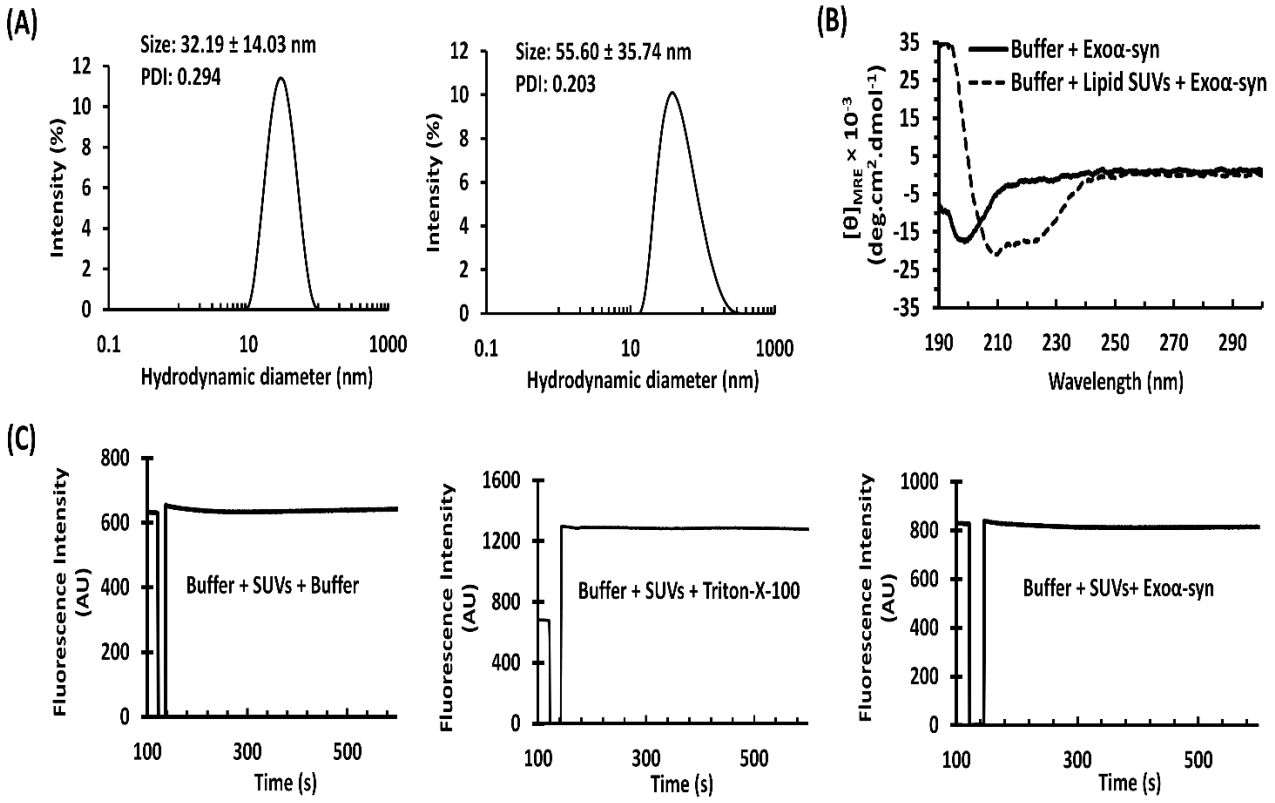

Figure 3.4 Characterization of liposomes (SUVs) and interaction with Exoα-syn protein. Graphs representing DLS size distribution profile of the plain and calcein-loaded SUVs (A). Circular dichroism spectra of Exoα-syn (2 μM) in phosphate buffer and in the presence of SUVs at protein:lipid ratio of 1:200 (B). Graphs representing fluorescence intensities of calcein-loaded SUVs in buffer, in the presence of Triton X-100 (1% v/v), and with Exoα-syn at 1:50 protein:lipid ratio (C).

Disruption of lipid vesicles upon Exoα-syn binding, if any, was investigated through calcein release assay. Calcein was loaded in the SUVs at self-quenching concentration. An increase in fluorescence intensity upon α-syn addition would imply membrane disruption. The extent of fluorescence is directly proportional to the extent of vesicle disruption. Treatment of calcein-loaded SUVs with Exoα-syn did not cause any appreciable enhancement in calcein fluorescence (Figure 3.4 C) suggesting that binding of Exoα-syn to SUVs does not disrupt them. The results obtained were in consonance with *in vitro* co-treatment study.

3.4.3 Effect of overexpression and silencing of α-syn on JEV replication

The overexpression study was carried out by transfecting neuro2a cells with plasmids encoding wild type α-syn and GFP, separately. Cellular protein analysis revealed about 68% reduction in JEV protein in α-syn overexpressing cells than GFP control. Concurrently, about 61% lower JEV titer was observed in α-syn overexpressing cells than JEV infected cells expressing GFP (Figure 3.5 A).

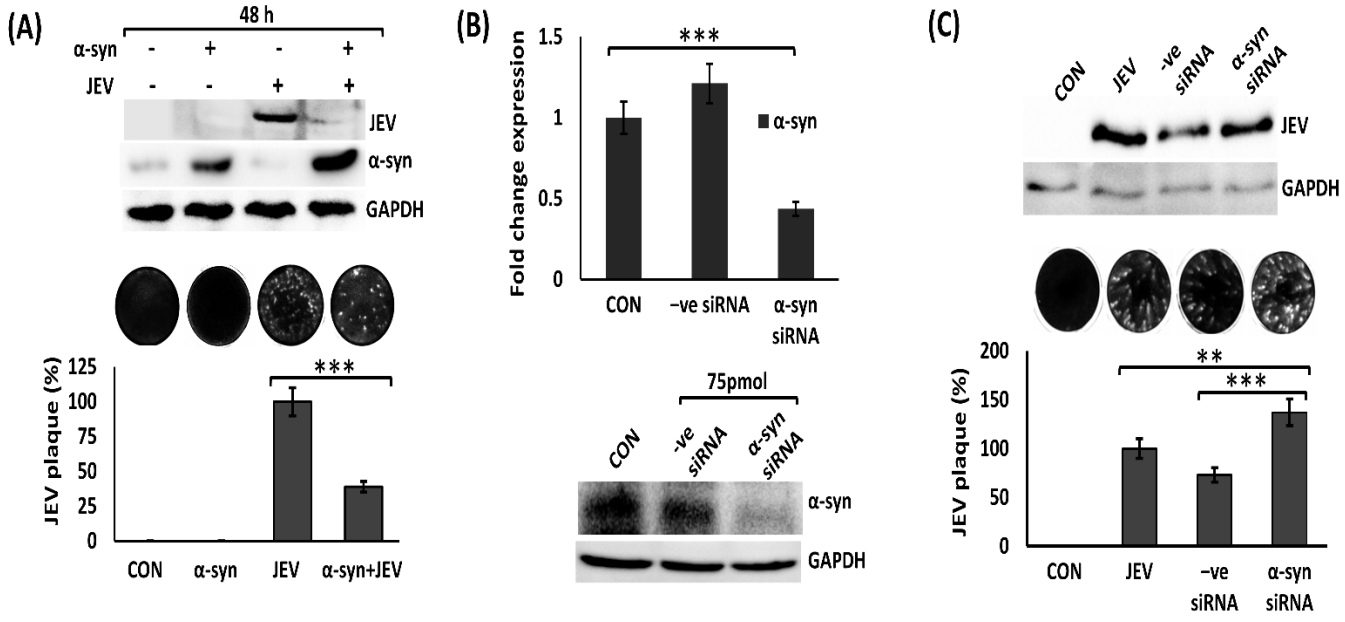

Figure 3.5 Modulation of JEV upon up and down regulations of α-syn gene. Western blot analysis of JEV protein after 48 h of its infection in cells transfected with plasmid expressing α-syn (A). The graph representing the percentage reduction in the plaque number. Downregulation of α-syn mRNA by siRNA treatment in neuro2a cells (B). Western blot analysis of JEV protein and plaque assay of neuronal cells transfected with siRNA and infected with JEV at 0.1 MOI (C).

Further, the silencing of endogenous α-syn was carried out through transfection of α-syn specific cocktail of two siRNAs. The downregulation was estimated using real time PCR and by western blot analyses. The endogenous α-syn mRNA was decreased by 57% and 64% compared to untransfected and -ve siRNA transfected neuro2a cells, respectively. A significant difference

was observed at protein level as well, where α-syn-specific siRNA transfection downregulated α-syn by more than 76% as estimated by ImageJ software (Figure 3.5 B). To estimate the replication of JEV upon α-syn silencing, cells were infected at 0.1 MOI after 12 h of transfection. Beside absence of any significant difference in viral protein, the JEV titer from the supernatant of α-syn-silenced cells showed up to 46% and 96% increase as compared to untransfected, and -ve siRNA-transfected JEV-infected cells, respectively (Figure 3.5 C).

3.4.4 α-syn modulates oxidative stress via decreasing ROS in neuro2a cells

We investigated the ROS levels upon JEV infection, and upon treatment with ascorbic acid, and H_2O_2, two oxidative stress modulators, and Exoα-syn protein. JEV was infected at 0.1 MOI in neuro2a cells and ROS was estimated using DCFH-DA dye using flow cytometry. ROS during early stage of infection was comparable to mock-infected neuro2a cells.

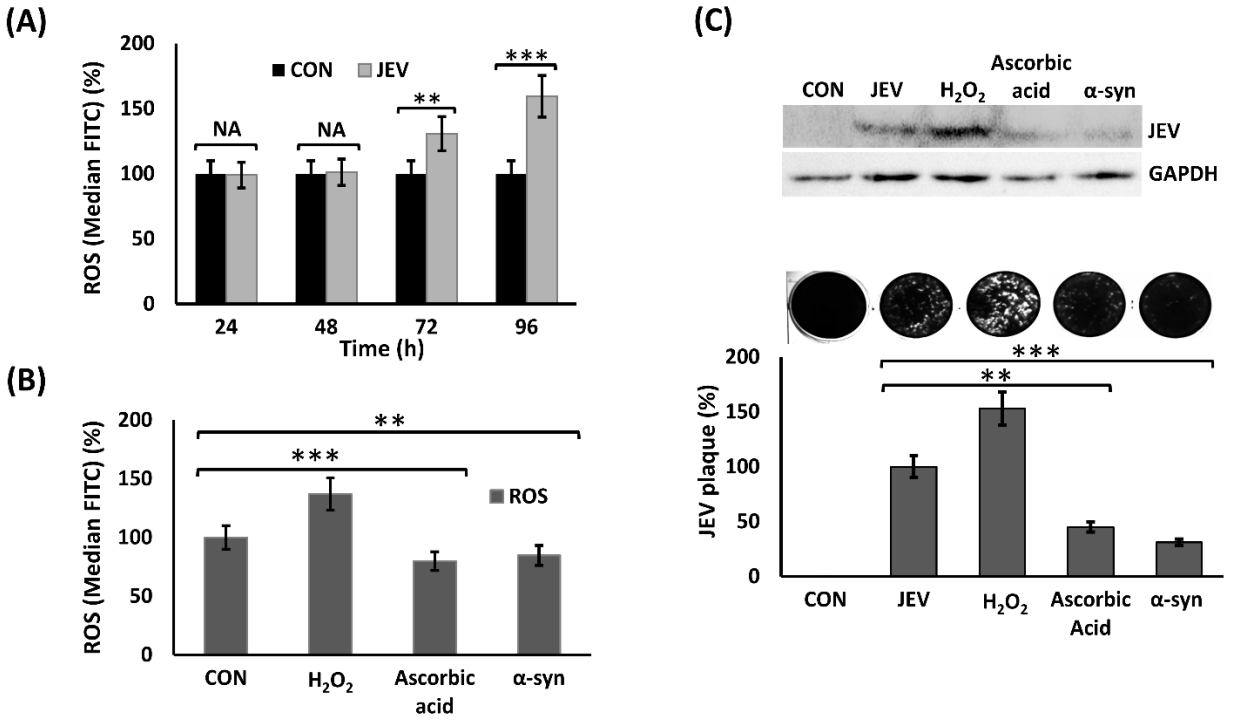

Figure 3.6 Reactive oxygen species (ROS) estimation using flow cytometry. Flow cytometry analysis to quantify ROS in JEV infection at 24 h interval till 96 h. DCFH-DA dye was used to stain the cells 30 min prior estimation in live cells in FITC channel. Graph representing median

FITC (%) in mock-infected and JEV-infected cells (A). Median FITC (%) of ROS estimation in cells 6 h post-treatment with H_2O_2, 12 h post-ascorbic acid and α-syn protein treatment and untreated control (B). Modulation of JEV infection post-treatment with H_2O_2, ascorbic acid, α-syn protein, and untreated control. Western blot analysis along with viral titration through plaque assay from the whole cell lysate and supernatant of the treated cells, respectively (C). Graph representing the percent plaque numbers in differentially treated cells.

Their level, however, increased by about 59% in JEV-infected cells 72 h post-infection (Figure 3.6 A). The H_2O_2 and ascorbic acid are positive and negative modulators of oxidative stress, respectively. As revealed by flow cytometric analysis, treatment with H_2O_2 resulted in ~37% more ROS compared to untreated control cells after 6 h of treatment. Ascorbic acid and Exoα-syn both decreased ROS by about 19% and 16%, respectively compared to untreated control after 12 h of treatment (Figure 3.6 B). These data revealed that Exoα-syn reduces intracellular ROS. Further, experiments were conducted to understand if JEV replication gets influenced by increase or decrease in ROS levels. We observed about 20% increase in JEV viral particle in the supernatant of H_2O_2 treated cells compared to untreated JEV-infected cells. Similar to Exoα-syn, ascorbic acid also negatively regulated JEV replication by approximately 38% compared to JEV control group (Figure 3.6 C).

3.4.5 α-syn positively regulates SOD1 expression

Neuro2a cells were treated with Exoα-syn at 0.25, 0.5, and 1 µM concentrations for 24 h, and cellular protein analyzed using western blotting. A significant increase in SOD1 level from ~2.2 to ~4.7-fold compared to untreated cells was observed with increasing concentration of Exoα-syn. No appreciable difference in SQSTM1, DJ-1, and NQO1 in either of the Exoα-syn concentrations was observed (Figure 3.7 A). To validate whether SOD1 is modulated via endogenous α-syn, the SOD1 expression post α-syn silencing was analyzed.

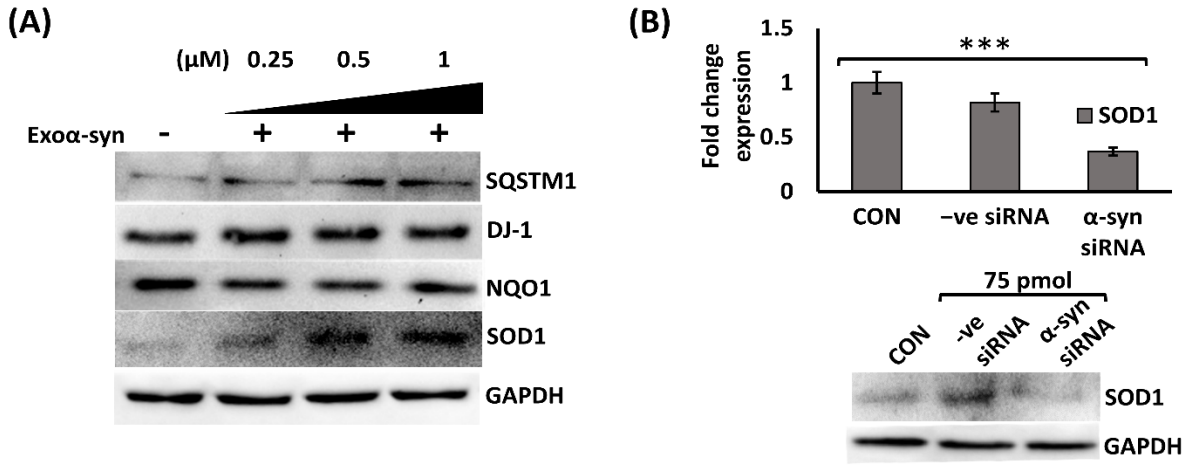

Figure 3.7 Modulation of genes involved in oxidative stress post-treatment with Exoα-syn protein at 0.25, 0.5, and 1 μM concentrations. Western blot analyses of SOD1, SQSTM1, DJ-1, and NQO1 proteins after 24 h of treatment. Untreated neuro2a cells are used as control cells and GAPDH as loading control (A). Modulation of SOD1 post-α-syn gene silencing. Real-time PCR and western blot analyses to estimate SOD1 specific mRNA and protein post α-syn siRNA treatment (B). Fold change is calculated by keeping SOD1 expression in untransfected (CON) cells as baseline.

SOD1-specific mRNA was reduced to about 37% and 56% compared to -ve siRNA-treated cells and untreated control cells, respectively. At protein level, SOD1 protein was upregulated by about 17% in -ve siRNA-treated cells compared to untreated cells. The SOD1 downregulation in α-syn knockdown cells was found to be reduced by around 59% and 42% compared to -ve siRNA-treated and untreated cells, respectively (Figure 3.7 B).

3.4.6 Increase in JEV infectivity post treatment with LCS-1

To check the role of SOD1 in JEV infection, the neuro2a cells were treated with LCS-1, a known inhibitor of SOD1 activity.

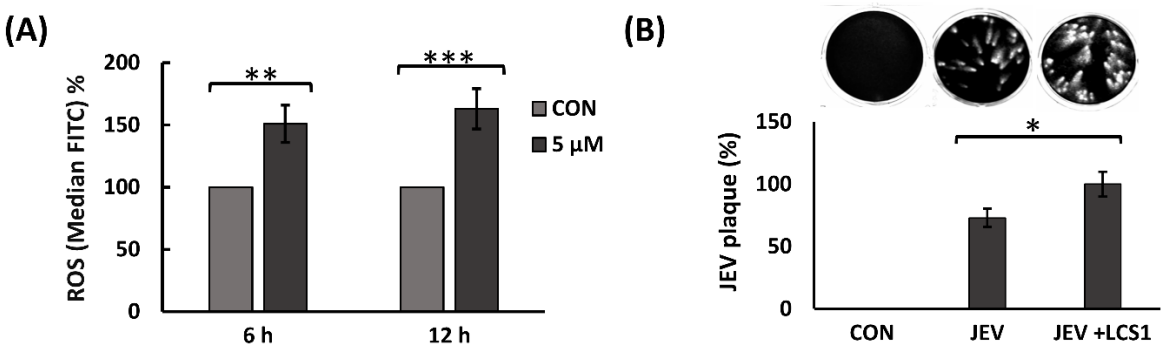

Figure 3.8 Modulation of ROS post-treatment with SOD1 inhibitor LCS-1. Graph representing median FITC (%) post 6 h and 12 h of 5 µM LCS-1 treatment in neuro2a cells (C). Untreated (CON) neuro2a cells are kept as control cells. Modulation of JEV post-treatment with 5 µM LCS-1. Viral titer analyses through plaque assay and graph representing plaques (%) in differentially-treated cells (D).

Intracellular ROS level was increased by ~51% and ~63% compared to untreated neuro2a cells after 6 h and 12 h treatment of 5 µM LCS-1, respectively (Figure 3.8 A). Moreover, it also enhanced the JEV replication by ~50% post 12 h LCS-1 treatment (Figure 3.8 B).

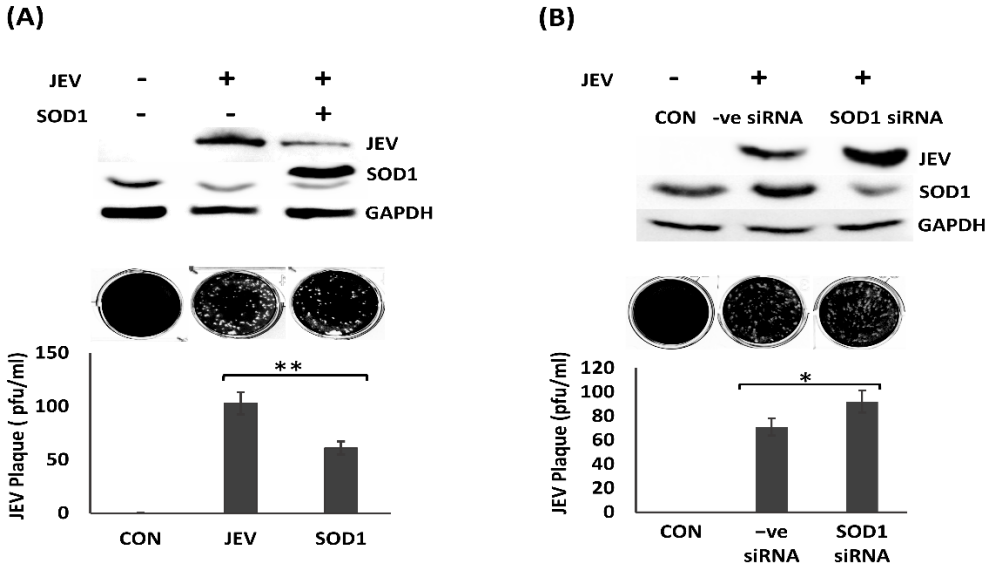

Figure 3.9 Modulation of JEV post-overexpression and silencing of SOD1. Modulation of JEV post-overexpression of SOD1. Western blot analyses were performed after 48 hours to estimate the JEV NS1-specific protein. Cells without infection (CON) and cells with JEV infection (JEV) were used as control groups. Graph representing the percentage of plaque obtained from the

supernatant of treated cells after 48 h (A). Modulation of JEV post-SOD1 siRNA treatment. Western blot analyses and plaque assays were carried out for virus titration in treated groups. Cells treated with universal scrambled siRNA were used as the control group. Graph representing the percentage of plaque obtained from the supernatant of the differentially treated groups post 48 h (B). Statistical analyses were determined using ordinary one-way ANOVA ($p<0.05$, $p<0.001$, and $p<0.001$ are described as *, **, and ***).

Further, overexpression and silencing of endogenous SOD1 were carried out in neuro2a cells. Overexpression of SOD1 decreased JEV replication as observed by ~54% and ~40% in JEV NS1 protein and viral titer, respectively, compared to only JEV-infected cells (Figure 3.9A). Approximately 76% knockdown of SOD1 was achieved compared to non-transfected cells via a cocktail of siRNAs targeting two different SOD1 exons. The silencing of endogenous SOD1 led to an increase in JEV NS1 protein by around 61% compared to -ve siRNA-treated cells. At the same time, virus titer was increased by almost ~30% (Figure 3.9B).

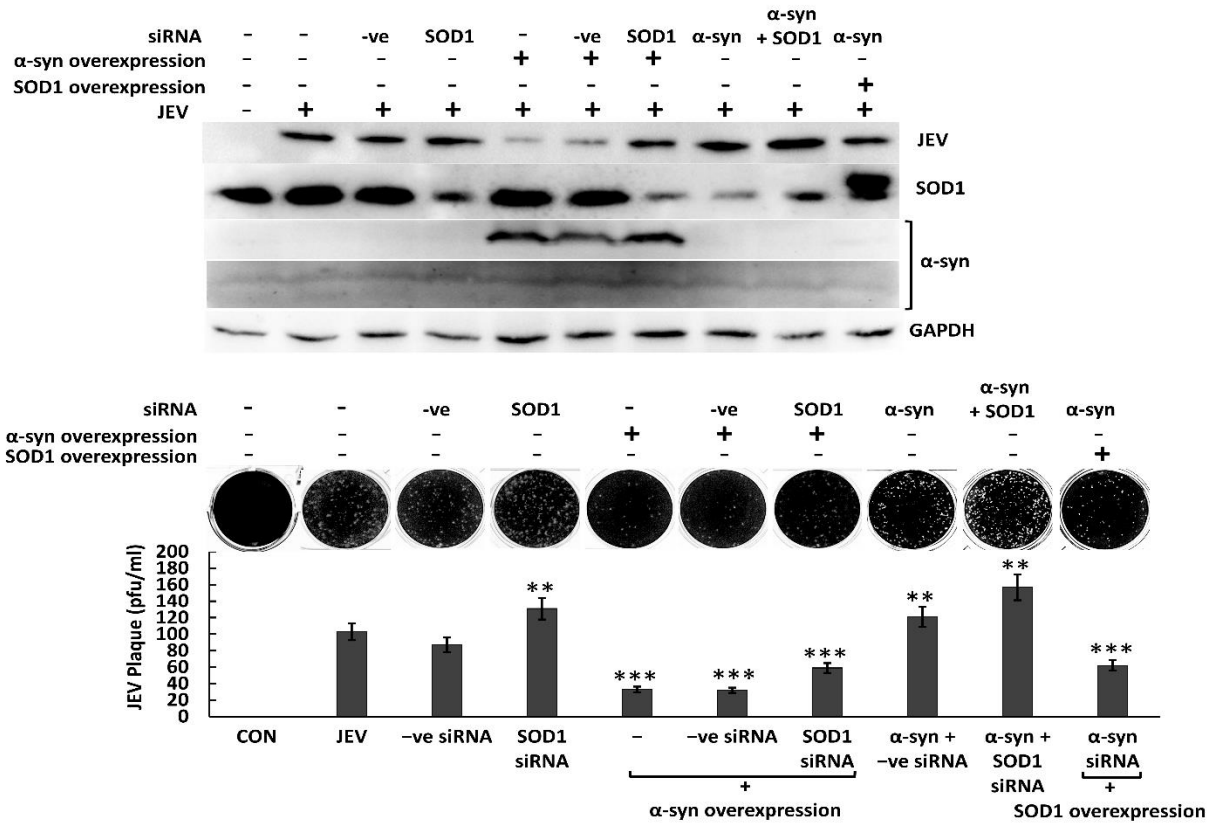

Figure 3.10 Modulation of JEV post overexpressing and silencing of α-syn along with SOD1

silencing and overexpression. Differential treated cells along with controls; non-transfected, -ve siRNA, SOD1 siRNA, α-syn siRNA, α-syn overexpression were infected with 0.1MO1 of JEV. Western blot analyses using GAPDH, NS1, SOD1, α-syn specific antibodies and plaque estimation were performed after 48 hours of JEV infection. Graph representing the percentage of plaque obtained from the supernatant of differentially treated cells. Statistical analyses were determined using ordinary two-way ANOVA ($p<0.05$, $p<0.001$, and $p<0.001$ are described as *, **, and ***).

To check whether anti-JEV activity of α-syn is directly linked through SOD1 activity, endogenous silencing of SOD1 was carried out in α-syn overexpressing cells infected with JEV. Additionally, the effect of overexpression of SOD1 in α-syn silenced cells along with appropriate controls were analyzed. Approximately 53% increase in NS1 protein was observed in α-syn overexpressing cells that were SOD1 silenced compared to -ve siRNA treated cells (Figure 3.10). In α-syn and SOD1 silenced cells, NS1 protein increased by ~39% compared to α-syn silenced cells whereas JEV titer increased by ~30%. The plaque assay revealed 78% and 38% increased JEV titer post-SOD1 silencing in α-syn overexpressing cells compared to non-treated and -ve siRNA-treated α-syn overexpressing cells, respectively. Additionally, SOD1 overexpression in α-syn silenced cells led to ~48% decrease in JEV titer compared to only α-syn silenced cells.

3.5 Discussion

Despite intensive research endeavors, the development of effective treatments against neurotropic viruses, mainly JEV has been impeded due to lack of comprehensive understanding of neurotropism (155, 156). To bridge these gaps and enhance therapeutic approaches, we investigated the function of a specific neuronal protein, α-syn in JEV pathogenesis. Recently, many clinical studies have uncovered the resemblance of Parkinson-like symptoms in JEV-infected patients. This prompted us to explore whether α-syn contributes to promoting JEV progression or inhibiting its replication.

We performed time-course expression analyses of α-syn in JEV-infected and mock-infected neuro2a cells. The results revealed a marked upregulation of endogenous α-syn at both mRNA and protein levels during the late phase of JEV replication in neuronal cells. This upregulation of α-syn is consistent with previous reports of increased α-syn levels in the brains of patients infected with other viruses, such as WNV and human immunodeficiency virus (HIV) (101, 102). To investigate the potential antiviral role of α-syn, we conducted experiments involving wild-type Exoα-syn. Pre- and post-treatment with Exoα-syn exhibited reduction in JEV infection. These findings align with previous studies that showed α-syn's antiviral properties against WNV, wherein the brains of α-syn-knockout mice exhibited increased infectious viral particles and mortality compared to control mice (101). Intriguingly, our co-treatment experiments, wherein α-syn was administered along with JEV, did not show a significant antiviral effect. We hypothesized that Exoα-syn exerted its antiviral function through modulation of host cellular mechanisms rather than direct interference with the physiochemical properties of JEV virion particles or the viral entry process. We explored this hypothesis via investigating the biophysical interaction between Exoα-syn and calcein dye-encapsulated SUVs designed to mimic the lipid membrane of JEV (157). Using circular dichroism spectroscopy and calcein release assay, we found that Exoα-syn underwent a conformational change from random coil to α-helical conformation upon interaction with SUVs. Remarkably, this interaction did not cause any disruption in the lipid SUVs, as no calcein release was observed. While α-syn is known to exhibit lipid binding affinity under cellular conditions, our results suggest that it does not significantly disrupt the viral lipid membrane or inhibit viral entry during JEV infection.

The behavior or function of α-syn seems to differ based on cell type, its mutational status, and the conformation of the protein (aggregated or non-aggregated). Several studies have

demonstrated a relationship between mutated and aggregated α-syn and oxidative stress, leading to neurotoxicity and its involvement in neurodegenerative diseases (158-160). However, besides the well-documented neurodegenerative activity of α-syn, the role of monomeric and wild-type α-syn has been found to be neuroprotective in many studies (161, 162). The toxicity of wild-type α-syn is specifically dependent on the presence of dopamine. In the absence of dopamine, in human cortical neurons, α-syn protects the cells and significantly increases neuronal survival (163). Additionally, wild-type α-syn has been reported to block rotenone- and maneb-induced ROS production and cell toxicity. In contrast, the mutated versions of α-syn, such as A30P, A53T, and E46K, aggravated ROS production induced by rotenone and maneb (115). Moreover, in one of the studies involving microglial cells, the administration of aggregated wild-type α-syn showed a dose-dependent increase in ROS production, while non-aggregated α-syn resulted in a slightly decreased ROS level (116). Thus, the ability of α-syn to modulate ROS appears to be dependent on the conformational form of the protein. In terms of JEV progression in neuronal cells, Exoα-syn was found to modulate oxidative stress inside the cell. Furthermore, it blocked the JEV-induced ROS generation during the late phase of JEV infection.

We investigated whether the anti-JEV activity exhibited by α-syn is mediated via modulation of ROS levels. The expression of anti-oxidative proteins like NQO1, SOSM1, and DJ-1, that are mainly involved in Nrf2-SQSTM1 pathway, was not altered with Exoα-syn protein treatment. However, there was upregulation of SOD1 with Exoα-syn treatment and conversely, endogenous α-syn silenced neuro2a cells had low SOD1 expression. This anti-oxidative mechanism of α-syn has been shown earlier, wherein SH-SY5Y cells expressing α-syn protein had increased SOD1 activity and significantly attenuated rotenone-induced cell apoptosis (121). SOD1 is known to convert the superoxide radicals arising from mitochondrial intermembrane space,

cytosol, and peroxisome into hydrogen peroxide and molecular oxygen through redox reactions. Overall, our results indicate that α-syn, through SOD1 upregulation directly or indirectly, contributes to a cellular environment that counteracts oxidative stress and restrains JEV propagation. This was supported by the data where inhibiting SOD1 activity using the compound LCS-1 led to an increased release of JEV particles outside the cells. We did not observe a significant difference in intracellular viral proteins with LCS-1 treatment, indicating the late response of SOD1 which may be during packaging or budding of viral particles outside cells. SOD1 is a known target of a plant lignan compound, arctigenin that shows anti-JEV activity via increasing SOD1 protein level inside cells (140). In JEV-infected *in vivo* and *in vitro* models, SOD1 is reported to be downregulated (140). Like SOD1, there are many other anti-oxidative proteins that are manipulated differentially by most of the *flaviviridae* members. JEV is reported to decrease ROS scavenging *via* downregulation of proteins like DJ-1 as well as Nrf2-mediated expression of SQSTM1 and thioredoxin (86, 152). Thus, there is a significant role of oxidative stress-induced ROS in shaping the cellular milieu to favor JEV propagation. This is further established by the data where administration of the oxidative stress inducer, hydrogen peroxide (H_2O_2), significantly increased viral replication within infected cells.

In conclusion, our study sheds light on the intricate interplay between oxidative stress, α-syn, and JEV infection. Apart from the current study, α-syn is reported to modulate the ER stress pathway (101). The levels of activating transcription factor 6 (Atf6), protein disulfide isomerase (PDI), and phosphorylated eIF2α proteins, all of which support viral infection in WNV were significantly increased in α-syn-knockout primary cortical neurons (101). Thus, there is possibility of more than one antiviral mechanism or pathway being involved in response to α-syn. It is noteworthy that we have not investigated the role of aggregated α-syn or Lewy bodies (LBs) in

JEV infection. Also, the role of JEV induced ROS in α-syn aggregation. As maintaining the physiologic levels of α-syn in neurons is important for their survival, overexpression of α-syn for prolonged time may lead to its aggregation even if it is in response of viral infection. Therefore, the role of LBs and aggregation of α-syn in viral pathogenesis remains an important question and an area of active interest.

Chapter 4. Understanding the effects of JEV replication on phosphorylation and oligomerization of α-syn

4.1 Abstract

The pathological implications of α-syn phosphorylation and oligomerization constitute a critical aspect in various neurodegenerative diseases. α-syn aggregation has been discerned in specific brain regions of animal models infected with coxsackievirus B3, influenza A, and western equine encephalitis viruses. In contrast, WNV infection exhibited no discernible variation in α-syn multimers in primary striatal neuron cultures compared to non-infected cells. Given the established association of α-syn aggregation with neurotoxicity in dopaminergic neurons, it becomes imperative to elucidate its role in JEV pathogenesis. Therefore, in the present study, we conducted a comprehensive time-course analysis of casein kinase 2 (CK2) and polo-like kinase 2 (PLK2), the kinases responsible for α-syn phosphorylation at the S129 position (pα-synS129) in neuronal cells. Our findings revealed a substantial reduction in both these kinases, specifically during the late phase of JEV replication. Concurrently, a decrease was also observed in pα-synS129 levels in JEV-infected cells. Moreover, we examined α-syn oligomerization through glutaraldehyde cross-linking and thioflavin T dye. Both results collectively indicated an overall increase in intracellular oligomerization of α-syn in JEV-infected neuro2a cells. To understand the role of phosphorylation and oligomerization in JEV prognosis, further investigations through *in vitro* and *in vivo* studies are required.

4.2 Introduction

Phosphorylated α-syn has been implicated in neurodegenerative diseases like dementia and PD. In a healthy brain, α-syn is primarily unphosphorylated; however, most aggregated α-syn in Lewy bodies of PD patients is phosphorylated at Ser129, presumed to be of pathological significance (137). The C-terminal tail of α-syn contains the majority of phosphorylation sites, but location S129 is known to be a major player involved in α-synucleinopathy. Various kinases like casein kinase 2 (CK2), polo-like kinase (PLK), and G protein-coupled receptor kinase (GRK) have been recognized to date that catalyzes S129 phosphorylation (164-166).

Both CK2 and PLK2 are serine/threonine protein kinases. CK2 is a tetrameric enzyme assembled from two catalytic subunits (CK2α and CK2α′) and a regulatory subunit (CK2β dimer). Casein kinase 2 is necessary for cell survival and is a crucial suppressor of apoptosis. Out of five known PLKs, PLK2 and PLK3 have better phosphorylation activity than PLK1 and PLK4. PLK5 lacks a functional kinase domain due to a premature stop codon in exon 6 and is thus incapable of phosphorylating α-syn. Interestingly, a significant reduction in α-syn phosphorylation has been observed in primary cortical neurons and the cerebral cortex of PLK2 knockout mice (167). These data suggest that PLK2 is critical for α-syn phosphorylation in the pathogenesis of α-synucleinopathy.

Whether phosphorylation serves as the constraining factor in facilitating aggregation remains ambiguous. Exposure to the exogenous α-syn fibrils results in intracellular aggregation in cell lines and primary neuronal cells, which is immunopositive to α-syn phosphorylated at Ser129 (168, 169). However, phosphorylation does not seem to be mandatory for the formation of cytoplasmic inclusions. The study indicated the presence of phosphorylated α-syn only in triton-

insoluble fraction, suggesting the modification in growing inclusions (169). Contradictory to the above findings, aggregation of α-syn has been suggested to be independent of phosphorylation in a few studies (170-172). No significant differences existed in dopaminergic cell loss, tyrosine hydroxylase expression, or nigrostriatal terminal density among the wild-type and pα-synS129 mutants. Furthermore, there were no differences in α-syn aggregate formation or distribution among wild-type or pα-synS129 mutants (172). In normal cells, the overexpression of α-syn leads to the formation of cytoplasmic inclusion bodies known as aggresomes, which have several morphologic and molecular similarities to LBs (173). Aggresomes are characterized by their localization to the centrosome and protect cells from the toxic effects of misfolded proteins (174).

In terms of neurotropic virus infection or JEV particularly, α-syn phosphorylation and aggregate are not explored. a number of kinases phosphorylate pα-synS129, however, their role in disease pathogenesis and relationship with α-synucleinopathy are yet to be understood. Thus, our study highlighted the time course analyses of CK2, PLK2, and pα-synS129 in JEV-infected cells. We have analyzed the effect of JEV replication on oligomerization of α-syn in neuro2a cells.

4.3 Material and Method

4.3.1 RNA and protein quantification of phosphokinases

mRNA and protein quantification of CK2 and PLK2 was carried out via real-time PCR and western blot analyses. The primers specific to CK2; For.P – GAGCACCCTTACTTCTACACTG, Rev.P- CTGGAACAGGTATCCCAAGTG and PLK2; For.P- AGGTGGGAGACTTTGGTTTG, Rev.P- TGGTTTCGAATGGAGGTCTTC, were used. For western blot analyses CK2 (2656, CST, USA) and PLK2 (A7066, Abclonal, USA) were used. Briefly, cells were seeded in 6 well plate at density 2×10^6 cells per well. After 12 h, 3 wells were kept non-infected and 3 wells were infected with JEV at 0.1MOI. Cells were harvested at 24 h interval for RNA and protein estimation.

4.3.2 Phosphorylated α-syn estimation

Phosphorylation of α-syn post JEV infection was carried out using a phosphorylated (S129) antibody (AP0450, Abclonal, USA). Plasmid pHM6-alpha-synuclein-WT from addgene was used for α-syn overexpression in neuro2a cells (151). Briefly, neuro2a cells were seeded in density 2×10^6 cells per well. Approximately 2 µg of pHM6-alpha-synuclein-WT plasmid was transfected per well using Lipofectamine3000 (Thermo, USA). Following incubation, the transfected cells were infected with JEV at 0.1 MOI. Cells were harvested post 48 h of JEV infection and protein lysates were prepared using 2X Laemmli buffer with 355 mM 2-mercaptoethanol. Samples were heated 10 min prior SDS-PAGE for protein estimation.

4.3.3 Aggregation of α-syn

Oligomerization of α-syn was analyzed post-treatment with protein crosslinking reagent, glutaraldehyde at 0.005%. Briefly, 2×10^6 cells per well were infected with 0.1MOI JEV along with appropriate controls. Post 72 h of incubation, cells were harvested in PBS. Cells were treated with 0.005% glutaraldehyde for 15 mins at room temperature and washed with cold PBS to analyze it for protein expression using α-syn specific antibody.

4.3.4 ThioflavinT Assay

ThioflavinT (ThT) dye was used to analyze aggregated cellular proteins in neuro2a cells post differential treatment. Briefly, two 35mm dishes having 2×10^6 cells per well were transfected with approximately 2 µg of pHM6-alphasynuclein-WT plasmid using Lipofectamine3000. Transfected cells from one dish were infected with 0.1MOI of JEV whereas other was kept as transfected uninfected control. Likewise, one dish of untransfected/uninfected cells and a second dish of untransfected cells with JEV infection were analyzed for ThT fluorescence. The samples were mixed with 300 µl of 20 µM ThT dye, and all the samples were

excited at 445 nm wavelength. ThT fluorescence intensities were estimated from 450 to 650 nm, slit 4 nm. CON cells without ThT were used to measure baseline fluorescence.

4.4 Results

4.4.1 Modulation of phosphokinases post JEV infection

Time course analyses of CK2 and PLK2 was done from 24 h till 72 h post-JEV infection. We observed a significant decrease in gene and protein expression of PLK2 and CK2 at 72 h. About 80% decrease in CK2 mRNA was observed post 48 h of JEV infection. PLK2 mRNA was decreased gradually over time up to 30% compared to non-infected cells (Figure 4.1A). Western blot analyses revealed better modulation of CK2 as compared to PLK2 at 24 h post-JEV infection (Figure 4.1B).

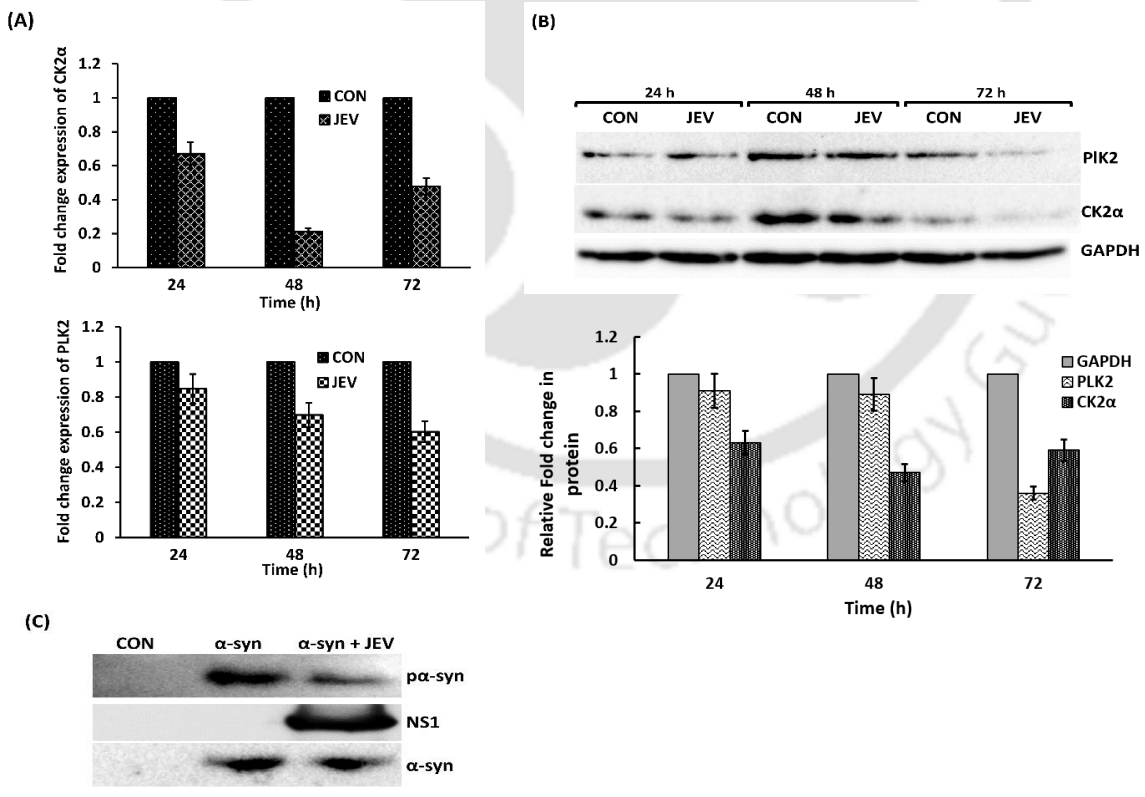

Figure 4.1 Real time gene expression analyses of CK2 and PLK2 in JEV infected compared to control neuro2a cells (CON). Fold change has been calculated keeping CON as base line

expression and GAPDH as control gene expression (A). The western blot analyses using PLK2, CK2 and GAPDH specific antibodies in JEV infected and CON cells at 24, 48, 72 h intervals (B). Western blot analyses to evaluate the pα-syn in JEV infected and non-infected neuro2a cells which are transfected α-syn expression plasmids (C). Total α-syn is kept as control to analyze the change in pα-syn

Around 37% and 52% decrease in CK2 protein level was observed at 24 h and 48 h post JEV infection, respectively. More than 62% and ~ 43% reduction in PLK2 and CK2 was observed respectively, in JEV infected cells compared to control cells at 72 h. Further, we visualized pα-synS129 protein level in α-syn overexpressing cells infected with JEV compared to uninfected cells. About 71% decrease in exogenous pα-synS129 level was observed post JEV infection compared to non-infected cells (Figure 4.1C).

4.4.2 Oligomerization of α-syn

The results indicated an overall increase in endogenous α-syn expression and an increase in α-syn specific oligomers of distinct sizes between ~15 kDa to 55 kDa in JEV-infected cells compared to non-infected neuro2a cells (Figure 4.2A). ThT fluorescence intensities showed higher intracellular protein aggregate in JEV-infected cells both in the absence and presence of α-syn overexpression compared to appropriate controls (Figure 4.2B). In JEV-infected cells higher peak maxima was observed at ~ 56000 units, whereas in CON cells, peak maxima was followed less than 40000 units. In α-syn+JEV cells peak maxima was found around 610000 and in α-syn cells it was around 50000 units.

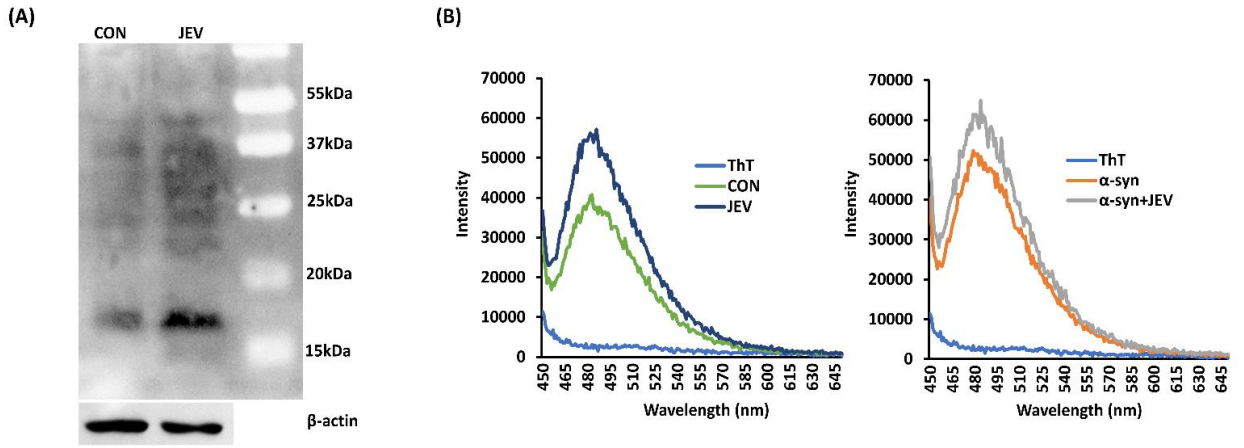

Figure 4.2. Analyses of aggregation α-syn by western blotting and ThT fluorescence. Western blot analyses of whole cell lysate post 0.05% glutaraldehyde mediated protein cross-linking. α-syn specific antibody was used to detect the oligomers of different sizes in CON and JEV infected sample (A). Spectrophotometric analyses of aggregated intracellular proteins via ThT dye. Graphs representing fluorescence intensities from 450 to 650 nm (B). CON cells without ThT is used to measure base line fluorescence from cells (ThT). The samples CON, JEV, α-syn and α-syn+JEV were mixed with 300 µl of 20 µM ThT dye and all the samples were excited at 445 nm wavelength.

4.5 Discussion

Many studies have indicated the importance of α-syn phosphorylation at Ser129 in regulating its aggregation and neurotoxicity (137, 175). Thus, the propensity by which kinases, particularly, CK2 and PLK2, are involved in phosphorylation and α-syn aggregation has been of significant importance. Characterizing these two kinases in other viruses has been indicated to play an important role. Our study suggested that CK2 and PLK2 got downregulated, particularly at late phase of JEV infection. As per previous reports, both of these kinases are proviral host factors (176, 177). CK2 is reported to regulate the phosphorylation of viral-specific proteins in HIV, HBV and HCV, CMV, HSV infection while PLK2 is found to be involved in viral-induced apoptosis (178-184). Although, the impact on α-syn phosphorylation has not been studied in former studies,

our data suggests a decrease in CK2 and PLK2 expression and reduced pα-synS129 protein in JEV infection.

Many studies have indicated the pα-synS129 protein may promote pα-syn oligomerization (185, 186). It has been estimated that 90% of aggregated α-syn present in LBs contains are phosphorylated at Serine129, implying that this specific phosphorylation event is connected to pathology (186). Thus, we checked the aggregation of α-syn in both JEV-infected and non-infected neuro2a cells. Glutaraldehyde-mediated cross-linking of intracellular proteins showed increased α-syn oligomers. The aggregated or oligomeric state of α-syn has been shown to bind with ThT dye, a benzothiazole salt and is widely used to visualize and quantify the presence of misfolded protein aggregates called amyloid, both *in vitro* and *in vivo*. Hence, spectrophotometry analyses of ThT dye confirmed that JEV replication leads to oligomerization of α-syn which further indicated that decreased α-syn phosphorylation did not alter its aggregation in JEV-infected cells. In previous animal studies, pα-synS129 neither promoted nor inhibited α-syn aggregate formation (170, 171). Studies have reported that S129 phosphorylation is present on monomeric and soluble α-syn and able to inhibit its fibril formation under certain conditions (187). However, others have proposed that pα-synS129 does not confer toxicity *in vivo* and may actually be a neuroprotective mechanism accelerating the clearance of aggregated α-syn (172, 188).

The interplay between phosphorylation and the non-phosphorylated state of α-syn has been important in gene transcriptional regulation (175). Serine-129 phosphorylation decreases the ability of α-syn to both bind and bend DNA, as α-syn binds 304 bp circular DNA forced into a bent shape, but pα-synS129 does not (189). We hypothesize that reduction in α-syn phosphorylation might be one of the key events that regulate the transcription of SOD1 is in JEV-infected cells as mentioned in chapter 3. Further, the oligomerization of α-syn in JEV infection

even at lower pα-synS129 level may indicate the formation of aggresomes, which are rather cytoprotective.

Beside this study, the exact role of pα-synS129 and α-syn aggregate in JEV pathogenesis is yet to be understood. In JE disease prognosis, the function of these phosphorylating enzymes like GRKs is still poorly understood (137). Also, as per a previous study, the propensity of α-syn to form cellular aggregates *in vivo* can be more pronounced as compared to *in vitro* (190). Thus, elaborate *in vivo* and *in vitro* studies is required to understand the dynamics of α-syn in JEV pathogenicity.

Chapter 5. 3. Designing and assessment of pyrazole derivatives against JEV infection.

5.1 Abstract

JEV is the leading causative agent of encephalitis and its associated mortality among children. JEV modulates host cell machinery for its advantage, such as oxidative damage, leading to stress responsive pathways. The present study analyzes new series of dinitroaryl substituted derivatives (1a-1f), containing a pyrazole moiety and explores its potential anti-JEV activity. Out of all synthesized derivatives, compounds 1b and 1f were selected based on minimal cytotoxicity. In vitro inhibition of more than 70% and 90% were observed with compounds 1b and 1f, respectively, in neuronal cells. Dose-response analyses highlighted 1f exhibiting better antiviral activity than 1b. The mice treated with compound 1b or 1f did not show any noticeable toxicity at a dose of 100 mg/kg/day when administered intraperitoneally for 96th h. Inhibition of up to 41% and 70% JEV RNA in the spleen and 33% to 43% in brain tissue was observed with compounds 1b and 1f, respectively. Both the compounds suppressed JEV induced ROS generation by significantly up-regulating the endogenous anti-oxidative proteins like NQO1 and HO-1 via increasing DJ-1 and SQSTM1 expression. The results suggest 1b and 1f regulated JEV replication through an interlocked positive feedback loops of NRF2-SQSTM1 signaling mechanism. The potential of these compounds can be further tested for broad-spectrum antiviral effects with other flaviviruses in the path towards the development of therapeutics.

5.2 Introduction

In the prognosis of JEV infection, many host factors have been identified as being involved in the various steps of the viral life cycle (74). Viral replication machinery perturbs cellular metabolism homeostasis, thus inducing a stress pressure on the host cell. Cell injury, disease, homeostasis or signaling alteration, increasingly produces ROS, as a byproduct in mitochondria, ER, and peroxisome compartments (73, 74).

Previous studies showed that elevated ROS can react to form peroxynitrite, which triggers the loss of ATP and mitochondrial membrane potential. This cascade further leads to the activation of caspase 3, causing neuronal apoptosis (87, 88). Thus, several potential anti-oxidative compounds like minocycline, arctigenin, fenofibrate, curcumin have been explored for anti-JEV activities, but only minocycline and ribavirin have been tested by randomized clinical trials (138, 140, 141, 191). However, the treatment with both the drugs showed no statistically significant differences in the mortality rate of JEV patients as compared to placebo-treated controls (192, 193).

Pyrazole derived compounds have recently been studied in various aspects of its biological applications (127). In this study, we have synthesized new pyrazole derivatives and checked their efficacies against JEV both *in vitro* and in animal model. Moreover, the study highlights the anti-oxidative properties of the pyrazole derivatives concurrently imparting the anti-JEV effect.

5.3 Materials and methods

5.3.1 General methods

All commercially available reagents of analytical grade were used without further purification and procured commercially (SD Fine, Loba Chemie, and Avra synthesis, India). An

open capillary tube method was used to determine melting points and ^{1}H (^{13}C) NMR spectra were recorded using $CDCl^{3}$ solvent (Bruker model 400 MHz instrument, USA). The chemical shifts (δ) were expressed in parts per million, and coupling constants (J) were calculated in hertz. Proton coupling patterns were illustrated as singlet (s), doublet (d), triplet (t), quartet (q), multiplet (m) and broad (br). The IR spectra were recorded on a FT-IR spectrometer using KBr pellets (Schimadzu, Japan). HRMS data were obtained in electron impact (EI) mode, and intensities were recorded as percentages relative to the base peak (I=100%). Chalcone and hydrazone derivatives have been synthesized as per the literature known procedures. The synthesis of pyrazole compounds have been previously reported by our research group (Gawandi et al., 2019). Some known and new pyrazole derivatives have been selected to perform anti-JEV studies.

5.3.2 General procedure for the synthesis of pyrazole derivatives

Substituted 2,4-dinitrophenyl hydrazones (1mM) and silica supported molybdic acid (1mM) were placed in a conical flask and heated at 80–120°C on a sand bath. The progress of the reaction was monitored by TLC intermittently. After completion of the reaction, the product was dissolved in ethyl acetate and filtered to recover the catalyst. The solvent was then evaporated under vacuum, and the crude product was recrystallized from n-hexane to afford the pure product. The newly synthesized compounds were characterized based on IR and NMR spectroscopic data. The catalyst was further recycled to carry out another batch of reactions.

5.3.3 Cytotoxicity assay of pyrazole-based compounds.

The cytotoxicity of the compounds was analyzed using 3-(4,5- dimethylthiazol-2-yl)-2,5-diphenyltetrazolium bromide (MTT) to 3- (4,5-dimethylthiazol-2-yl)-2,5-diphenyltetrazolium bromide formazan conversion assay. Neuro2a cells were seeded in a 96 well plate with a seeding density of 10^{4} cells/well before the experiment. Further, the cells were incubated with six

compounds (100 µM to 100 nM) for 48hr. The absorbance was taken at 570 nm using the microplate reader (Multiscan go, Thermo scientific, USA), and the percentage of cell viability was calculated taking DMSO as vehicle control.

5.3.4 *In vitro* antiviral assay of pyrazole compounds

The Neuro2a cells were seeded in 12 well plate at a density of 2×10^5 cells per well. For co-treatment, JEV at 0.01 MOI in infection medium was incubated with pyrazole compounds at 15µM for half an hour in 1.5ml tubes. Following incubation, 200µl of infection medium was added on top of cells. After 2 h of adsorption, the medium was removed, and fresh DMEM with 2% FBS was added. For post-treatment, compounds were added after 2 h of JEV adsorption. Cells and supernatant from differentially treated (virus-infected, virus along with compound treated, mock-infected, and compound control) samples were collected at 72 h time point. Virus titration was done using plaque assay along with viral vRNA and JEV NS1 protein detection through real-time and western blot analyses, respectively.

5.3.5 *In vitro* time-dependent kinetics of JEV

To examine the replication of JEV, Neuro2a cells were treated in four different conditions: mock-infected, compound treated cells, virus along with DMSO treated, virus along with compound treated. Initially, cells were seeded in 6 well plate at a density of 2×10^6 cells/well and kept for 12 h at 5% CO_2 at 37°C incubator. Further, 0.01 MOI of JEV infection was given for 2 h. Post virus adsorption, infection media was removed and DMEM containing 2% FBS along with compound at 15µM concentration were added. For analyses, the cultured media at 24, 48, 72, 96, and 120th h were harvested for virus titration using $\log_{10}$ $TCID_{50}$.

5.3.6 *In vitro* dose-dependent response of JEV

For dose-response analyses, Neuro2a cells were seeded in a 12 well plate at a density of 2 × 10^5 cells/well. The cells were infected with 0.01 MOI of JEV for 2 h. Post-virus adsorption, different doses of final shortlisted compounds (1b and 1f) starting from 15μM to 5μM in DMEM containing 2% FBS were used to treat cells. Supernatant and whole-cell lysate were collected at 72 h post-infection. The JEV NS1 and GAPDH specific bands were detected in western blot to check the virus inhibition and for loading control, respectively. Inhibitory concentrations (IC_{50}) of both the compounds were calculated by treating the cells at four different concentrations ranging from 15 to 1μM. Briefly, Neuro2a cells were seeded in 6 well plates and infected with JEV at MOI 0.01 after which cells were incubated for 72 h. Cells and supernatant were harvested post incubation, and JEV particles were titrated by plaque assay.

5.3.7 Dose and time-course study of compounds in mice

For dose-determination study, non-toxic concentrations of 1b and 1f were determined by administering intraperitoneal 10, 50, and 100mg/ kg body weight of the compound in different groups (n = 5) of 4-weekold BALB/c mice. All mice were observed for seven days for loss or gain in weight and other evidence of toxicity like ruffled fur compared with the mice injected with plain DMSO. Dilutions of compounds were prepared accordingly to inject only 50μl for every three mentioned concentrations. Further, in the time course study, separate groups of mice (n = 5) were treated with a different dosage of selected concentrations of compounds from the first study. The dosage was administered intraperitoneal every 24 h for four days. The toxicity of compounds in mice of each group was observed for seven days.

5.3.8 Evaluation of anti-JEV effect of the compounds in mice

Four-week-old BALB/c mice were randomly divided into six groups (10 mice/group). In three groups, 10^4 PFU/mice of live attenuated vaccine strain of JEV SA-14-14-2 was administered intracerebrally. Following two hours of JEV injection, compounds 1b or 1f with dosage 100 mg/kg/day per mice were injected intraperitoneally into two out of three JEV injected groups. Third group was treated as JEV infected group and was infected intraperitoneally with DMSO (30 µl). Fourth group received intracerebral injection of PBS (30 µl) and intraperitoneal DMSO (30 µl) to serve as 'mock infected group'. Fifth and sixth groups served as 'only drug control' thus received 100mg/kg/day per mice of 1b or 1f, respectively. The treatment of compounds was given from 1st day post-infection, daily, for up to four days. Following a day, three mice from each group were sacrificed every 24 h. The spleen and brain harvested from each mouse were used for virus quantification and gene expression studies. For viral vRNA quantification, total RNA from the brain and spleen were isolated using TriZol method and converted into cDNA using (iScript™ cDNA Synthesis Kit, Biorad). All the in vivo experiments were done at Maharshi Dayanand University, Rohtak, India. The study was conducted following the guidelines of the institutional animal ethics and biosafety committee vide sanction CAH 76-85 dated 26-02-2021.

5.3.9 ROS estimation

For flow cytometry analyses, Neuro2a cells were seeded in 2×10^6 cells/well density in 6-well plate and incubated for 12 h at 37°C, 5% CO_2 incubator. JEV infection were given in three wells at 0.1MOI. The 1b and 1f treatment was given at 15µM concentration separately in JEV infected and non-infected cells 2 h post-infection. Untreated and uninfected controls were kept along with one DMSO (0.1%) control. After 48 h of incubation, cells were pelleted and washed with 1% phosphate buffer saline (PBS, pH 7.4). Further, cells were suspended in 500 µl of 1%

PBS and incubated with 10 μM 2′ ,7′ -dichlorodihydrofluorescin diacetate (H2DCF-DA) for 30 min at 37°C. The stained live cells were analyzed using flow cytometry (BC, CytoFlex S Analyser). The DJ-1(5933, CST, USA), SQSTM1 (39749, CST, USA), HO-1 (43966, CST, USA), NQO1 (62262, CST, USA), antibodies were used to explore the modulation of NRF2- SQSTM1 pathway in the cells. Antibodies dilutions of 1:5000 were prepared in 2% Bovine serum albumin in PBS. The β-actin was used as a loading control for all the experiments (MA1-91399, Invitrogen).

5.4 Results

5.4.1 Synthesis of pyrazole derivatives

The synthesis of 1,3,5-trisubstituted pyrazoles were achieved using our reported methodology involving oxidative cyclization of synthesized 2,4-dinitrophenyl hydrazone derivatives in the presence of silica molybdic acid as catalyst. At the beginning, the synthesis of substituted chalcones was obtained employing the literature known Claisen Schmidt condensation procedure, followed by treatment with 2, 4-dinitrophenyl hydrazine under hot acidic conditions in methanol to yield respective hydrazone derivatives. These hydrazone derivatives were then subjected to oxidative cyclization under solvent-free, neat heat conditions using silica molybdic acid as a catalyst (Figure 5.1 [A, B]). The formation of compounds 1a-1f were confirmed by ^{1}H NMR and ^{13}C NMR spectral analysis (Figure 5.2).

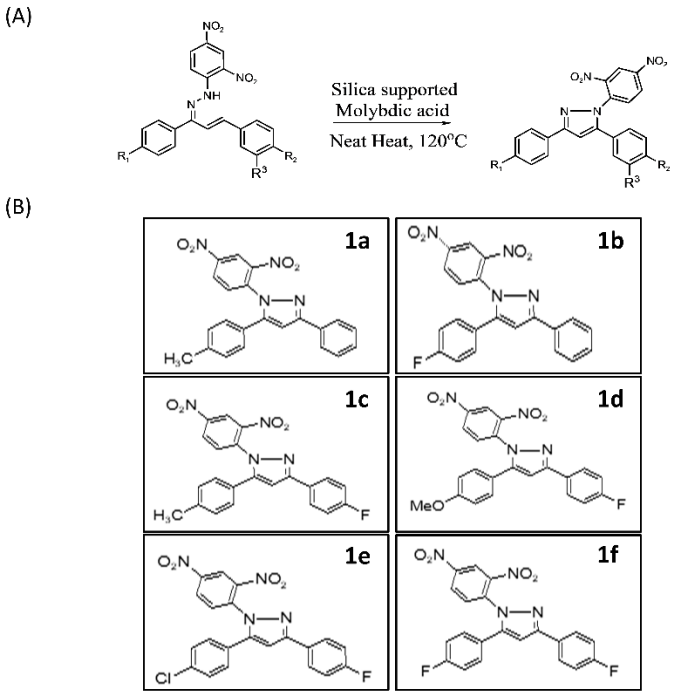

Figure 5.1 Substrate scope of the synthesized 2,4-dinitrophenyl pyrazole derivatives (**A**). Structural representation newly synthesized six pyrazole derivatives (**B**).

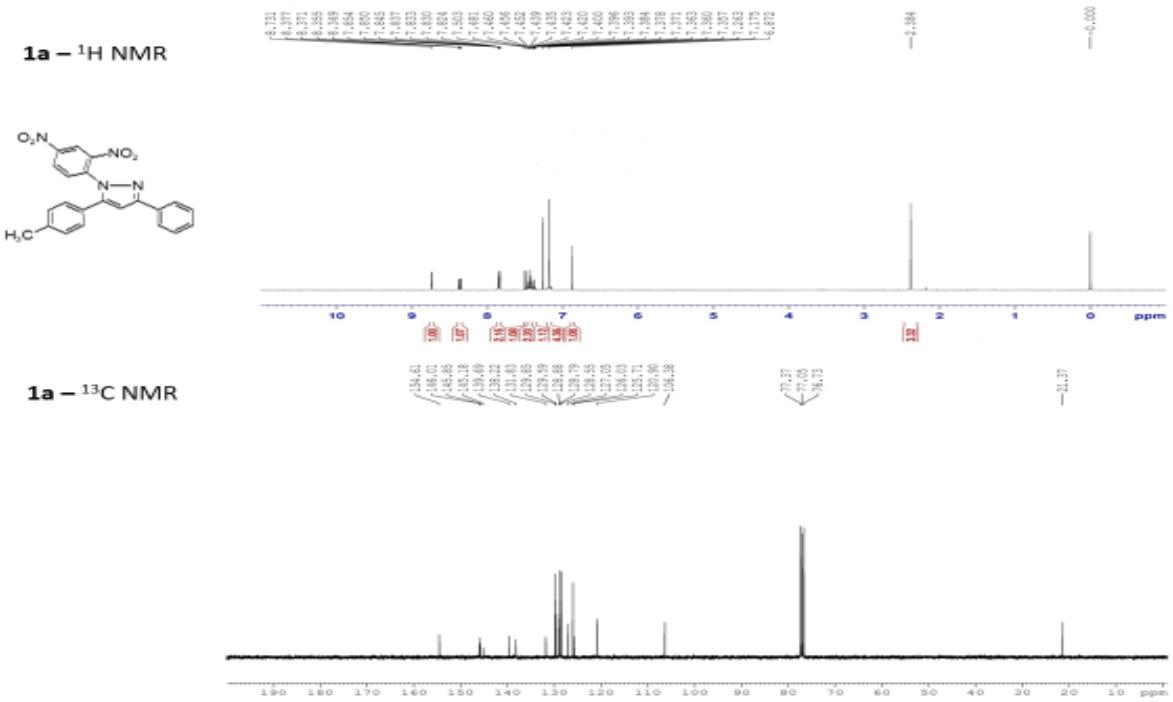

1b – ^{1}H NMR

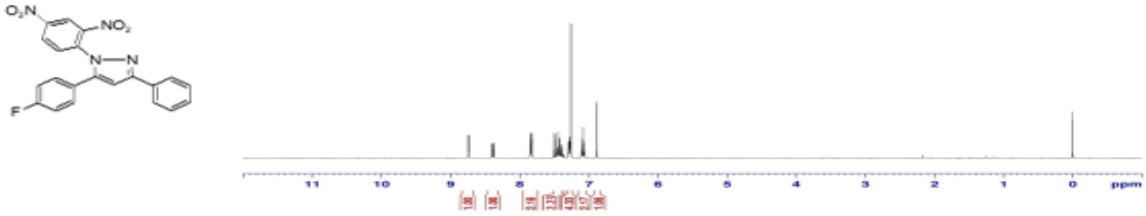

1b – ^{13}C NMR

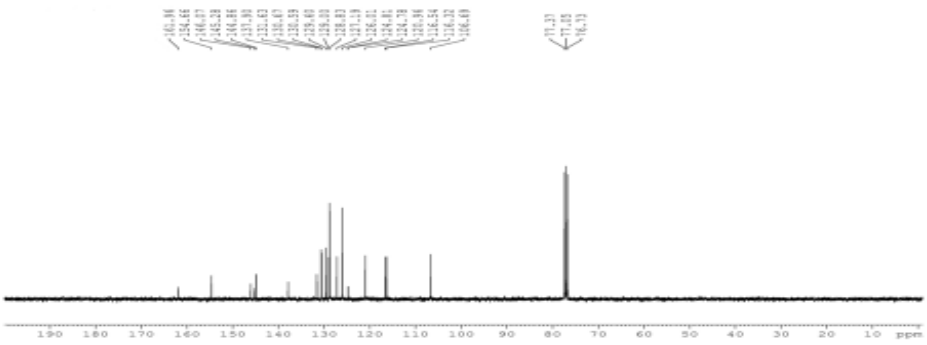

1c – ^{1}H NMR

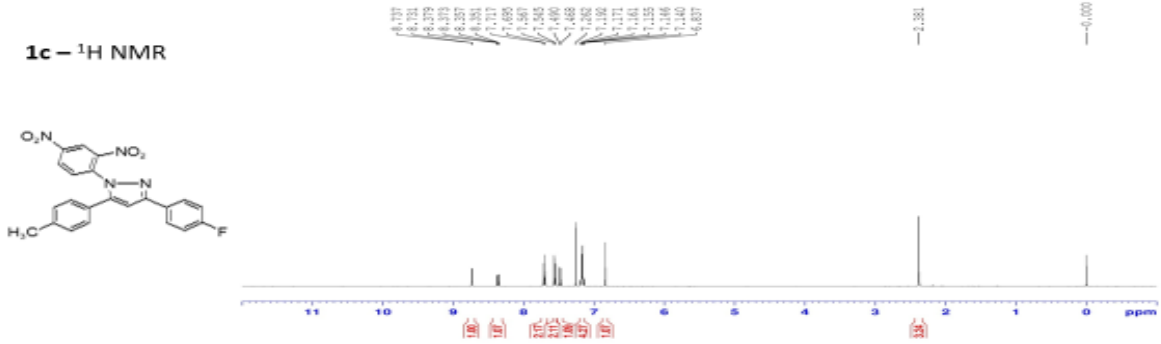

1c – ^{13}C NMR

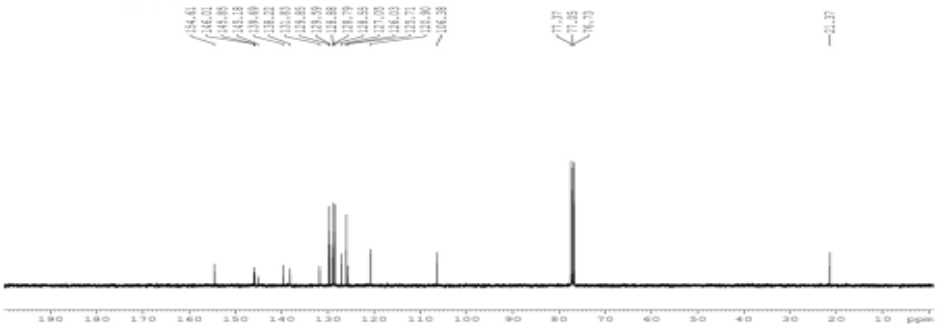

1d – ^{1}H NMR

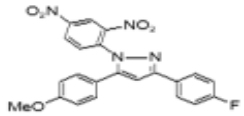

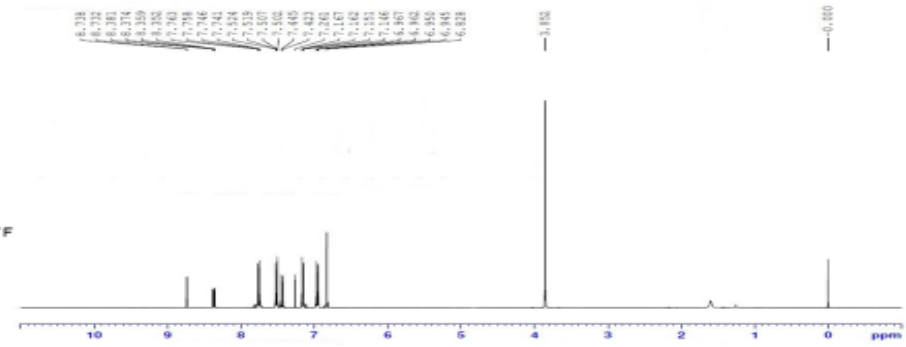

1d – ^{13}C NMR

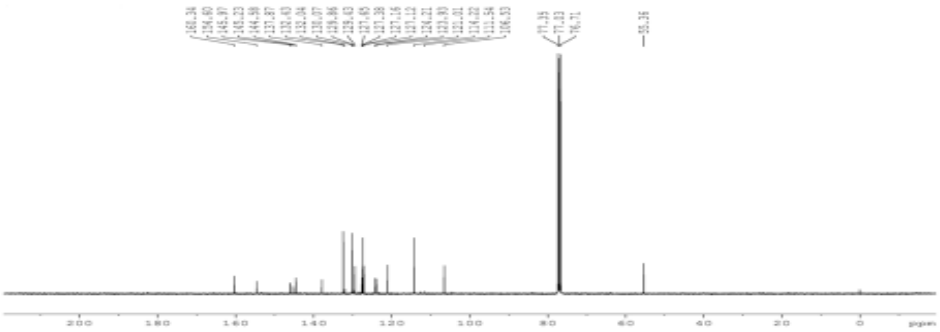

1e – ^{1}H NMR

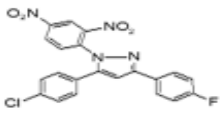

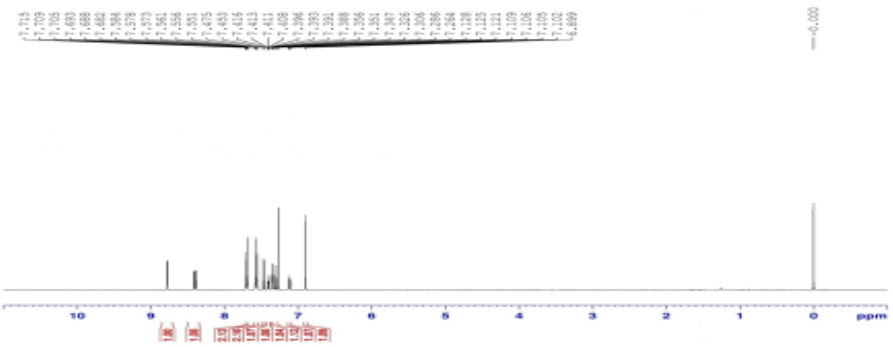

1e – ^{13}C NMR

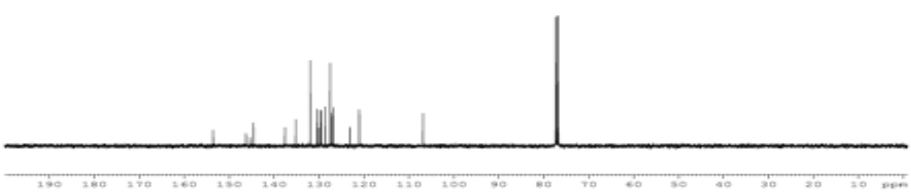

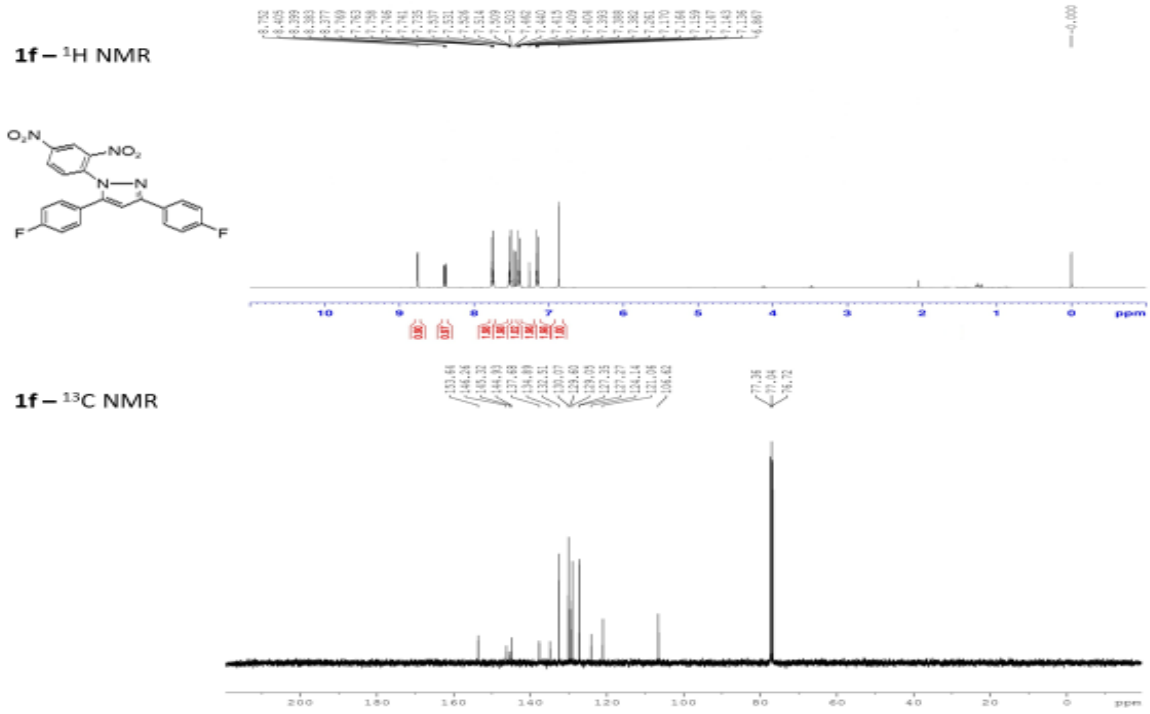

Figure 5.2 ^{1}H NMR and ^{13}C NMR spectral analysis of compounds 1a-1f.

5.4.2 Evaluation of the anti-JEV effect of compounds in cells

Mean cellular toxicity (CC_{50}) of pyrazole derivative 1a was recorded at around 10µM, for 1c, 1d, 1e at around 1µM, whereas CC_{50} values of 1b and 1f were calculated around 50µM and 75µM, respectively (Figure 5.3). Compound 1a showed about 10% reduction in viral plaque at 5µM concentration but was not selected due to high cellular toxicity beyond 10µM (data not shown). Also, no anti-JEV activity were observed with 1c, 1d, or 1e treated cells, at different concentration.

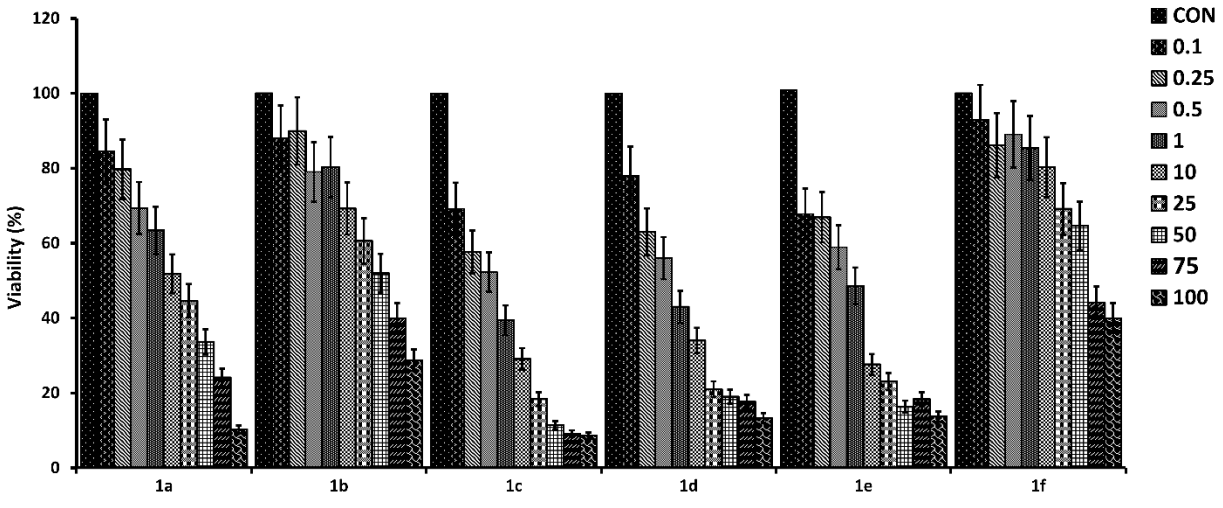

Figure 5.3 Cytotoxicity analyses of six compounds in Neuro2a cells. MTT assay was done after 48hr. Concentrations from 100µM to 100nM were selected for the experiment (**A**). Data are shown as the mean ± SD.

In order to examine the anti-JEV effects of two-hit compounds 1b and 1f, Neuro2a cells infected with JEV at 0.01 MOI were co-treated and post-treated with the compounds separately (Figure 5.4A). At 72 h post-infection, viral titer of the supernatant were calculated through plaque assay by diluting it in ratio 1:10. The results showed up to 70% and 90% less viral particles in post-treated and about 55% to 82% reduced particles in co-treated cells with 1b and 1f, respectively (Figure 5.4B). Viral vRNA from the cells was quantified by qRT-PCR by gene-specific primers and normalized with GAPDH. The results indicated 83%- and 98%-fold decrease in viral vRNA at 72 h with 1b and 1f in post-treated cells (Figure 5.4C). The anti-JEV effect of both compounds was higher in post-treated than in co-treated cells. Concurrent results were observed at the protein level as well. About 60% and 78% reduction in the viral protein was observed in 1b co-treated and post-treated cells, respectively. The 1f treated cells showed more than 95% reduction (Figure 5.4D).

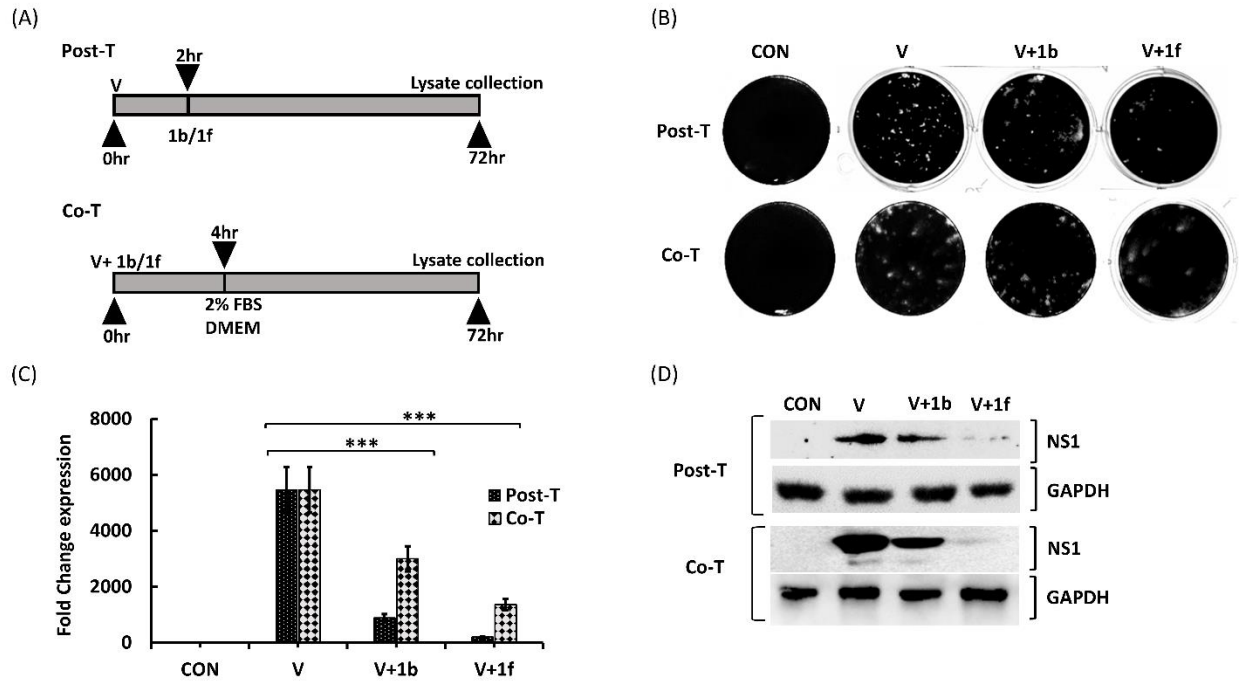

Figure 5.4 Evaluation of antiviral effect of 1b and 1f derivatives in Neuro2a cells. Different treatment groups are marked as: cell control (CON), virus infected (V), virus along with 1b treated cells (V+1b) and virus along with 1f treated (V+1f). Schematic presentation of post-treatment and co-treatment performed for 72 h at 15µM concentration (**A**). Virus titration using plaque assay of supernatant collected from post and co-treated cells after 72 h of incubation (**B**). Real-time analyses of viral RNA using JEV E gene specific amplification (**C**). For all the treated groups CON, V,V+1b, V+1f analyses is done at 72 h time points. GAPDH is used as an internal control and values are represented as mean fold change in multiple of 100 with respect to cell control. *** representing p-value < 0.001. Western blot analyses using JEV NS1 specific monoclonal antibody (GTX633820, GeneTex) and GAPDH (BB-AB0060, BioBharti) as an internal control (**D**). Analyses was done using whole cell lysates after 72 h of treatments. JEV NS1 band is detected at ~45 kDa normalised with protein band of GAPDH at around 37 kDa.

5.4.3 Time and dose-dependent kinetics of JEV in cells

Virus titration in Neuro2a showed maximum inhibition at 96th h with either of the compounds (V+1b and V+1f) treated cells compared to control. A maximum of 6 $\log_{10}$ $TCID_{50}$ value was observed at 96th h for the virus control compared to 5.25 and 4.25 $\log_{10}$ $TCID_{50}$ for compounds 1b and 1f, respectively (Figure 5.5A). Results highlighted slow replication of JEV

from the early phase of infection in compound treated groups. Supernatant from the mock-infected group showed no cytopathic effect.

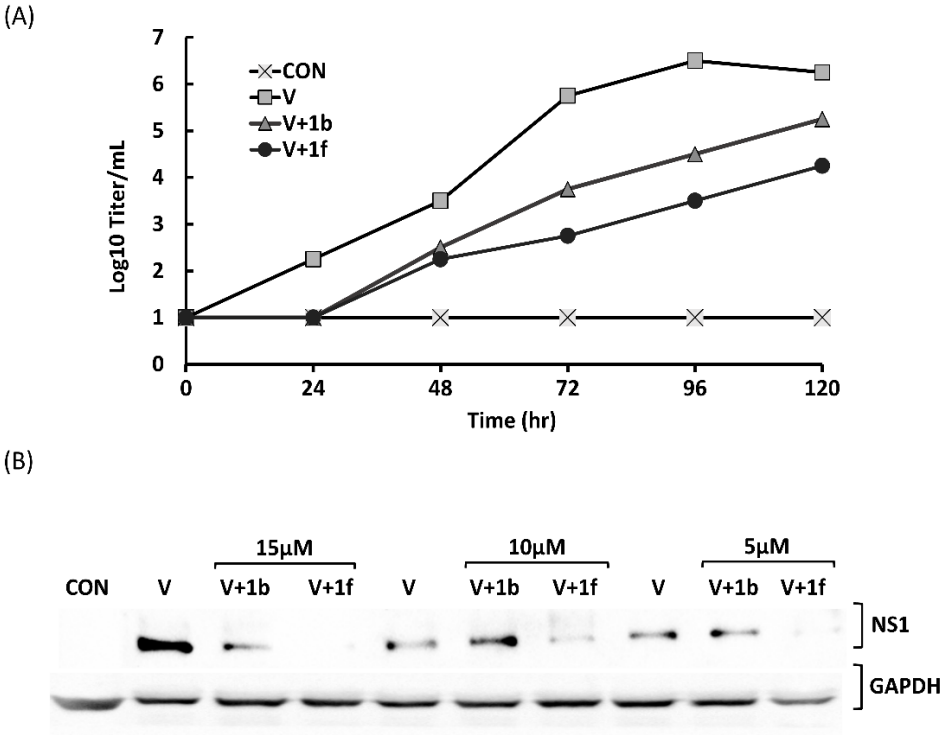

Figure 5.5 Time and Dose-dependent kinetics of JEV in Neuro2a cells. Multi-step growth kinetics of the JEV in Neuro2a cells upon treatment with 15µM of 1b and 1f (**A**). Cells from CON are shown as base line. Supernatant were collected after every 24 h till 120th h post treatment and replaced with equal volume of fresh medium. Virus yield were determined by log_{10} $TCID_{50}$. Standard deviations indicated as error bars. Dose response analyses of JEV from (15 to 5)µM concentration of 1b and 1f (**B**). Western blot analyses with JEV NS1 and GAPDH specific antibody post. Whole cell lysates collected post 72 h of treatment were used for analyses.

Different doses of 1b and 1f treatment were given to Neuro2a cells starting from 15µM to 5µM. Protein analyses from whole cell lysate revealed more reduction in JEV protein with compound 1f as compared to 1b (Figure 5.5B). The decrease in JEV protein was dependent upon the concentration of 1b, while inhibition by 1f was consistent even at lower concentrations.

The IC_{50} value of compound 1b was calculated ~5µM with about 59% reduction in JEV as compared to controls. Compound 1f showed five times lower IC_{50} value than 1b (Figure 5.6 [A, B]). Approximately, 67% reduction in JEV was observed at 1µM concentration suggesting IC_{50} value of 1f to be around <1µM.

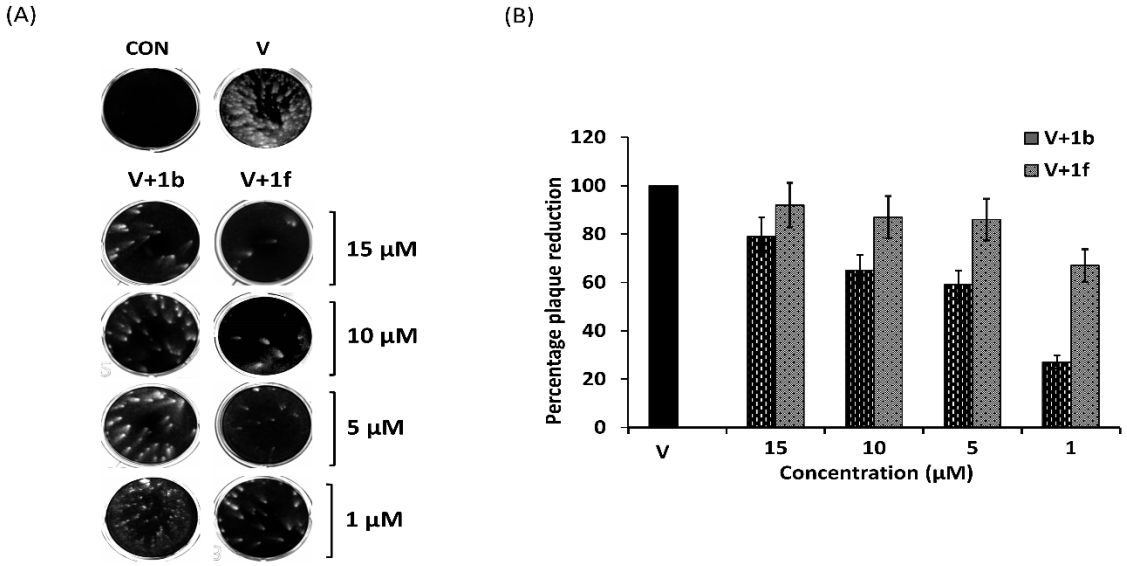

Figure 5.6 Evaluation of IC_{50} value of 1b and 1f through plaque assay at 72th h. (**A**). Graph representing percentage of plaque reduction at 15 µM, 10 µM, 5 µM and 1 µM (**B**).

5.4.4 Anti-JEV potential of 1b and 1f in mice

No significant change in body weight due to intraperitoneal injection of the compound was observed. Also, no change in fur color, tremors or activeness was observed at any time till seven days in either time-escalation or dose-escalation study (Figure 5.7 [A–D]).

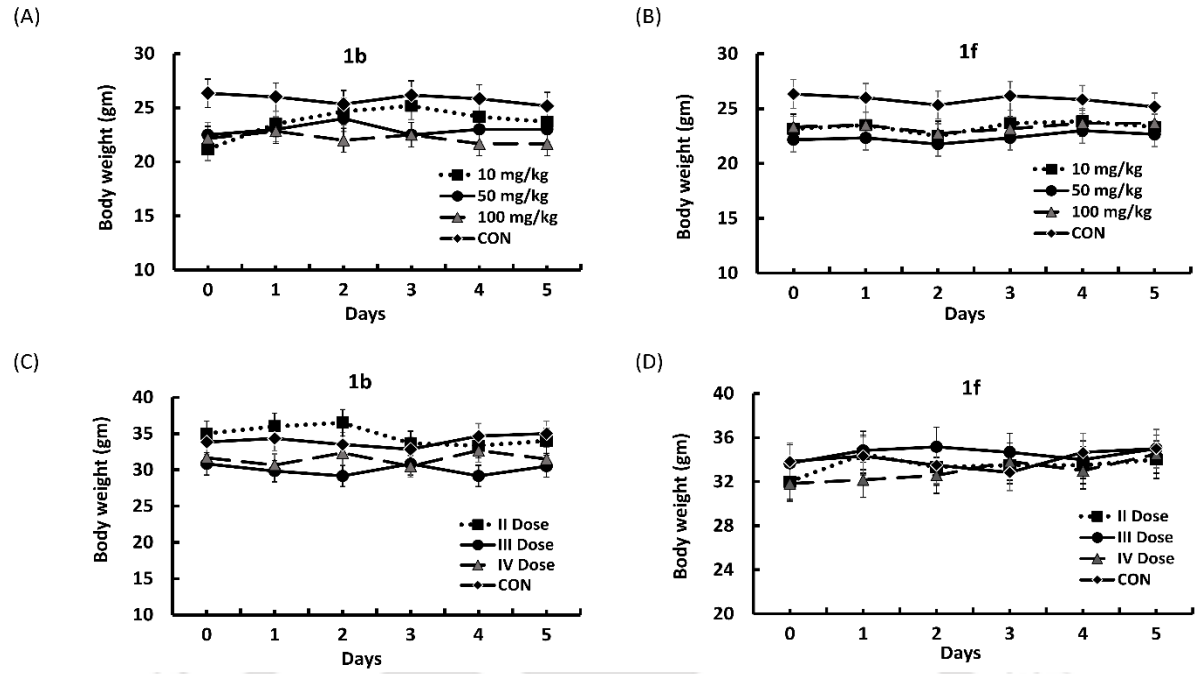

Figure 5.7 Graph representing time escalation study of 1b and 1f in mice (**A-B**). Mice wereinjected intraperitoneal with 10, 50 and 100mg/kg of 1b or 1f first day in different groups (n=3). Mice of control group received DMSO of equal volume. Body weight of each mouse were observed till five days and plotted as mean body weight in grams. Graph representing dose escalation study of compounds in mice (**C-D**). Intraperitoneal injection of 100mg/kg of 1b or 1f were given two, three and four times at 24 h interval in different groups. Body weight of each mouse was observed till 5th day of experiment and plotted in graph as mean body weight in grams

Further, the anti-JEV efficacy was analyzed till five days of antiviral study (Figure 5.8A). No visible symptoms of infection were observed in mice of any group injected with intracerebral JEV at 10^4 PFU/mice. The protective efficacy of compounds on mice was determined by viral RNA quantification through real-time analyses in brain and spleen samples every 24 h. Treatment with either compound 1b or 1f considerably reduced viral RNA by more than 41% and 70% in spleen tissue and about 33% and 43%, respectively, in brain tissue compared to untreated controls. Data suggested reduced JEV replication starting from an early phase of infection with most significant inhibition in the spleen than in the brain (Figure 5.8 [B, C]).

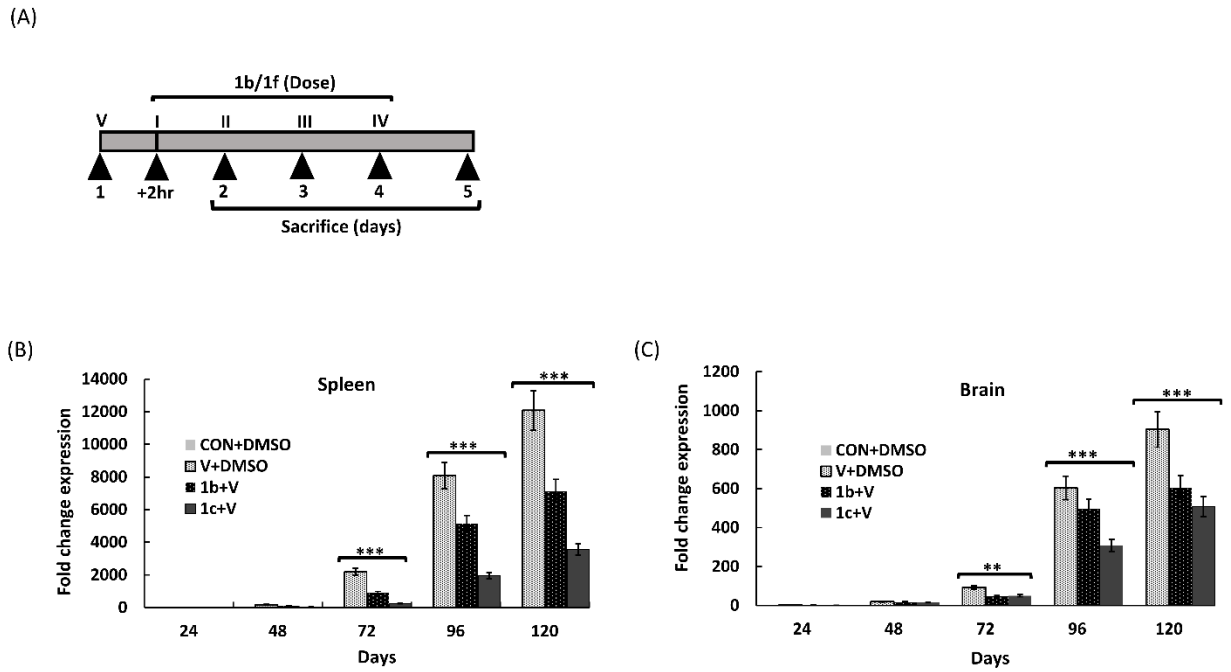

Figure 5.8 Schematic presentation of anti-JEV experiment in mice (**A**). Real time analyses of JEV E viral RNA in spleen (**B**) and brain (**C**) tissues harvested at 24, 48, 72, 96, 120th h time points. Graph representing JEV E RNA fold change in multiple of 100 with respect to group CON+DMSO. GAPDH is used as internal control**.** *** representing p-value < 0.001. Standard deviations indicated as error bars.

5.4.5 Anti-JEV mechanism

The expression of DJ-1 and SQSTM1 proteins were analyzed along with anti-oxidative proteins; HO-1 and NQO1 48 h of post treatment and/or infection. DMSO (solvent in which compound was dissolved) did not show significant modulation of any of the proteins except HO-1 with 0.76-fold decrease compared to mock control. Significant up-regulation of all the proteins were observed post 1b and 1f treatment. DJ-1 and SQSTM1 proteins showed 5.4- and 2.6-folds higher expression compared to untreated/uninfected control for 1b and 1f, respectively. Conversely, JEV infected cells showed a decrease in both the protein level by ~25% compared to untreated and uninfected control. No suppression of DJ-1 or SQSTM1 was observed in JEV infected cells when treated with 1b or 1f compounds (Figure 5.9A). Further, analyses of anti-oxidative proteins, NQO1 and HO-1 indicated a substantial increase by around 14 and 2.9 folds

with either of the compound treatment. In the contrary, no significant difference was observed in either NQO1 or HO-1 in JEV infected cells. Further, flow cytometry analyses was performed to estimate ROS generation post 48 h. About 27% and 32% reduction in median FITC intensity was observed in 1b and 1f treated cells, respectively, compared to untreated and uninfected cells (Figure 5.9B). On the other side, approximately 50% increase in ROS was observed in JEV infected cells. Conversely, no increase in ROS was observed in JEV infected cells post 1b or 1f compound treatment (V+1b, V+1f). Around 15% low FITC intensity was obtained in V+1f treated cells compared to JEV infected cells.

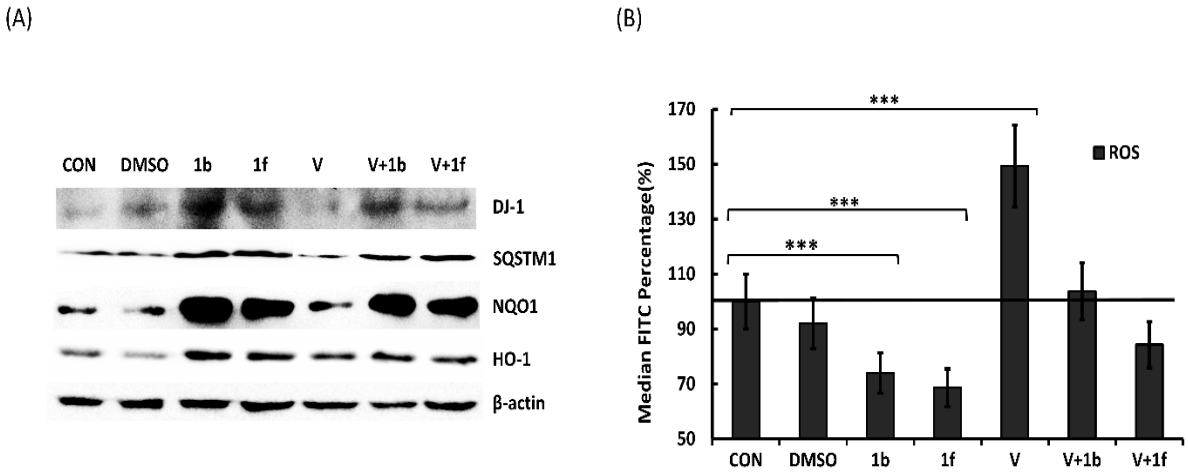

Figure 5.9 Western blot analyses using DJ-1 (SQSTM1 (8025, CST) specific antibody and beta-actin as a loading control (MA1-91399, Invitrogen) at 48th h. **(A).** Flow cytometry analyses to estimate ROS generation in differential treated group with respect to CON group at 48th h in Neuro2a cells **(B).** FITC channel is used to detect fluorescence of DCFH-DA dye. Y-axis representing median FITC intensity**.** Base line drawn at intensity of CON group. *** representing p-value < 0.001

5.5 Discussion

JEV infection causes up-regulation of ROS and down-regulation of endogenous anti-oxidative mechanism (73). The endogenous (or adaptive) anti-oxidants are of both enzymatic and

non-enzymatic molecules. As discussed before, many of these enzymatic anti-oxidants (e.g., NQO1 peroxiredoxins, HO-1, SOD, catalase, and GPx) are encoded by the NRF2 -Keap1 pathway (194). Upon cellular oxidative stress, SQSTM1 prevents Keap1 from binding to NRF2, thereby up-regulation of ARE-containing genes (195, 196). NRF2 has also been found to get stabilized with DJ-1 protein. It is a redox-sensitive protein that triggers activation of anti-oxidant pathway through NRF2/ARE system by ubiquitination and facilitates its nuclear translocation(195, 196). Knockdown of DJ-1 have indicated decrease in NRF2 as well as NRF2 dependent decrease in NQO1, HO-1 enzymes (195, 196)). In the present study, we have tried understanding the anti-oxidative characteristics of synthesized pyrazole derivatives via NRF2-SQSTM1 pathway attributing towards anti-JEV properties.

Out of six pyrazole derivatives, only two compounds 1b and 1f inhibited JEV up to ~70 and ~90%, respectively. We observed a higher reduction of JEV infection in post-treatment than co-treatment probably due to the prevention of re-infection of virus particles present in the supernatant. Further, dose-dependent response of JEV showed significant reduction at protein level even at 5µM concentration of compound 1f. Whereas, with 1b the level of JEV reduction was dependent on concentration and was ineffective at 5µM concentration. Time-dependent kinetics of JEV conferred inhibition from the early stage of viral entry till the late phase of virus replication and release of viral particles. Our study reflects that fluoro substituent is essential for optimal anti-JEV activity. Pyrazole 1f, which contains two fluorine substituents, showed better activity than compound 1b, which has only one fluoro substituent. Further, having established anti-JEV role *in vitro*, we investigated its therapeutic potential in mouse.

In our *in vivo* study, all 3-week old mice infected with up to 10^4 PFU/mouse of SA14-14-2 remained healthy and displayed no clinical signs of JEV infection up to 120^{th} h. In previous

research, high pathogenicity of SA14-14-2 strain was observed when injected via intracerebral route than intraperitoneal or intramuscular route (197). In our study, the intraperitoneal administration of (100mg/kg/day) of 1b and 1f did not affect the visible sign of health and behavior in mice, thus bypassing toxicity limitations. In mouse model, although both of the compounds inhibited JEV infection but did not suppress JEV replication completely. At 120th h notable inhibition by 40.9% and 70.5% in spleen and by 33.3% and 43.7% in brain tissues were achieved by 1b and 1f, respectively. The data suggests that 1f compound suppressed the JEV infection more effectively than 1b and both compounds showed higher inhibition in spleen than in brain tissue. We assume that the distribution and reach of the compounds to different organs or blood brain barrier penetration could be the factor for their limiting performance. Also, the route of virus inoculation or pathogenic nature of JEV strain may influence the extent of inhibition in different tissues. Further work can be done to improve the delivery method or its formulation. In previous studies, anti-JEV effect of Nitazoxanide was shown following its delivery directly to the stomach (198).

In our study, pyrazole compounds 1b and 1f significantly induced the expression of DJ-1 and SQSTM1, thereby mediating NRF2-driven pronounced increase in NQO1 and HO-1 protein level at 48th h of its treatment. Concurrently, opposite (negative) regulation of DJ-1 and SQSTM1 was observed in JEV infected cells. In various studies role of SQSTM1 in flavivirus pathogenesis have been contradictory. During the progression of dengue infection, SQSTM1/p62 levels have been found to reduce via proteasomal degradation. Importantly, stable overexpression of SQSTM1 significantly suppressed dengue replication, suggesting it as a viral restriction factor (199). Dual functionality of SQSTM1 in autophagy and JEV infection supports its role in viral pathogenesis. Increased levels of SQSTM1 are seen in JEV-infected cells and are hypothesized to block

autophagosome maturation and accumulation of misfolded proteins (200, 201). Our results correlate with the findings that SQSTM1 levels in cells are dependent on viral replication or on the stage of infection. Unlike SQSTM1, few studies have been done reporting regulation of DJ-1 in JEV infected cells. Previously, DJ-1 as well as NRF2 mediated expression of thioredoxin, SOD were down-regulated, leading to decrease in ROS scavenging and activation of p38-MAPK induced apoptosis in JEV infected cells (199). In various studies, the role of NQO1 and HO-1 have found to be antiviral and the propagation of RNA viruses like Zika, Dengue, HCV are known to suppress its induction thus bypassing the host antiviral response against increasing ROS (195, 196). In contrast, in our study, JEV infection mediated DJ-1 and SQSTM1 down-regulation did not affect the NRF2 mediated regulation of downstream proteins like NQO1 or HO-1. We hypothesize that, depending on the cellular contexts and oxidative stress levels, viral infection exerts a differential influence on the NRF2 pathway. Apart from this report conflicting results overturned the findings describing the up-regulation of NQO1 and HO-1 in most of the viral infections (199). Studies have confirmed the mechanism of detoxification by NQO1 is based on the two electron mediated reduction of quinones to hydroquinones and bypassing semiquinone radical via redox cycling reactions (199). On the other side, HO-1 is a stress-inducible enzyme that catabolizes heme into biliverdin, ferrous iron, and carbon monoxide contributing to the cytoprotective effect of HO-1 by acting as anti-oxidant, anti-inflammatory, and immunomodulatory molecules (199). Our results showed marked decrease in ROS (27% and 32%) in 1b or 1f treated cells via NRF2 downstream up-regulation of NQO1 and HO-1, respectively. Altogether, even slight increase in DJ-1 and SQSTM1 protein significantly induced NQO1 and HO-1 by 14-fold and 3-fold compared to mock-treated cells. The activity of our compounds corresponds to interlocked positive feedback loops of NRF2-SQSTM1 signaling mechanism

(196). In previous reports, pyrazole itself have been shown to increase both, nuclear NRF2 protein level and NRF2-ARE binding activity in both *in vitro* as well as *in vivo* systems, indicating the vast target potential of pyrazole derivatives (131, 202).

Among many reported studies, few pyrazole derivatives were found to be ineffective, similar to our compounds 1a, 1c, 1d, and 1e (142). In this study, we have used the most prevailing synthetic route known for the synthesis of 1,3,5-trisubstituted pyrazole which includes annulations initiated by condensation of 1,3-diketones with hydrazines, 1,3-dipolar cycloaddition of diazo compounds with alkynes from aryl hydrazones and the reaction of α, β-unsaturated aldehydes and ketones with hydrazines (203-207). In our previous study, we have synthesized similar series of 1,3,5-trisubstituted pyrazole derivatives and were screened biologically against different cancer cells (208).

Many recently reported anti-JEV compounds are found to be active against multiple viruses (198, 209). Since, 1b and 1f have been found to be more effective in inhibiting JEV infection both in neuronal cells and in mouse, these may impart a possibility for developing therapeutics against other flaviviruses. Antiviral therapies based on anti-oxidants could provide potential targets for generating therapeutics against JEV. Compounds with direct radical scavenging properties or modulating anti-oxidative enzymes like SOD, catalase, GPx, GST can be explored for their likely antiviral effects.

Chapter 6. Conclusions

JEV is a serious vector-borne cause of encephalitis and a major public health problem leading to high morbidity and mortality. Within endemic areas, it leads to approximately 25-30% rate mortality and severe residual neurological or psychiatric complications (6). Neurological complications associated with the critical phase of the illness include encephalopathy, movement disorders such as parkinsonism (46, 47). Parkinsonism includes symptoms like tremors, a masked face, microphonia, impaired consciousness, saccadic eye tracking and neck stiffness (48, 49). Since there are no therapeutics for the treatment of JEV infected patients, identifying a biomarker could be a way forward to develop its therapeutics and diagnostics.

Neuron-specific proteins in JEV infection play major role in JEV prognosis in CNS. The normal function of α-syn is associated with synapses, such as synaptic plasticity, neurotransmitter release, dopamine metabolism, and vesicle trafficking α-syn. However, this protein has been directly and indirectly linked with JEV pathogenesis. Overexpression of α-syn is reported in the brain of JEV-infected patients. Also, JEV exploits dopamine signaling and modulates its level to facilitate viral infection, which is regulated by α-syn protein.

Thus, we tried to understand the role of α-syn in JEV replication, including the mechanism, phosphorylation, and oligomerization. We also focused on utilizing a similar mechanism to design anti-JEV therapeutic candidates and characterize them *in vitro* and *in vivo*. Our results suggested that α-syn exerts an anti-JEV effect by regulating protein involved in oxidative stress inside neuronal cells. Briefly, we found significant increase in endogenous α-syn expression in JEV-infected cells. Additionally, treatment with Exoα-syn led to a substantial reduction in JEV replication, suggesting its anti-viral effect. Furthermore, Exoα-syn treatment led to the

upregulation of SOD1 and reduction in ROS. The results were validated by endogenous α-syn-silencing, which decreased SOD1 and raised ROS levels in neuronal cells. Similarly, the SOD1 inhibition via LCS-1 also intensified ROS and JEV infection.

Further, an increase in endogenous α-syn expression in JEV-infected neuro2a, leads to its altered α-synS129 phosphorylation and formation of α-syn oligomers. Our study revealed protein expression of phosphokinases like PLK2 and CK2 that are found to regulate α-syn were significantly downregulated, specifically at late phase of JEV replication. Parallelly, we observed significant decrease in pα-synS129 in JEV-infected cells. Since the interplay between phosphorylation and the non-phosphorylated state of α-syn has been important in gene transcriptional regulation, we hypothesize that it might increase SOD1 gene expression as shown in our first objective. Further, the oligomerization of α-syn in JEV-infected cells was increased compared to non-infected neuro2a cells.

The modulation of anti-oxidative pathways could be a way to interfere with JEV replication. Thus, we analyzed new series of dinitroaryl substituted derivatives of pyrazole moiety that can directly modulate anti-oxidative pathway. We. Out of six tested pyrazole derivatives, only two compounds showed anti-JEV effect. Pyrazole compounds significantly induced the expression of DJ-1 and SQSTM1, which were otherwise negatively regulated in JEV-infected cells. Our results indicated anti-oxidative properties of pyrazoles derivatives through up-regulation of NQO1 and HO-1 leading to marked decrease in ROS. The activity of our compounds corresponds to interlocked positive feedback loops of NRF2-SQSTM1 signaling mechanism. The combined results of all objectives reflect the molecular and functional insight of the anti-JEV role of cellular anti-oxidative machinery, which can be modulated via endogenous neuronal protein like α-syn or directly by exogenous pyrazole compounds.

Chapter 7. Future prospects

The present study ponders on the functional characterization of α-syn in JEV replication and probable therapeutic candidates against its infection.

The study revealed the anti-viral role of α-syn via modulating SOD1 protein. Since the normal function of α-syn is found to be related to synaptic plasticity, we hypothesize multiple roles of α-syn in JEV pathogenesis. Hence, an elaborate study is required to be performed to analyze all other aspects. Notably, we have not investigated the role of aggregated α-syn or LBs in JEV infection. Therefore, in viral pathogenesis, it remains an important question to answer. In depth *in vivo* study will provide molecular details of α-synucleinopathy in JEV infection.

Apart from current study, α-syn is reported to modulate ER stress pathway (101). The levels of activating transcription factor 6 (Atf6), protein disulfide isomerase (PDI), and phosphorylated eIF2α proteins, all of which support viral infection in WNV, were significantly increased in α-syn-knockout primary cortical neurons (101). Also, the detailed analyses of mutated α-syn like A53T, A30P can deliver a broader understanding of functional characteristics of α-syn in JEV replication. Also, our findings corroborate with the previous studies indicating the unrelated behavior of pα-synS129 with the oligomerization of α-syn. This can be validated using a mouse model or in clinical samples.

In the present study, we examined temporal expression of cellular CK2 and PLK2. However, other kinases like GRK5, PLK1 are left to be investigated. The relation of pα-synS129 in JE progression is still left to be uncovered. Additionally, *in vitro* and *in vivo* analyses of the antiviral activity of pyrazole compounds highlighted their potential to develop therapeutics against JEV. However, its role in other flaviviruses like WNV, DENV are yet to be analyzed.

Additionally, pyrazole derivatives modulating α-syn expression can be an interesting area to explore. Antiviral therapies based on anti-oxidants could provide potential targets for generating therapeutics against JEV. Compounds with direct radical scavenging properties or modulating anti-oxidative enzymes like SOD, catalase, GPx, GST can be explored for their likely antiviral effects.

Bibliography

1. Bandyopadhyay B, Bhattacharyya I, Adhikary S, Mondal S, Konar J, Dawar N, Biswas A, Bhattacharya N. 2013. Incidence of Japanese encephalitis among acute encephalitis syndrome cases in West Bengal, India. Biomed Res Int 2013:896749.
2. Kumar R, Mathur A, Kumar A, Sharma S, Saksena PN, Chaturvedi UC. 1988. Japanese encephalitis--an important cause of acute childhood encephalopathy in Lucknow, India. Postgrad Med J 64:18-22.
3. Schweitzer BK, Chapman NM, Iwen PC. 2009. Overview of the With an Emphasis on the Japanese Encephalitis Group Viruses. Labmedicine 40:493-499.
4. Solomon T, Ni H, Beasley DW, Ekkelenkamp M, Cardosa MJ, Barrett AD. 2003. Origin and evolution of Japanese encephalitis virus in southeast Asia. J Virol 77:3091-8.
5. Kabilan L, Rajendran R, Arunachalam N, Ramesh S, Srinivasan S, Samuel PP, Dash AP. 2004. Japanese encephalitis in India: an overview. Indian J Pediatr 71:609-15.
6. Upadhyay RK. 2013. Japanese Encephalitis Virus Generated Neurovirulence, Antigenicity, and Host Immune Responses. International Scholarly Research Notices 2013:1-24.
7. Ghosh D, Basu A. 2009. Japanese Encephalitis - A Pathological and Clinical Perspective. Plos Neglected Tropical Diseases 3.
8. Sumiyoshi H, Mori C, Fuke I, Morita K, Kuhara S, Kondou J, Kikuchi Y, Nagamatu H, Igarashi A. 1987. Complete nucleotide sequence of the Japanese encephalitis virus genome RNA. Virology 161:497-510.
9. de Leeuw O, Peeters B. 1999. Complete nucleotide sequence of Newcastle disease virus:: evidence for the existence of a new genus within the subfamily. Journal of General Virology 80:131-136.
10. Sahoo GC, Dikhit MR, Das P. 2008. Functional assignment to JEV proteins using SVM. Bioinformation 3:1-7.
11. Villordo SM, Gamarnik AV. 2009. Genome cyclization as strategy for flavivirus RNA replication. Virus Research 139:230-239.
12. Mukhopadhyay S, Kuhn RJ, Rossmann MG. 2005. A structural perspective of the life cycle. Nature Reviews Microbiology 3:13-22.
13. Zhang Y, Corver J, Chipman PR, Zhang W, Pletnev SV, Sedlak D, Baker TS, Strauss JH, Kuhn RJ, Rossmann MG. 2003. Structures of immature flavivirus particles. EMBO J 22:2604-13.
14. Chang HH, Huber RG, Bond PJ, Grad YH, Camerini D, Maurer-Stroh S, Lipsitch M. 2017. Systematic analysis of protein identity between Zika virus and other arthropod-borne viruses. Bulletin of the World Health Organization 95:517-525.
15. Zai J, Mei L, Wang C, Cao S, Fu ZF, Chen H, Song Y. 2013. N-glycosylation of the premembrane protein of Japanese encephalitis virus is critical for folding of the envelope protein and assembly of virus-like particles. Acta Virologica 57:27-33.
16. Kolaskar AS, Kulkarni-Kale U. 1999. Prediction of three-dimensional structure and mapping of conformational epitopes of envelope glycoprotein of Japanese encephalitis virus. Virology 261:31-42.
17. Luca VC, AbiMansour J, Nelson CA, Fremont DH. 2012. Crystal Structure of the Japanese Encephalitis Virus Envelope Protein. Journal of Virology 86:2337-2346.

18. Gritsun TS, Holmes EC, Gould EA. 1995. Analysis of Flavivirus Envelope Proteins Reveals Variable Domains That Reflect Their Antigenicity and May Determine Their Pathogenesis. Virus Research 35:307-321.
19. Bollati M, Alvarez K, Assenberg R, Baronti C, Canard B, Cook S, Coutard B, Decroly E, de Lamballerie X, Gould EA, Grard G, Grimes JM, Hilgenfeld R, Jansson AM, Malet H, Mancini EJ, Mastrangelo E, Mattevi A, Milani M, Moureau G, Neyts J, Owens RJ, Ren JS, Selisko B, Speroni S, Steuber H, Stuart DI, Unge T, Bolognesi M. 2010. Structure and functionality in flavivirus NS-proteins: Perspectives for drug design. Antiviral Research 87:125-148.
20. Poonsiri T, Wright GSA, Diamond MS, Turtle L, Solomon T, Antonyuk SV. 2018. Structural Study of the C-Terminal Domain of Nonstructural Protein 1 from Japanese Encephalitis Virus. Journal of Virology 92.
21. Liu WJ, Wang XJ, Clark DC, Lobigs M, Hall RA, Khromykh AA. 2006. A single amino acid substitution in the West Nile virus nonstructural protein NS2A disables its ability to inhibit alpha/beta interferon induction and attenuates virus virulence in mice. J Virol 80:2396-404.
22. Liu WJ, Wang XJ, Mokhonov VV, Shi PY, Randall R, Khromykh AA. 2005. Inhibition of interferon signaling by the New York 99 strain and Kunjin subtype of West Nile virus involves blockage of STAT1 and STAT2 activation by nonstructural proteins. J Virol 79:1934-42.
23. Kummerer BM, Rice CM. 2002. Mutations in the yellow fever virus nonstructural protein NS2A selectively block production of infectious particles. J Virol 76:4773-84.
24. Leung JY, Pijlman GP, Kondratieva N, Hyde J, Mackenzie JM, Khromykh AA. 2008. Role of nonstructural protein NS2A in flavivirus assembly. J Virol 82:4731-41.
25. Edward Z, Takegami T. 1993. Localization and functions of Japanese encephalitis virus nonstructural proteins NS3 and NS5 for viral RNA synthesis in the infected cells. Microbiol Immunol 37:239-43.
26. Mackenzie J. 2005. Wrapping things up about virus RNA replication. Traffic 6:967-77.
27. Youn S, Li T, McCune BT, Edeling MA, Fremont DH, Cristea IM, Diamond MS. 2012. Evidence for a Genetic and Physical Interaction between Nonstructural Proteins NS1 and NS4B That Modulates Replication of West Nile Virus. Journal of Virology 86:7360-7371.
28. Zmurko J, Neyts J, Dallmeier K. 2015. Flaviviral NS4b, chameleon and jack-in-the-box roles in viral replication and pathogenesis, and a molecular target for antiviral intervention. Rev Med Virol 25:205-23.
29. Ray D, Shah A, Tilgner M, Guo Y, Zhao YW, Dong HP, Deas TS, Zhou YS, Li HM, Shi PY. 2006. West nile virus 5′-cap structure is formed by sequential guanine N-7 and ribose 2′-O methylations by nonstructural protein 5. Journal of Virology 80:8362-8370.
30. Zhou Y, Ray D, Zhao Y, Dong H, Ren S, Li Z, Guo Y, Bernard KA, Shi PY, Li H. 2007. Structure and function of flavivirus NS5 methyltransferase. J Virol 81:3891-903.
31. Miyake M. 1964. The Pathology of Japanese Encephalitis. A Review. Bull World Health Organ 30:153-60.
32. Solomon T. 2006. Control of Japanese encephalitis--within our grasp? N Engl J Med 355:869-71.
33. Paranjpe S, Banerjee K. 1996. Phylogenetic analysis of the envelope gene of Japanese encephalitis virus. Virus Res 42:107-17.

34. Uchil PD, Satchidanandam V. 2001. Phylogenetic analysis of Japanese encephalitis virus: Envelope gene based analysis reveals a fifth genotype, geographic clustering, and multiple introductions of the virus into the Indian subcontinent. American Journal of Tropical Medicine and Hygiene 65:242-251.
35. Nawa M, Takasaki T, Yamada KI, Kurane I, Akatsuka T. 2003. Interference in Japanese encephalitis virus infection of Vero cells by a cationic amphiphilic drug, chlorpromazine. J Gen Virol 84:1737-1741.
36. Chu PWG, Westaway EG. 1985. Replication Strategy of Kunjin Virus - Evidence for Recycling Role of Replicative Form Rna as Template in Semiconservative and Asymmetric Replication. Virology 140:68-79.
37. Chambers TJ, Hahn CS, Galler R, Rice CM. 1990. Flavivirus genome organization, expression, and replication. Annu Rev Microbiol 44:649-88.
38. Kim YG, Yoo JS, Kim JH, Kim CM, Oh JW. 2007. Biochemical characterization of a recombinant Japanese encephalitis virus RNA-dependent RNA polymerase. BMC Mol Biol 8:59.
39. Yun SI, Choi YJ, Song BH, Lee YM. 2009. 3′-Acting Elements That Contribute to the Competence and Efficiency of Japanese Encephalitis Virus Genome Replication: Functional Importance of Sequence Duplications, Deletions, and Substitutions. Journal of Virology 83:7909-7930.
40. van den Hurk AF, Ritchie SA, Mackenzie JS. 2009. Ecology and geographical expansion of Japanese encephalitis virus. Annu Rev Entomol 54:17-35.
41. Kimura-Kuroda J, Ichikawa M, Ogata A, Nagashima K, Yasui K. 1993. Specific tropism of Japanese encephalitis virus for developing neurons in primary rat brain culture. Arch Virol 130:477-84.
42. Yang KD, Yeh WT, Chen RF, Chuon HL, Tsai HP, Yao CW, Shaio MF. 2004. A model to study neurotropism and persistency of Japanese encephalitis virus infection in human neuroblastoma cells and leukocytes. J Gen Virol 85:635-642.
43. Ghosh D, Basu A. 2009. Japanese encephalitis-a pathological and clinical perspective. PLoS Negl Trop Dis 3:e437.
44. Basumatary LJ, Raja D, Bhuyan D, Das M, Goswami M, Kayal AK. 2013. Clinical and radiological spectrum of Japanese encephalitis. J Neurol Sci 325:15-21.
45. Srivastava R, Kalita J, Khan MY, Gore MM, Bondre VP, Misra UK. 2013. Temporal changes of Japanese encephalititis virus in different brain regions of rat. Indian J Med Res 138:219-23.
46. Tadokoro K, Ohta Y, Sato K, Maeki T, Sasaki R, Takahashi Y, Shang J, Takemoto M, Hishikawa N, Yamashita T, Lim CK, Tajima S, Abe K. 2018. A Japanese Encephalitis Patient Presenting with Parkinsonism with Corresponding Laterality of Magnetic Resonance and Dopamine Transporter Imaging Findings. Intern Med 57:2243-2246.
47. Misra UK, Kalita J. 2002. Prognosis of Japanese encephalitis patients with dystonia compared to those with parkinsonian features only. Postgrad Med J 78:238-41.
48. DeMaagd G, Philip A. 2015. Parkinson's Disease and Its Management: Part 1: Disease Entity, Risk Factors, Pathophysiology, Clinical Presentation, and Diagnosis. P T 40:504-32.
49. Jankovic J, Tan EK. 2020. Parkinson's disease: etiopathogenesis and treatment. J Neurol Neurosurg Psychiatry 91:795-808.

50. Limphaibool N, Iwanowski P, Holstad MJV, Kobylarek D, Kozubski W. 2019. Infectious Etiologies of Parkinsonism: Pathomechanisms and Clinical Implications. Front Neurol 10:652.
51. Hopkins HK, Traverse EM, Barr KL. 2022. Viral Parkinsonism: An underdiagnosed neurological complication of Dengue virus infection. PLoS Negl Trop Dis 16:e0010118.
52. Kimurakuroda J, Ichikawa M, Ogata A, Nagashima K, Yasui K. 1993. Specific Tropism of Japanese Encephalitis-Virus for Developing Neurons in Primary Rat-Brain Culture. Archives of Virology 130:477-484.
53. Chen T, He X, Zhang P, Yuan Y, Lang X, Yu J, Qin Z, Li X, Zhang Q, Zhu L, Zhang B, Wu Q, Zhao W. 2019. Research advancements in the neurological presentation of flaviviruses. Rev Med Virol 29:e2021.
54. Laureti M, Narayanan D, Rodriguez-Andres J, Fazakerley JK, Kedzierski L. 2018. Flavivirus Receptors: Diversity, Identity, and Cell Entry. Front Immunol 9:2180.
55. Perez RG, Waymire JC, Lin E, Liu JJ, Guo F, Zigmond MJ. 2002. A role for alpha-synuclein in the regulation of dopamine biosynthesis. J Neurosci 22:3090-9.
56. Butler B, Saha K, Rana T, Becker JP, Sambo D, Davari P, Goodwin JS, Khoshbouei H. 2015. Dopamine Transporter Activity Is Modulated by alpha-Synuclein. J Biol Chem 290:29542-54.
57. Lee FJ, Liu F, Pristupa ZB, Niznik HB. 2001. Direct binding and functional coupling of alpha-synuclein to the dopamine transporters accelerate dopamine-induced apoptosis. FASEB J 15:916-26.
58. Sidhu A, Wersinger C, Vernier P. 2004. alpha-Synuclein regulation of the dopaminergic transporter: a possible role in the pathogenesis of Parkinson's disease. FEBS Lett 565:1-5.
59. Burre J, Sharma M, Sudhof TC. 2018. Cell Biology and Pathophysiology of alpha-Synuclein. Cold Spring Harb Perspect Med 8.
60. Bussell R, Jr., Eliezer D. 2003. A structural and functional role for 11-mer repeats in alpha-synuclein and other exchangeable lipid binding proteins. J Mol Biol 329:763-78.
61. Liu C, Zhao Y, Xi H, Jiang J, Yu Y, Dong W. 2021. The Membrane Interaction of Alpha-Synuclein. Front Cell Neurosci 15:633727.
62. Pfefferkorn CM, Jiang Z, Lee JC. 2012. Biophysics of alpha-synuclein membrane interactions. Biochim Biophys Acta 1818:162-71.
63. Fusco G, De Simone A, Gopinath T, Vostrikov V, Vendruscolo M, Dobson CM, Veglia G. 2014. Direct observation of the three regions in α-synuclein that determine its membrane-bound behaviour. Nature Communications 5.
64. Bisi N, Feni L, Peqini K, Perez-Pena H, Ongeri S, Pieraccini S, Pellegrino S. 2021. alpha-Synuclein: An All-Inclusive Trip Around its Structure, Influencing Factors and Applied Techniques. Front Chem 9:666585.
65. Kanaan NM, Manfredsson FP. 2012. Loss of functional alpha-synuclein: a toxic event in Parkinson's disease? J Parkinsons Dis 2:249-67.
66. Li J, Uversky VN, Fink AL. 2001. Effect of familial Parkinson's disease point mutations A30P and A53T on the structural properties, aggregation, and fibrillation of human alpha-synuclein. Biochemistry 40:11604-13.
67. Ono K, Ikeda T, Takasaki J, Yamada M. 2011. Familial Parkinson disease mutations influence alpha-synuclein assembly. Neurobiol Dis 43:715-24.
68. Westphal CH, Chandra SS. 2013. Monomeric synucleins generate membrane curvature. J Biol Chem 288:1829-40.

69. Mizuno N, Varkey J, Kegulian NC, Hegde BG, Cheng N, Langen R, Steven AC. 2012. Remodeling of lipid vesicles into cylindrical micelles by alpha-synuclein in an extended alpha-helical conformation. J Biol Chem 287:29301-11.
70. Oueslati A, Fournier M, Lashuel HA. 2010. Role of post-translational modifications in modulating the structure, function and toxicity of alpha-synuclein: implications for Parkinson's disease pathogenesis and therapies. Prog Brain Res 183:115-45.
71. Mittal M, Siddiqui MR, Tran K, Reddy SP, Malik AB. 2014. Reactive oxygen species in inflammation and tissue injury. Antioxid Redox Signal 20:1126-67.
72. Schieber M, Chandel NS. 2014. ROS function in redox signaling and oxidative stress. Curr Biol 24:R453-62.
73. Zhang Z, Rong L, Li YP. 2019. Flaviviridae Viruses and Oxidative Stress: Implications for Viral Pathogenesis. Oxid Med Cell Longev 2019:1409582.
74. Schneider WM, Hoffmann HH. 2022. Flavivirus-host interactions: an expanding network of proviral and antiviral factors. Curr Opin Virol 52:71-77.
75. Srivastava S, Khanna N, Saxena SK, Singh A, Mathur A, Dhole TN. 1999. Degradation of Japanese encephalitis virus by neutrophils. Int J Exp Pathol 80:17-24.
76. Raung SL, Kuo MD, Wang YM, Chen CJ. 2001. Role of reactive oxygen intermediates in Japanese encephalitis virus infection in murine neuroblastoma cells. Neurosci Lett 315:9-12.
77. Liao SL, Raung SL, Chen CJ. 2002. Japanese encephalitis virus stimulates superoxide dismutase activity in rat glial cultures. Neurosci Lett 324:133-6.
78. Lin RJ, Liao CL, Lin YL. 2004. Replication-incompetent virions of Japanese encephalitis virus trigger neuronal cell death by oxidative stress in a culture system. Journal of General Virology 85:521-533.
79. Ghoshal A, Das S, Ghosh S, Mishra MK, Sharma V, Koli P, Sen E, Basu A. 2007. Proinflammatory mediators released by activated microglia induces neuronal death in Japanese encephalitis. Glia 55:483-96.
80. Kumar S, Misra UK, Kalita J, Khanna VK, Khan MY. 2009. Imbalance in oxidant/antioxidant system in different brain regions of rat after the infection of Japanese encephalitis virus. Neurochem Int 55:648-54.
81. Al-Alimi AA, Ali SA, Al-Hassan FM, Idris FM, Teow SY, Mohd Yusoff N. 2014. Dengue virus type 2 (DENV2)-induced oxidative responses in monocytes from glucose-6-phosphate dehydrogenase (G6PD)-deficient and G6PD normal subjects. PLoS Negl Trop Dis 8:e2711.
82. Basu M, Courtney SC, Brinton MA. 2017. Arsenite-induced stress granule formation is inhibited by elevated levels of reduced glutathione in West Nile virus-infected cells. Plos Pathogens 13.
83. Kuzmenko YV, Smirnova OA, Ivanov AV, Starodubova ES, Karpov VL. 2016. Nonstructural Protein 1 of Tick-Borne Encephalitis Virus Induces Oxidative Stress and Activates Antioxidant Defense by the Nrf2/ARE Pathway. Intervirology 59:111-117.
84. Li G, Poulsen M, Fenyvuesvolgyi C, Yashiroda Y, Yoshida M, Simard JM, Gallo RC, Zhao RY. 2017. Characterization of cytopathic factors through genome-wide analysis of the Zika viral proteins in fission yeast. Proceedings of the National Academy of Sciences of the United States of America 114:E376-E385.
85. Olagnier D, Peri S, Steel C, van Montfoort N, Chiang C, Beljanski V, Slifker M, He Z, Nichols CN, Lin R, Balachandran S, Hiscott J. 2014. Cellular oxidative stress response

controls the antiviral and apoptotic programs in dengue virus-infected dendritic cells. PLoS Pathog 10:e1004566.
86. Yang TC, Lai CC, Shiu SL, Chuang PH, Tzou BC, Lin YY, Tsai FJ, Lin CW. 2010. Japanese encephalitis virus down-regulates thioredoxin and induces ROS-mediated ASK1-ERK/p38 MAPK activation in human promonocyte cells. Microbes Infect 12:643-51.
87. Guo C, Sun L, Chen X, Zhang D. 2013. Oxidative stress, mitochondrial damage and neurodegenerative diseases. Neural Regen Res 8:2003-14.
88. Higuchi M, Honda T, Proske RJ, Yeh ET. 1998. Regulation of reactive oxygen species-induced apoptosis and necrosis by caspase 3-like proteases. Oncogene 17:2753-60.
89. Mishra MK, Kumawat KL, Basu A. 2008. Japanese encephalitis virus differentially modulates the induction of multiple pro-inflammatory mediators in human astrocytoma and astroglioma cell-lines. Cell Biol Int 32:1506-13.
90. El Safadi D, Paulo-Ramos A, Hoareau M, Roche M, Krejbich-Trotot P, Viranaicken W, Lebeau G. 2023. The Influence of Metabolism on Immune Response: A Journey to Understand Immunometabolism in the Context of Viral Infection. Viruses 15.
91. Ighodaro O, Akinloye O. 2018. First line defence antioxidants-superoxide dismutase (SOD), catalase (CAT) and glutathione peroxidase (GPX): Their fundamental role in the entire antioxidant defence grid. Alexandria journal of medicine 54:287-293.
92. Kaspar JW, Niture SK, Jaiswal AK. 2009. Nrf2:INrf2 (Keap1) signaling in oxidative stress. Free Radic Biol Med 47:1304-9.
93. Kageyama S, Gudmundsson SR, Sou YS, Ichimura Y, Tamura N, Kazuno S, Ueno T, Miura Y, Noshiro D, Abe M, Mizushima T, Miura N, Okuda S, Motohashi H, Lee JA, Sakimura K, Ohe T, Noda NN, Waguri S, Eskelinen EL, Komatsu M. 2021. p62/SQSTM1-droplet serves as a platform for autophagosome formation and anti-oxidative stress response. Nature Communications 12.
94. Gan L, Johnson DA, Johnson JA. 2010. Keap1-Nrf2 activation in the presence and absence of DJ-1. Eur J Neurosci 31:967-77.
95. Im JY, Lee KW, Woo JM, Junn E, Mouradian MM. 2012. DJ-1 induces thioredoxin 1 expression through the Nrf2 pathway. Human Molecular Genetics 21:3013-3024.
96. Clements CM, McNally RS, Conti BJ, Mak TW, Ting JP. 2006. DJ-1, a cancer- and Parkinson's disease-associated protein, stabilizes the antioxidant transcriptional master regulator Nrf2. Proc Natl Acad Sci U S A 103:15091-6.
97. Vazquez C, Jurado KA. 2022. Neurotropic RNA Virus Modulation of Immune Responses within the Central Nervous System. Int J Mol Sci 23.
98. Goldstein L, Fogel-Grinvald H, Steiner I. 2019. Hepatitis B and C virus infection as a risk factor for Parkinson's disease in Israel-A nationwide cohort study. J Neurol Sci 398:138-141.
99. Tsai HH, Liou HH, Muo CH, Lee CZ, Yen RF, Kao CH. 2016. Hepatitis C virus infection as a risk factor for Parkinson disease: A nationwide cohort study. Neurology 86:840-6.
100. Wu WY, Kang KH, Chen SL, Chiu SY, Yen AM, Fann JC, Su CW, Liu HC, Lee CZ, Fu WM, Chen HH, Liou HH. 2015. Hepatitis C virus infection: a risk factor for Parkinson's disease. J Viral Hepat 22:784-91.
101. Beatman EL, Massey A, Shives KD, Burrack KS, Chamanian M, Morrison TE, Beckham JD. 2015. Alpha-Synuclein Expression Restricts RNA Viral Infections in the Brain. J Virol 90:2767-82.

102. Khanlou N, Moore DJ, Chana G, Cherner M, Lazzaretto D, Dawes S, Grant I, Masliah E, Everall IP, Group H. 2009. Increased frequency of alpha-synuclein in the substantia nigra in human immunodeficiency virus infection. J Neurovirol 15:131-8.
103. Gupta A, Mohapatra A, Kaur H, Sharma A, Chaudhary N, Kumar S. 2023. Alpha-synuclein expression in neuron modulates the Japanese encephalitis virus infection. bioRxiv:2023.09.25.559402.
104. Wu Z, Zhang X, Huang Z, Ma K. 2022. SARS-CoV-2 Proteins Interact with Alpha Synuclein and Induce Lewy Body-like Pathology In Vitro. Int J Mol Sci 23.
105. Semerdzhiev SA, Fakhree MAA, Segers-Nolten I, Blum C, Claessens M. 2022. Interactions between SARS-CoV-2 N-Protein and alpha-Synuclein Accelerate Amyloid Formation. ACS Chem Neurosci 13:143-150.
106. Jang H, Boltz D, Sturm-Ramirez K, Shepherd KR, Jiao Y, Webster R, Smeyne RJ. 2009. Highly pathogenic H5N1 influenza virus can enter the central nervous system and induce neuroinflammation and neurodegeneration. Proc Natl Acad Sci U S A 106:14063-8.
107. Ait Wahmane S, Achbani A, Ouhaz Z, Elatiqi M, Belmouden A, Nejmeddine M. 2020. The Possible Protective Role of alpha-Synuclein Against Severe Acute Respiratory Syndrome Coronavirus 2 Infections in Patients With Parkinson's Disease. Mov Disord 35:1293-1294.
108. Lesteberg KE, Beckham JD. 2019. Immunology of West Nile Virus Infection and the Role of Alpha-Synuclein as a Viral Restriction Factor. Viral Immunol 32:38-47.
109. Massey AR, Beckham JD. 2016. Alpha-Synuclein, a Novel Viral Restriction Factor Hiding in Plain Sight. DNA Cell Biol 35:643-645.
110. Grozdanov V, Bousset L, Hoffmeister M, Bliederhaeuser C, Meier C, Madiona K, Pieri L, Kiechle M, McLean PJ, Kassubek J, Behrends C, Ludolph AC, Weishaupt JH, Melki R, Danzer KM. 2019. Increased Immune Activation by Pathologic alpha-Synuclein in Parkinson's Disease. Ann Neurol 86:593-606.
111. Bernal-Conde LD, Ramos-Acevedo R, Reyes-Hernandez MA, Balbuena-Olvera AJ, Morales-Moreno ID, Arguero-Sanchez R, Schule B, Guerra-Crespo M. 2019. Alpha-Synuclein Physiology and Pathology: A Perspective on Cellular Structures and Organelles. Front Neurosci 13:1399.
112. Irwin DJ, Lee VM, Trojanowski JQ. 2013. Parkinson's disease dementia: convergence of alpha-synuclein, tau and amyloid-beta pathologies. Nat Rev Neurosci 14:626-36.
113. Benskey MJ, Perez RG, Manfredsson FP. 2016. The contribution of alpha synuclein to neuronal survival and function - Implications for Parkinson's disease. J Neurochem 137:331-59.
114. Khan FH, Sen T, Maiti AK, Jana S, Chatterjee U, Chakrabarti S. 2005. Inhibition of rat brain mitochondrial electron transport chain activity by dopamine oxidation products during extended in vitro incubation: implications for Parkinson's disease. Biochim Biophys Acta 1741:65-74.
115. Choong CJ, Say YH. 2011. Neuroprotection of alpha-synuclein under acute and chronic rotenone and maneb treatment is abolished by its familial Parkinson's disease mutations A30P, A53T and E46K. Neurotoxicology 32:857-63.
116. Thomas MP, Chartrand K, Reynolds A, Vitvitsky V, Banerjee R, Gendelman HE. 2007. Ion channel blockade attenuates aggregated alpha synuclein induction of microglial reactive oxygen species: relevance for the pathogenesis of Parkinson's disease. J Neurochem 100:503-19.

117. Lin RJ, Liao CL, Lin YL. 2004. Replication-incompetent virions of Japanese encephalitis virus trigger neuronal cell death by oxidative stress in a culture system. J Gen Virol 85:521-533.
118. Chen TH, Tang P, Yang CF, Kao LH, Lo YP, Chuang CK, Shih YT, Chen WJ. 2011. Antioxidant defense is one of the mechanisms by which mosquito cells survive dengue 2 viral infection. Virology 410:410-7.
119. Gupta A, Gawandi S, Vandna, Yadav I, Mohan H, Desai VG, Kumar S. 2023. Analysis of fluoro based pyrazole analogues as a potential therapeutics candidate against Japanese encephalitis virus infection. Virus Res 323:198955.
120. Somayaji M, Lanseur Z, Choi SJ, Sulzer D, Mosharov EV. 2021. Roles for alpha-Synuclein in Gene Expression. Genes (Basel) 12.
121. Liu YY, Zhao HY, Zhao CL, Duan CL, Lu LL, Yang H. 2006. [Overexpression of alpha-synuclein in SH-SY5Y cells partially protected against oxidative stress induced by rotenone]. Sheng Li Xue Bao 58:421-8.
122. Kumar V, Kaur K, Gupta GK, Sharma AK. 2013. Pyrazole containing natural products: synthetic preview and biological significance. Eur J Med Chem 69:735-53.
123. Miura T, OGOSHI Y, UEYAMA K, MOTODA D, IWAYAMA T, SUZAWA K, NAGAMORI H, UENO H, TAKAHASHI A, SUGIMOTO K. 2020. PYRAZOLE COMPOUND AND PHARMACEUTICAL USE THEREOF FOR INHIBITING SGLT1 patent CA 2845127WO2013/031922.
124. Barbara Nave JD, Peter Nesvadba, Mihiret Tekeste Sisay, Alexander Wissemeier, Wolfram Zerulla, Gregor Pasda, Olof Wallquist, Allan F. Cunningham. 2018. THIOETHER COMPOUNDS AS NITRIFICATION INHIBITORS.
125. Karrouchi K, Radi S, Ramli Y, Taoufik J, Mabkhot YN, Al-Aizari FA, Ansar M. 2018. Synthesis and Pharmacological Activities of Pyrazole Derivatives: A Review. Molecules 23.
126. Khan MF, Alam MM, Verma G, Akhtar W, Akhter M, Shaquiquzzaman M. 2016. The therapeutic voyage of pyrazole and its analogs: A review. Eur J Med Chem 120:170-201.
127. Naim MJ, Alam O, Nawaz F, Alam MJ, Alam P. 2016. Current status of pyrazole and its biological activities. J Pharm Bioallied Sci 8:2-17.
128. Rashad AE, Ali MA. 2006. Synthesis and antiviral screening of some thieno[2,3-d]pyrimidine nucleosides. Nucleosides Nucleotides Nucleic Acids 25:17-28.
129. Tanaka H, Baba M, Hayakawa H, Sakamaki T, Miyasaka T, Ubasawa M, Takashima H, Sekiya K, Nitta I, Shigeta S, Walker RT, Balzarini J, Declercq E. 1991. A New Class of Hiv-1-Specific 6-Substituted Acyclouridine Derivatives - Synthesis and Anti-Hiv-1 Activity of 5-Substituted or 6-Substituted Analogs of 1-[(2-Hydroxyethoxy)Methyl]-6-(Phenylthio)Thymine (Hept). Journal of Medicinal Chemistry 34:349-357.
130. Goodell JR, Puig-Basagoiti F, Forshey BM, Shi PY, Ferguson DM. 2006. Identification of compounds with anti-West Nile Virus activity. Journal of Medicinal Chemistry 49:2127-2137.
131. Bae SH, Sung SH, Lee HE, Kang HT, Lee SK, Oh SY, Woo HA, Kil IS, Rhee SG. 2012. Peroxiredoxin III and sulfiredoxin together protect mice from pyrazole-induced oxidative liver injury. Antioxid Redox Signal 17:1351-61.
132. Gong PF, Cederbaum AI. 2006. Nrf2 is increased by CYP2E1 in rodent liver and HepG2 cells and protects against oxidative stress caused by CYP2E1. Hepatology 43:144-153.

133. Wang Y, He M, Li X, Chai J, Jiang Q, Peng C, He G, Huang W. 2021. Design, Synthesis, and Biological Evaluation of Pyrano[2,3-c]-pyrazole-Based RalA Inhibitors Against Hepatocellular Carcinoma. Front Chem 9:700956.
134. Ali SA, Awad SM, Said AM, Mahgoub S, Taha H, Ahmed NM. 2020. Design, synthesis, molecular modelling and biological evaluation of novel 3-(2-naphthyl)-1-phenyl-1H-pyrazole derivatives as potent antioxidants and 15-Lipoxygenase inhibitors. J Enzyme Inhib Med Chem 35:847-863.
135. Simanjuntak Y, Liang JJ, Lee YL, Lin YL. 2017. Japanese Encephalitis Virus Exploits Dopamine D2 Receptor-phospholipase C to Target Dopaminergic Human Neuronal Cells. Front Microbiol 8:651.
136. Kim SJ, Kim SY, Na YS, Lee HJ, Chung KC, Baik JH. 2006. Alpha-synuclein enhances dopamine D2 receptor signaling. Brain Res 1124:5-9.
137. Kawahata I, Finkelstein DI, Fukunaga K. 2022. Pathogenic Impact of alpha-Synuclein Phosphorylation and Its Kinases in alpha-Synucleinopathies. Int J Mol Sci 23.
138. Mishra MK, Ghosh D, Duseja R, Basu A. 2009. Antioxidant potential of Minocycline in Japanese Encephalitis Virus infection in murine neuroblastoma cells: correlation with membrane fluidity and cell death. Neurochem Int 54:464-70.
139. Sehgal N, Kumawat KL, Basu A, Ravindranath V. 2012. Fenofibrate reduces mortality and precludes neurological deficits in survivors in murine model of Japanese encephalitis viral infection. PLoS One 7:e35427.
140. Swarup V, Ghosh J, Mishra MK, Basu A. 2008. Novel strategy for treatment of Japanese encephalitis using arctigenin, a plant lignan. J Antimicrob Chemother 61:679-88.
141. Turtle L, Solomon T. 2018. Japanese encephalitis - the prospects for new treatments. Nat Rev Neurol 14:298-313.
142. Goodell JR, Puig-Basagoiti F, Forshey BM, Shi PY, Ferguson DM. 2006. Identification of compounds with anti-West Nile Virus activity. J Med Chem 49:2127-37.
143. Murgod UA, Muthane UB, Ravi V, Radhesh S, Desai A. 2001. Persistent movement disorders following Japanese encephalitis. Neurology 57:2313-5.
144. Banerjee A, Tripathi A. 2019. Recent advances in understanding Japanese encephalitis. F1000Res 8.
145. Stefanis L. 2012. alpha-Synuclein in Parkinson's disease. Cold Spring Harb Perspect Med 2:a009399.
146. Heiden DL, Monogue B, Ali MDH, Beckham JD. 2023. A functional role for alpha-synuclein in neuroimmune responses. J Neuroimmunol 376:578047.
147. Roodveldt C, Labrador-Garrido A, Gonzalez-Rey E, Fernandez-Montesinos R, Caro M, Lachaud CC, Waudby CA, Delgado M, Dobson CM, Pozo D. 2010. Glial innate immunity generated by non-aggregated alpha-synuclein in mouse: differences between wild-type and Parkinson's disease-linked mutants. PLoS One 5:e13481.
148. Schaser AJ, Osterberg VR, Dent SE, Stackhouse TL, Wakeham CM, Boutros SW, Weston LJ, Owen N, Weissman TA, Luna E, Raber J, Luk KC, McCullough AK, Woltjer RL, Unni VK. 2019. Alpha-synuclein is a DNA binding protein that modulates DNA repair with implications for Lewy body disorders. Sci Rep 9:10919.
149. Mohapatra A, Bohara VS, Kumar S, Chaudhary N. 2021. Polymyxin B accelerates the alpha-synuclein aggregation. Biophys Chem 277:106628.

150. Mohapatra A, Lokappa SB, Chaudhary N. 2020. Interaction of cavin-1/PTRF leucine zipper domain 2 and its congenital generalized lipodystrophy mutant with model membranes. Biochem Biophys Res Commun 521:732-738.
151. Furlong RA, Narain Y, Rankin J, Wyttenbach A, Rubinsztein DC. 2000. Alpha-synuclein overexpression promotes aggregation of mutant huntingtin. Biochem J 346 Pt 3:577-81.
152. Gupta A, Gawandi S, Vandna, Yadav I, Mohan H, Desai VG, Kumar S. 2022. Analysis of fluoro based pyrazole analogues as a potential therapeutics candidate against Japanese encephalitis virus infection. Virus Res 323:198955.
153. Mohapatra A, Hans A, Chaudhary N. 2023. Interfacial properties of alpha-synuclein's Parkinsonian variants. Biophys Chem 297:107006.
154. Mohapatra A, Chaudhary N. 2021. N-terminal acetylation does not alter alpha-synuclein's interfacial properties. Int J Biol Macromol 174:69-76.
155. Al-Obaidi MMJ, Bahadoran A, Wang SM, Manikam R, Raju CS, Sekaran SD. 2018. Disruption of the blood brain barrier is vital property of neurotropic viral infection of the central nervous system. Acta Virol 62:16-27.
156. Pardridge WM. 2012. Drug transport across the blood-brain barrier. J Cereb Blood Flow Metab 32:1959-72.
157. Wewer CR, Khandelia H. 2018. Different footprints of the Zika and dengue surface proteins on viral membranes. Soft Matter 14:5615-5621.
158. Angelova PR, Horrocks MH, Klenerman D, Gandhi S, Abramov AY, Shchepinov MS. 2015. Lipid peroxidation is essential for alpha-synuclein-induced cell death. J Neurochem 133:582-9.
159. Harischandra DS, Jin H, Anantharam V, Kanthasamy A, Kanthasamy AG. 2015. alpha-Synuclein protects against manganese neurotoxic insult during the early stages of exposure in a dopaminergic cell model of Parkinson's disease. Toxicol Sci 143:454-68.
160. Zhu M, Qin ZJ, Hu D, Munishkina LA, Fink AL. 2006. Alpha-synuclein can function as an antioxidant preventing oxidation of unsaturated lipid in vesicles. Biochemistry 45:8135-42.
161. Kim JY, Jeon BS, Kim HJ, Ahn TB. 2013. Nanomolar concentration of alpha-synuclein enhances dopaminergic neuronal survival via Akt pathway. Neural Regen Res 8:3269-74.
162. Kaul S, Anantharam V, Kanthasamy A, Kanthasamy AG. 2005. Wild-type alpha-synuclein interacts with pro-apoptotic proteins PKCdelta and BAD to protect dopaminergic neuronal cells against MPP+-induced apoptotic cell death. Brain Res Mol Brain Res 139:137-52.
163. Xu J, Kao SY, Lee FJ, Song W, Jin LW, Yankner BA. 2002. Dopamine-dependent neurotoxicity of alpha-synuclein: a mechanism for selective neurodegeneration in Parkinson disease. Nat Med 8:600-6.
164. Mbefo MK, Paleologou KE, Boucharaba A, Oueslati A, Schell H, Fournier M, Olschewski D, Yin G, Zweckstetter M, Masliah E, Kahle PJ, Hirling H, Lashuel HA. 2010. Phosphorylation of synucleins by members of the Polo-like kinase family. J Biol Chem 285:2807-22.
165. Waxman EA, Giasson BI. 2008. Specificity and regulation of casein kinase-mediated phosphorylation of alpha-synuclein. J Neuropathol Exp Neurol 67:402-16.
166. Pronin AN, Morris AJ, Surguchov A, Benovic JL. 2000. Synucleins are a novel class of substrates for G protein-coupled receptor kinases. J Biol Chem 275:26515-22.
167. Inglis KJ, Chereau D, Brigham EF, Chiou SS, Schobel S, Frigon NL, Yu M, Caccavello RJ, Nelson S, Motter R, Wright S, Chian D, Santiago P, Soriano F, Ramos C, Powell K,

Goldstein JM, Babcock M, Yednock T, Bard F, Basi GS, Sham H, Chilcote TJ, McConlogue L, Griswold-Prenner I, Anderson JP. 2009. Polo-like kinase 2 (PLK2) phosphorylates alpha-synuclein at serine 129 in central nervous system. J Biol Chem 284:2598-2602.

168. Volpicelli-Daley LA, Luk KC, Patel TP, Tanik SA, Riddle DM, Stieber A, Meaney DF, Trojanowski JQ, Lee VM. 2011. Exogenous alpha-synuclein fibrils induce Lewy body pathology leading to synaptic dysfunction and neuron death. Neuron 72:57-71.
169. Luk KC, Song C, O'Brien P, Stieber A, Branch JR, Brunden KR, Trojanowski JQ, Lee VM. 2009. Exogenous alpha-synuclein fibrils seed the formation of Lewy body-like intracellular inclusions in cultured cells. Proc Natl Acad Sci U S A 106:20051-6.
170. Weston LJ, Cook ZT, Stackhouse TL, Sal MK, Schultz BI, Tobias ZJC, Osterberg VR, Brockway NL, Pizano S, Glover G, Weissman TA, Unni VK. 2021. In vivo aggregation of presynaptic alpha-synuclein is not influenced by its phosphorylation at serine-129. Neurobiol Dis 152:105291.
171. Azeredo da Silveira S, Schneider BL, Cifuentes-Diaz C, Sage D, Abbas-Terki T, Iwatsubo T, Unser M, Aebischer P. 2009. Phosphorylation does not prompt, nor prevent, the formation of alpha-synuclein toxic species in a rat model of Parkinson's disease. Hum Mol Genet 18:872-87.
172. McFarland NR, Fan Z, Xu K, Schwarzschild MA, Feany MB, Hyman BT, McLean PJ. 2009. Alpha-synuclein S129 phosphorylation mutants do not alter nigrostriatal toxicity in a rat model of Parkinson disease. J Neuropathol Exp Neurol 68:515-24.
173. Iqbal A, Baldrighi M, Murdoch JN, Fleming A, Wilkinson CJ. 2020. Alpha-synuclein aggresomes inhibit ciliogenesis and multiple functions of the centrosome. Biol Open 9.
174. Tanaka M, Kim YM, Lee G, Junn E, Iwatsubo T, Mouradian MM. 2004. Aggresomes formed by alpha-synuclein and synphilin-1 are cytoprotective. J Biol Chem 279:4625-31.
175. Pinho R, Paiva I, Jercic KG, Fonseca-Ornelas L, Gerhardt E, Fahlbusch C, Garcia-Esparcia P, Kerimoglu C, Pavlou MAS, Villar-Pique A, Szego E, Lopes da Fonseca T, Odoardi F, Soeroes S, Rego AC, Fischle W, Schwamborn JC, Meyer T, Kugler S, Ferrer I, Attems J, Fischer A, Becker S, Zweckstetter M, Borovecki F, Outeiro TF. 2019. Nuclear localization and phosphorylation modulate pathological effects of alpha-synuclein. Hum Mol Genet 28:31-50.
176. St-Denis NA, Litchfield DW. 2009. Protein kinase CK2 in health and disease: From birth to death: the role of protein kinase CK2 in the regulation of cell proliferation and survival. Cell Mol Life Sci 66:1817-29.
177. Pohl MO, von Recum-Knepper J, Rodriguez-Frandsen A, Lanz C, Yángüez E, Soonthornvacharin S, Wolff T, Chanda SK, Stertz S. 2017. Identification of Polo-like kinases as potential novel drug targets for influenza A virus. Scientific Reports 7.
178. Conner J. 1999. The unique N terminus of herpes simplex virus type 1 ribonucleotide reductase large subunit is phosphorylated by casein kinase 2, which may have a homologue in Escherichia coli. J Gen Virol 80 (Pt 6):1471-1476.
179. Meggio F, D'Agostino DM, Ciminale V, Chieco-Bianchi L, Pinna LA. 1996. Phosphorylation of HIV-1 Rev protein: implication of protein kinase CK2 and pro-directed kinases. Biochem Biophys Res Commun 226:547-54.
180. Wadd S, Bryant H, Filhol O, Scott JE, Hsieh TY, Everett RD, Clements JB. 1999. The multifunctional herpes simplex virus IE63 protein interacts with heterogeneous ribonucleoprotein K and with casein kinase 2. J Biol Chem 274:28991-8.

181. Enomoto M, Sawano Y, Kosuge S, Yamano Y, Kuroki K, Ohtsuki K. 2006. High phosphorylation of HBV core protein by two alpha-type CK2-activated cAMP-dependent protein kinases in vitro. FEBS Lett 580:894-9.
182. Franck N, Le Seyec J, Guguen-Guillouzo C, Erdtmann L. 2005. Hepatitis C virus NS2 protein is phosphorylated by the protein kinase CK2 and targeted for degradation to the proteasome. Journal of Virology 79:2700-2708.
183. Quan R, Wei L, Hou L, Wang J, Zhu S, Li Z, Lv M, Liu J. 2020. Proteome Analysis in a Mammalian Cell line Reveals that PLK2 is Involved in Avian Metapneumovirus Type C (aMPV/C)-Induced Apoptosis. Viruses 12.
184. Shapira SD, Gat-Viks I, Shum BO, Dricot A, de Grace MM, Wu L, Gupta PB, Hao T, Silver SJ, Root DE, Hill DE, Regev A, Hacohen N. 2009. A physical and regulatory map of host-influenza interactions reveals pathways in H1N1 infection. Cell 139:1255-67.
185. Walker DG, Lue LF, Adler CH, Shill HA, Caviness JN, Sabbagh MN, Akiyama H, Serrano GE, Sue LI, Beach TG, Arizona Parkinson Disease C. 2013. Changes in properties of serine 129 phosphorylated alpha-synuclein with progression of Lewy-type histopathology in human brains. Exp Neurol 240:190-204.
186. Fujiwara H, Hasegawa M, Dohmae N, Kawashima A, Masliah E, Goldberg MS, Shen J, Takio K, Iwatsubo T. 2002. α-Synuclein is phosphorylated in synucleinopathy lesions. Nature Cell Biology 4:160-164.
187. Paleologou KE, Schmid AW, Rospigliosi CC, Kim HY, Lamberto GR, Fredenburg RA, Lansbury PT, Jr., Fernandez CO, Eliezer D, Zweckstetter M, Lashuel HA. 2008. Phosphorylation at Ser-129 but not the phosphomimics S129E/D inhibits the fibrillation of alpha-synuclein. J Biol Chem 283:16895-905.
188. Machiya Y, Hara S, Arawaka S, Fukushima S, Sato H, Sakamoto M, Koyama S, Kato T. 2010. Phosphorylated alpha-synuclein at Ser-129 is targeted to the proteasome pathway in a ubiquitin-independent manner. J Biol Chem 285:40732-44.
189. Dent SE, King DP, Osterberg VR, Adams EK, Mackiewicz MR, Weissman TA, Unni VK. 2022. Phosphorylation of the aggregate-forming protein alpha-synuclein on serine-129 inhibits its DNA-bending properties. J Biol Chem 298:101552.
190. Waxman EA, Giasson BI. 2010. A novel, high-efficiency cellular model of fibrillar α-synuclein inclusions and the examination of mutations that inhibit amyloid formation. Journal of Neurochemistry 113:374-388.
191. Lv BM, Tong XY, Quan Y, Liu MY, Zhang QY, Song YF, Zhang HY. 2018. Drug Repurposing for Japanese Encephalitis Virus Infection by Systems Biology Methods. Molecules 23.
192. Kumar R, Basu A, Sinha S, Das M, Tripathi P, Jain A, Kumar C, Atam V, Khan S, Singh AS. 2016. Role of oral Minocycline in acute encephalitis syndrome in India - a randomized controlled trial. BMC Infect Dis 16:67.
193. Kumar R, Tripathi P, Baranwal M, Singh S, Tripathi S, Banerjee G. 2009. Randomized, controlled trial of oral ribavirin for Japanese encephalitis in children in Uttar Pradesh, India. Clin Infect Dis 48:400-6.
194. Ighodaro OM, Akinloye OA. 2018. First line defence antioxidants-superoxide dismutase (SOD), catalase (CAT) and glutathione peroxidase (GPX): Their fundamental role in the entire antioxidant defence grid. Alexandria Journal of Medicine 54:287-293.
195. Kageyama S, Gudmundsson SR, Sou YS, Ichimura Y, Tamura N, Kazuno S, Ueno T, Miura Y, Noshiro D, Abe M, Mizushima T, Miura N, Okuda S, Motohashi H, Lee JA,

Sakimura K, Ohe T, Noda NN, Waguri S, Eskelinen EL, Komatsu M. 2021. p62/SQSTM1-droplet serves as a platform for autophagosome formation and anti-oxidative stress response. Nat Commun 12:16.
196. Taniguchi K, Yamachika S, He F, Karin M. 2016. p62/SQSTM1-Dr. Jekyll and Mr. Hyde that prevents oxidative stress but promotes liver cancer. FEBS Lett 590:2375-97.
197. Yun SI, Song BH, Kim JK, Yun GN, Lee EY, Li L, Kuhn RJ, Rossmann MG, Morrey JD, Lee YM. 2014. A molecularly cloned, live-attenuated japanese encephalitis vaccine SA14-14-2 virus: a conserved single amino acid in the ij Hairpin of the Viral E glycoprotein determines neurovirulence in mice. PLoS Pathog 10:e1004290.
198. Shi Z, Wei J, Deng X, Li S, Qiu Y, Shao D, Li B, Zhang K, Xue F, Wang X, Ma Z. 2014. Nitazoxanide inhibits the replication of Japanese encephalitis virus in cultured cells and in a mouse model. Virol J 11:10.
199. Metz P, Chiramel A, Chatel-Chaix L, Alvisi G, Bankhead P, Mora-Rodriguez R, Long G, Hamacher-Brady A, Brady NR, Bartenschlager R. 2015. Dengue Virus Inhibition of Autophagic Flux and Dependency of Viral Replication on Proteasomal Degradation of the Autophagy Receptor p62. J Virol 89:8026-41.
200. Sharma M, Bhattacharyya S, Nain M, Kaur M, Sood V, Gupta V, Khasa R, Abdin MZ, Vrati S, Kalia M. 2014. Japanese encephalitis virus replication is negatively regulated by autophagy and occurs on LC3-I- and EDEM1-containing membranes. Autophagy 10:1637-51.
201. Tasaki T, Nukuzuma S, Takegami T. 2016. Impaired Japanese encephalitis virus replication in p62/SQSTM1 deficient mouse embryonic fibroblasts. Microbiol Immunol 60:708-711.
202. Gong P, Cederbaum AI. 2006. Nrf2 is increased by CYP2E1 in rodent liver and HepG2 cells and protects against oxidative stress caused by CYP2E1. Hepatology 43:144-53.
203. Aggarwal VK, de Vicente J, Bonnert RV. 2003. A novel one-pot method for the preparation of pyrazoles by 1,3-dipolar cycloadditions of diazo compounds generated in situ. J Org Chem 68:5381-3.
204. Desai VG, Satardekar PC, Polo S, Dhumaskar K. 2012. Regioselective Synthesis of 1,3,5-Trisubstituted Pyrazoles. Synthetic Communications 42.
205. Ivonin SP, Kurpil BB, Rusanov EB, Grygorenko OO, Volochnyuk DM, -. 2014. N-Alkylhydrazones of aliphatic ketones in the synthesis of 1, 3, 4-trisubstituted non-symmetric pyrazoles. Tetrahedron Letters 55.
206. Jin W, Yu H, Yu Z. 2011. Regioselective synthesis of multisubstituted pyrazoles via cyclocondensation of β-thioalkyl-α,β-unsaturated ketones with hydrazines. Tetrahedron Letters 52:5884-5887.
207. Wei W, Wang Z, Yang X, Yu W, Chang J, -. 2017. Divergent Synthesis of 1H-Indazoles and 1H-Pyrazoles from Hydrazones via Iodine-Mediated Intramolecular Aryl and sp3 C–H Amination. Advanced Synthesis & Catalysis 359.
208. Gawandi SJ, Desai VG, Shingade SG. 2019. Design, synthesis, and biological evaluation of 1,3,5-trisubstituted pyrazoles as tyrosine kinase inhibitors. Medicinal Chemistry Research 28.
209. Antony F, Vashi Y, Morla S, Vandna, Mohan H, Kumar S. 2020. Therapeutic potential of Nitazoxanide against Newcastle disease virus: A possible modulation of host cytokines. Cytokine 131:155115.

Research Achievements

Publications from thesis research work

1. **Gupta A**, Mohapatra A, Kaur H, Sharma A, Chaudhary N*, Kumar S* (2023) Alpha-synuclein expression in neuron modulates the Japanese encephalitis virus infection. https://doi.org/10.1101/2023.09.25.559402 [Manuscript Submitted]

2. **Gupta A**, Gawandi S, Vandna, Yadav I, Mohan Hari, Desai VG, Kumar S* [2022] Analysis of fluoro based pyrazole analogues as a potential therapeutics candidate against Japanese encephalitis virus infection. ***Virus Res.*** https://doi.org/10.1016/j.virusres.2022.198955

3. **Gupta A**, Bohara VS, Kumar S* (2023) Alpha-Synuclein and RNA viruses: exploring the Neuronal Nexus. ***Virology.*** https://doi.org/10.1016/j.virol.2024.110141

Publications from other collaborative research work

1. Kalita S, Kalita S, Kawa AH, Shill S, **Gupta A,** Kumar S, Mandal B [2022] Copper Chelating Cyclic Peptidomimetic Inhibits Aβ Fibrillogenesis. ***RSC Med. Chem.*** https://doi.org/10.1039/D2MD00019A

2. Das NM, Prusty BM, Pradhan N, **Gupta A**, Carmena-Bargueño M, Karn R, Pérez-Sánchez H, Kumar S, Manna D* [2023] Evaluation of mode of indoleamine 2,3-dioxygenase 1 inhibition by 4,7-dichloroquinolines. ***EJMCR.*** https://doi.org/10.1016/j.ejmcr.2023.100110

3. Pradhan N, Akhtar N, Nath B, Pena-Garcia J, **Gupta A,** Perez-Sanchez H, Kumar S, Manna D, [2021] Inhibition of Immunosuppressive Indoleamine 2,3-Dioxygenase by Targeting the Heme and Apo form, ***Chemical Communications.*** 57, 395-398. https://doi.org/10.1039/D0CC06942F

4. **Gupta A**, Deka P, Kumar S* [2020] Resiquimod inhibits Newcastle disease virus replication by modulating host cytokines: An understanding towards its possible therapeutics. ***Cytokine***.125: 154811. https://doi.org/10.1016/j.cyto.2019.154811

5. Dey S, **Gupta A**, Saha A, Pal S, Kumar S*, Manna D* [2020] Sunlight-Mediated Thiol-Ene/Yne Click Reaction: Synthesis and DNA Transfection Efficiency of New Cationic Lipids. ***ACS Omega***. 5:1, 735–750. https://pubs.acs.org/doi/10.1021/acsomega.9b03413

6. Sarmah H, Shah M, Pathak M, Barman NN, Koul M, **Gupta A**, Sahariah PJ, Neher S, Das SK, Gogoi SM, Kumar S*, [2020] Pathodynamics of circulating strains of duck enteritis virus: A step forward to understand its pathogenesis. ***Avian Dis.*** 64(2):166-173. https://doi.org/10.1637/0005-2086-64.2.166

7. Shah M, Bharadwaj M, **Gupta A**, Kumar R, Kumar S* [2019] Chicken viperin inhibits Newcastle disease virus infection in vitro: A possible interaction with the viral matrix protein. ***Cytokine.*** 120:28-40. https://doi.org/10.1016/j.cyto.2019.04.007

Awards

2023 **Global Scholar Travel award** for poster and flash talk presentation at American Society of Virology Conference (ASV) 2023, University of Georgia, Athens, USA

2023 **Best Poster presentation award** at 63rd International conference of Association of Microbiologists of India (AMI), MDU, Rohtak, Haryana

2022 **Second best oral presentation award** at National Seminar on "Advances in Basic and Translational Research in Biology (ABTRiB), Tezpur University, Assam, India.

CONFERENCES/ WORKSHOPS

2023 **Flash Talk and poster presentation** on "Role and mechanism of Alpha-Synuclein in Japanese Encephalitis virus infectivity in neuronal cells: An insight towards its anti-viral effect" at ASV 2023 annual conference, University of Georgia, Athens, USA.

2022 **Oral presentation** on "Analysis of fluoro based pyrazole analogues as a potential therapeutics candidate against Japanese encephalitis virus infection" at National Seminar on "Advances in Basic and Translational Research in Biology (ABTRiB), Tezpur University, Assam, India

2022 **Member of organizing committee** of "DIAGNOSTIC APPROACHES IN VIROLOGY: RECENT ADVANCEMENTS" at the Indian Institute of Technology Guwahati, May 13-15, 2022.

2020 **Member of organizing committee** of "DIAGNOSTIC APPROACHES IN VIROLOGY" at the Indian Institute of Technology Guwahati, March 4- 6, 2020.

2019 **Poster presentation** on "Resiquimod induces proinflammatory cytokines and inhibits Newcastle disease virus replication in chicken embryo fibroblast cells and in ovo" at 19th Indian Veterinary Congress, XXVI Annual Conference of IAAVR, Kolkata, India

2018 **Poster presentation** on "Resiquimod induces proinflammatory cytokines and inhibits Newcastle disease virus replication in chicken embryo fibroblast cells" at National Conference and Annual Convention of ISVIB and VIBCON-2018, Nagaland, India